THE DISPERSION OF THE NONLINEAR OPTICAL SUSCEPTIBILITY OF SOME WURTZITE AND ZINC
PARSONS, FREDERICK GEORGE
ProQuest Dissertations and Theses; 1971; ProQuest Dissertations & Theses Global

INFORMATION TO USERS

This dissertation was produced from a microfilm copy of the original document. While the most advanced technological means to photograph and reproduce this document have been used, the quality is heavily dependent upon the quality of the original submitted.

The following explanation of techniques is provided to help you understand markings or patterns which may appear on this reproduction.

1. The sign or "target" for pages apparently lacking from the document photographed is "Missing Page(s)". If it was possible to obtain the missing page(s) or section, they are spliced into the film along with adjacent pages. This may have necessitated cutting thru an image and duplicating adjacent pages to insure you complete continuity.
2. When an image on the film is obliterated with a large round black mark, it is an indication that the photographer suspected that the copy may have moved during exposure and thus cause a blurred image. You will find a good image of the page in the adjacent frame.
3. When a map, drawing or chart, etc., was part of the material being photographed the photographer followed a definite method in "sectioning" the material. It is customary to begin photoing at the upper left hand corner of a large sheet and to continue photoing from left to right in equal sections with a small overlap. If necessary, sectioning is continued again — beginning below the first row and continuing on until complete.
4. The majority of users indicate that the textual content is of greatest value, however, a somewhat higher quality reproduction could be made from "photographs" if essential to the understanding of the dissertation. Silver prints of "photographs" may be ordered at additional charge by writing the Order Department, giving the catalog number, title, author and specific pages you wish reproduced.

University Microfilms
300 North Zeeb Road
Ann Arbor, Michigan 48106
A Xerox Education Company

Reproduced with permission of the copyright owner. Further reproduction prohibited without permission.

72-17,152

PARSONS, Frederick George, 1945-
THE DISPERSION OF THE NONLINEAR OPTICAL
SUSCEPTIBILITY OF SOME WURTZITE AND ZINC-
BLENDE SEMICONDUCTORS.

Yale University, Ph.D., 1971
Physics, solid state

University Microfilms, A XEROX Company, Ann Arbor, Michigan

The Dispersion of the Nonlinear Optical Susceptibility of Some Wurtzite and Zinc-Blende Semiconductors.

by

Frederick George Parsons

A Dissertation
Presented to the Faculty of
the Graduate School of Yale University
in Candidacy for the Degree of
Doctor of Philosophy

1971

ABSTRACT

The dispersions of the nonlinear susceptibility modulus, $|\chi^{NL}_{14}(2\omega)|$, of GaAs, InAs, InSb, InP, and ZnTe have been measured by reflection with tunable dye lasers. Within the fundamental wavelength range (.73 to 1.02μ) sharp structure has been observed. This structure has been correlated, in most cases, with structure in the linear optical susceptibility at the fundamental and/or second harmonic. Dispersion in Miller's coefficients has also been observed. In most instances it is less pronounced than dispersion in $|\chi^{NL}_{14}(2\omega)|$.

The dispersion of the nonlinear optical susceptibility moduli $|\chi^{NL}_{15}(2\omega)|$, $|\chi^{NL}_{31}(2\omega)|$, and $|\chi^{NL}_{33}(2\omega)|$ of CdS and CdSe have also been measured by reflection over the wavelength range .73 to 1.02μ. Enhancement of the CdS nonlinear susceptibilities has been observed when the harmonic photon energy is coincident with the exciton energy. Near this photon energy dispersion of Robinson's ratio $|\chi^{NL}_{33}|/|\chi^{NL}_{31}|$ has also been observed. No dispersion was evident in $|\chi^{NL}_{15}|/|\chi^{NL}_{31}|$. Miller's coefficients are also determined.

A new method of measuring the relative phase of wurtzite nonlinear susceptibilities by reflection is presented. The relative phases of $\chi^{NL}_{33}(2\omega)$ and $\chi^{NL}_{15}(2\omega)$ to $\chi^{NL}_{31}(2\omega)$ in CdS and CdSe have been determined at some discrete wavelengths.

ACKNOWLEDGEMENTS

The author wishes to express his sincere appreciation to Professor Richard K. Chang, his research advisor, who has both assisted and counciled him through every phase of this work.

The author would also like to express his appreciation to Professors Richard C. Barker, Traugott E. Fischer, and Authur M. Yelon for serving on his dissertation committee.

Special thanks should go to Dr. Peter J. Kindlmann for the design of the pulse amplitude encoder used for all the harmonic intensity measurements.

Acknowledgement goes to Edward Chen for his assistance in data taking for Chapter 5.

The author also acknowledges with appreciation the financial support of Yale University and the Department of Engineering and Applied Science.

TABLE OF CONTENTS

Chapter 1

General Introduction

Since the advent of high intensity lasers, many nonlinear optical phenomena have been observed. One of these was optical second harmonic generation. Now, with the arrival of a tunable high intensity laser (the dye laser), nonlinear spectroscopy of materials can be examined.

Experimental data on the linear optical properties of materials has provided much of the groundwork for constructing the present electronic band structure models. The dispersion of the linear susceptibility has helped us to determine the shape of the Brillouin zone, in particular the locations of the critical points in the joint density of states. The dispersion of the nonlinear susceptibility should, in principle, provide new information on the electronic band structure. The details of this will be developed throughout this thesis.

Nonlinear spectroscopy was extremely difficult before the advent of the dye laser. Chang et. al. (Chang, Ducuing, and Bloembergen, 1965) had measured the nonlinear susceptibility of four zinc-blende semiconductors at nine discrete wavelengths.

Dispersion in the nonlinear susceptibility was observed. However, detailed fine structure in the dispersion could not be probed with the then existing discrete sources. With the recently developed dye laser, a continuously tunable intense source of monochromatic light covering the whole visible spectrum and the near infared (to 1.1 μ) was avalible. A decision was made to construct a dye laser operating over the wavelength range .7 to 1.1μ. Chapter 2 describes its operation and specifications.

1.1 The Nonlinear Susceptibility Tensor

Second harmonic light is generated whenever an intense beam impinges on a crystal which lacks inversion symmetry (Franken and Ward, 1963). To second order, the polarization of the crystal can then be expressed as:

eq. 1.1 $$\bar{P}(t) = \chi^{L}\bar{E}(t) + \chi^{NL}\bar{E}(t)\bar{E}(t)$$

where $\bar{E}(t)$ is the electric field of the intense beam, χ^{L} is the linear susceptibility and χ^{NL} is the nonlinear susceptibility of the crystal. The electric field oscillating at frequency ω will then give rise to a polarization oscillating at 2ω. This polarization will be called the "nonlinear polarization", P^{NLS}. The nonlinear polarization is related to the incident electric field through a third rank tensor, the nonlinear susceptibility tensor χ^{NL}:

eq. 1.2 $$P_i^{NLS} = \chi_{ijk} E_j E_k$$

Subscripts i, j, k designate Cartesian axes x, y, z.

The existence of a center of inversion (centro-symmetric) excludes any second harmonic generation. In fact, the second harmonic tensor has the same symmetry properties as the piezoelectric tensor (Yariv, 1967). Noting that the order in the electric fields is immaterial leads to a convenient contraction of indices of eq. 2.1. (Franken and Ward, 1963). The 27 components of the third rank tensor can be expressed in terms of an 18 component contracted tensor. That is, χ_{ijk} is now replaced by χ_{im}. The subscript i still designates the Cartesian components of P^{NLS} (i=1, 2, 3), and m now designates the components of the electric field product as follows:

m =	1	2	3	4	5	6
	xx	yy	zz	yz	xz	xy

This contracted form is often used to describe the piezoelectric tensor (Nye, 1957). Each of the 21 non-centro-symmetric crystal classes have their own tensors. The tensor elements must satsify the group symmetry of the crystal. For zinc-blende materials ($\bar{4}3m$) there exist only one independent tensor element. For wurtzite materials (6mm) there are three independent tensor elements.

1.2 Reflected Second Harmonic Radiation

Through Maxwell's wave equations, the nonlinear polarization can be related to the second harmonic intensity generated by the material. Boundary conditions require a field at 2ω to propagate in the same direction as the reflected beam of the incident ray. Thus second harmonic light can be observed in both the transmission and reflection direction. However, if the crystal absorbs the harmonic light and/or the incident light, measurements of the nonlinear susceptibilities by transmission are imprecise.(Bloembergen, Chang, and Ducuing, 1966). More accurate measurements are possible by measuring the reflected harmonic intensity. All the crystals that will be studied do absorb the second harmonic and in some crystals the fundamental radiation is also absorbed. Bloembergen and Pershan (Bloembergen and Pershan, 1962) have solved the wave equations that tie the nonlinear susceptibility to the reflected harmonic intensity for zinc-blende materials. Their results are used when measuring the nonlinear susceptibility of these materials by reflection.

The role of surface damage must be examined before meaningful measurements can be made by the reflection technique. It has been shown by several authors (Ducuing and Bloembergen, 1963; Chang and

Bloembergen, 1966) that with careful surface preparations, the second harmonic radiation exhibits the polarization selection rules associated with the bulk of the media. In this thesis some observations are made concerning the effect of surface quality on the measured nonlinear susceptibility value.

1.3 The Dispersion of χ^{NL} in Zinc-Blende

One aim of this thesis is to study the dispersion of the nonlinear susceptibility in zinc-blende semiconductors. The measured dispersion of five zinc-blende compounds ZnTe, InP, InAs, InSb, and GaAs are presented in Chapter 3.

The quantum mechanical description for the nonlinear susceptibility, derived elsewhere, (Bloembergen, Chang, and Ducuing, 1966) is reviewed in Chapter 3. Close attention is paid to the correlation between the nonlinear susceptibility structure and the critical points in the joint density of states. In most cases, one observes close correlation.

The quantum mechanical description also shows that the nonlinear susceptibility contains a triple product of momentum matrix elements. One recalls that the linear susceptibility only contains a double product of momentum matrix elements. This important difference between the nonlinear and linear susceptibilities should make the former yield more information about the band structure.

1.4 ADP as a Reference Standard

The nonlinear susceptibility of the semiconductors will be measured relative to the known nonlinear susceptibility of ADP (Ammonium Dihydrogen Phosphate). The nonlinear susceptibility of ADP has been carefully measured (Francois, 1966) using a cw HeNe single mode laser.

1.5 Dispersion of χ^{NL} in Wurtzite

The wurtzite structured semiconductors have uniaxial linear optical properties. Their symmetry (6mm) dictates there are three nonlinear susceptibilities χ_{15}, χ_{31}, and χ_{33}. The connection between these nonlinear susceptibilities and the reflected second harmonic intensity was attempted by Fischer (Fischer, 1967), however the correct solution was not obtained. In Chapter 4 the correct solution is derived. The result is used to obtain the dispersion of the nonlinear susceptibilities of CdS and CdSe by measurement of the reflected second harmonic intensities from them. The results are presented in Chapter 4.

1.6 Additional Relationships between χ^{NL} Tensors

Kleinman (1962) has suggested that an additional relationship can exist between nonlinear susceptibility tensor elements. Kleinman's relationships are additional to those dictated by symmetry. Kleinman used a reversible thermodynamic argument. Thus these additional relationships apply only to lossless and dispersionless media. The consequence in wurtzite materials is $\chi_{31} = \chi_{15}$. Experiments have shown this relationship to be correct when the crystal is transparent to both the harmonic and fundamental radiations. This thesis will examine the validity of $\chi_{15} = \chi_{31}$ in the absorbing region of the crystal. In Chapter 4 the dispersions of $\frac{|\chi_{15}|}{|\chi_{31}|}$ in CdS and CdSe are presented for the photon energy range were the second harmonic is strongly absorbed.

In wurtzite crystals Robinson (Robinson, 1968) has further postulated that $-2 \cdot \chi_{31} = \chi_{33}$ and $\chi_{15} = \chi_{31}$. Robinson's postulate rests on the anharmonic bond-charge model for the nonlinear susceptibility. The bond charge model again only applies to a lossless and dispersionless medium. Chapter 4 presents the behavior of $\frac{|\chi_{33}|}{|\chi_{31}|}$ for CdS and CdSe in the region where these crystals strongly absorb second harmonic radiation. From the dispersions of $\frac{|\chi_{33}|}{|\chi_{31}|}$ and $\frac{|\chi_{15}|}{|\chi_{31}|}$ more insight might be gained into the anharmonic bond charge model's characteristics.

1.7 The Phase of χ^{NL}.

The nonlinear susceptibility can have a phase associated with it. χ^{NL} can be either a positive or negative real number when the crystal is transparent to both the harmonic and fundamental light. This phase is exemplified in Robinson's postulate that $\chi_{33} = -2\chi_{31}$ while $\chi_{15} = \chi_{31}$. Most intensity measurements, as those found in Chapter 4, only give information on the moduli of the nonlinear susceptibility. All phase information is lost. A new method of obtaining the relative phases between nonlinear coefficients for wurtzite materials is discussed in Chapter 5. Relative phase information will serve as a further test of Kleinman's and Robinson's relationships in the absorbing region of CdS and CdSe.

1.8 Miller's Rule

In the transparency region of the crystal, Miller (1964) has empirically shown that a constant coefficient δ_{ijk} relates the nonlinear and linear susceptibilities of this given class of materials. This constant coefficient, often referred to as the "Miller δ", is defined as:

eq. 1.3
$$\delta_{ijk} = \frac{\chi_{ijk}^{NL}}{\chi_{ii}^{L}(2\omega)\,\chi_{jj}^{L}(\omega)\,\chi_{kk}^{L}(\omega)}$$

where $\chi^{L}(2\omega)$ and $\chi^{L}(\omega)$ designate the linear susceptibilities at 2ω and ω, respectively. The subscripts specify the crystal axes. Miller's δ was found to be $1.46 \pm .88 \times 10^{-6}$ esu in 72 transparent crystals (Bloembergen, 1970). The variation of χ^{NL} in all these crystals is three orders of magnitude. In the quest to find materials with large nonlinear susceptibilities, Miller's δ can be a useful parameter for estimating the magnitude of the nonlinear susceptibilities once the linear susceptibilities are known.

One major purpose of this thesis is the investigation of Miller's delta for III-V and II-VI semiconductors. In particular, the dispersion of Miller's delta is examined in the absorbing region of these semiconductors.

In summary, this thesis deals with the nonlinear optical spectroscopy of semiconductors using a tunable dye laser from $.7\mu$ to 1.1μ. Dispersion of the nonlinear susceptibilities was found to exist and cannot, in all cases, be directly correlated to the dispersion of the linear susceptibility. This thesis also derives the correct formulation for the nonlinear reflection from a uniaxial crystal. A new technique for measuring the relative phase between the nonlinear coefficients of wurtzite materials is also presented.

Chapter 2

The Experimental Apparatus

2.1 The Tunable Radiation Source

The tunable radiation source for all the nonlinear experiments reported in this work was a liquid dye laser. In 1966 P. P. Sorokin and J. R. Lankard first observed stimulated emission from an organic dye, Chloro Aluminum Phthalocyanine (Sorokin and Lankard, 1966). Since then the class of organic dyes that have been made to lase is extensive. Continuously tunable laser emission has been observed from $.37\mu$ to 1.1μ .

Dye lasers can be pumped by flashlamps (Sorokin, Lankard, Moruzzi, and Hammond, 1967) or other lasers (Sorokin, Lankard, Hammond, and Moruzzi, 1967). The class of dyes that can be flashlamp pumped is smaller than that of laser pumped dyes. This is due to the high lasing threshold for some dyes and the possibility of excited state absorption (SLMH, 1967). The dye laser used in this thesis was pumped by a passively Q switched ruby laser ($Al_2O_3:Cr^{+3}$) at $.694\mu$. The geometric arrangement is shown in Figure 2.1. This is called off-axis logitudinal geometry (Bradley, Gale, Moore and Smith, 1968). There are several advantages of this geometry over transverse geometry, where the incident pump direction and the dye lasing direction are orthogonal: i) smaller beam divergences and ii) higher pumping efficiencies (SLHM, 1967).

The ruby laser beam (3/8" diameter) was either focused or not focused. Focusing into the dye cell was used when attempting to lase high threshold dyes.

2.2 The Ruby Laser

The ruby laser was a Spacerays Model 101-5PS. The power supply was capable of delivering 4000 joules at 4000 VDC. The linear xenon flashlamp (FX-47C) had a pulse duration of approximately 500 microseconds, which matched the ruby fluorescence lifetime. The ruby rod was 3/8" in diameter and was 6" long. Both the rod and the lamp were water cooled by using a closed cycle temperture controlled circulator (Neslab Model HX-75) running at 15° C and at 5 gal/min. The plane parallel ends of the ruby rod and the silvered elliptical cavity were both purged with standard nitrogen gas flowing at a rate of 7 ml/min.

The laser cavity was formed by a 100% plane flat dielectric reflector and a sapphire etalon of about 20% reflectivity at .69 μ.

To achieve a Q-switch ruby pulse (spoiling the optical feedback until a large inverted population has been achieved) a liquid bleachable absorber (Sorokin, Luzzi, Lankard, and Pettit, 1964) was used. This absorber was placed in a 1 mm path length absorption cell, which was inserted between the 100% reflector and the ruby rod. The cell contained a mixture of nitrobenzene and vanadyl phthalocyanine whose concentration was adjusted for 43% transmission at .694 μ. For Q-switch lasers operating at low intensities phthalocyanines have two advantanges over cryptocyanines dyes (Degiorgio and Potenza, 1967). First the phthalocyanine has a lower residual loss at low powers than the cryptocyanine (Hercher, Chu and Stockman, 1968). Second phthalocyanine is less sensitive to ultraviolet light which readily decomposes the cryptocyanines.

Single Q-switch pulses occured when the flashlamp voltage was 2200 ± 25 volts. Larger voltages produced multiple Q-switch pulses while smaller voltages produced no lasing. The Q-switch ruby laser pulse had a full width at half maximum of approximately 35 nanoseconds. The peak power was 3 to 5 Megawatts.

Over a period of weeks the flashlamp voltage would gradually have to be increased. Several factors caused this: i) degradation of the flashlamp; ii) discoloration of the silvered cavity; iii) pitting of the glass envelope of the flashlamp; iv) pitting of the absorption cell; and v) deterioration of the dielectric reflector. Periodically the silvered cavity and the lamp envelope must be cleaned and/or polished with a fine alumina abrasive mixed with distilled water. The dielectric reflector and absorption cell must periodically be changed. The pitting of the absorption cell is not due to dust or dirt on the surface, as it was placed in a dust proof box and continously purged with nitrogen gas. Pitting perhaps occurs due to impurities in the glass itself. If the phthalocyanine concentration was raised higher than already indicated, Q-switch pulses of much higher energy (> 10 MW) would be produced. This would pit the cell within one or two pulses.

To ensure single pulse operation with repeatable and identical pulses it was observed that overall physical rigidity was the single most important factor. The lamp, rod, mirrors, and Q-switch cell should all be tightly clamped to a common base plate.

2.3 The Dye Laser Material

The polymethine dyes used for lasers in this work were all reported previously (Miyazoe and Maeda, 1968). The dyes, typically in powder form, were all dissolved in dimethyl sulfoxide (commonly referred to as DMSO). DMSO has been reported (SLHM, 1967) to be the best "host" solvent for the polymethine dyes.

The dyes used lased from .72μ to 1.02μ (see Appendix A). The dyes were all contained in standard absorption cells of one to five centimeters in length.

It has been reported (Miyazoe and Maeda, 1970) that these dyes decompose quite readily upon irradiation with white light. The author verified this effect which was more pronounced with some dyes than with others. Decomposition occured in room light, while much less decomposition was noted when irradiated only with ruby light. Thus a Corning CS-2-64 filter was inserted between the dye cell and the ruby laser to prevent the broadband light of the flash-lamp from reaching the dye cell. Excess dye solution could be preserved in a refrigerator for several days before noticable decrease in a dyes lasing efficiency was observed.

2.4 The Dye Laser Cavity

The optical cavity of the dye laser is shown in Figure 2.1. For a given dye the optical amplification takes place over a broad frequency range centered near the dye fluorescence peak (SLHM, 1967). Spectral narrowing is achieved by inserting a grating in a Littrow geometry in place of the usual 100% rear reflector (Soffer and McFarland, 1967). Laser linewidth of less than 1 Å was achieved.

The optical feedback for the dye laser consists of an etalon element as the front reflector and a grating as the rear reflector.

The etalon element was made by Laser Optics. It had a reflectivity of 66% over a broad wavelength range. This element was mounted in a Oriel Optics presision laser mirror mount (B-44-66). The grating was a standard plane Bausch and Lomb grating used in a littrow geometry. It was placed in an Oriel Optics presision laser mirror mount also. The peak reflectivity of the grating was about 80% at the blazed wavelength. Two different gratings were used, one blazed at 1.0μ and the other blazed at $.75\mu$. Both gratings had 1200 lines/mm and were 35X35 mm^2.

The typical dye laser pulse intensity was 3 MW with a pulse duration of 10 to 50 nanoseconds. The conversion efficiencies from the ruby laser to the dye laser could be as high as 30%. The dye laser beam diameter varied from 3/8" to 3/16" depending upon wavelength and whether the ruby beam was focused. The dye laser beam divergence was less than 5 mr in all cases.

2.5 The Optics

The output beam of the dye laser, see Figure 2.2, was sampled by a glass slide. The light reflected from this slide was directed to a 1/4 meter Jarrell-Ash spectrometer and a photodiode (E.G.&G. #SGD-100). This spectrometer was used to determine the dye laser wavelength within ±5 A. The main portion of the output beam was vertically polarized by a Glan Thompson prism (Karl Lambrecht #GLS-D√-12) and then apertured through an iris diaphram of 3/16" diameter.

It has been observed (Miller and Savage, 1962; Armstrong and Ducuing, 1963) that there lacks a one-to-one correlation between the amplitudes of the fundamental and the corresponding second harmonic radiations. This has been attributed to the many modes which exist in the fundamental beam. It has been shown experimentally (Ducuing and Bloembergen, 1964) that the harmonic intensity correlation between two samples irradiated from a single source was excellent. In this work the fundamental intensity was monitored by the amount of second harmonic a z-cut quartz platelet produced. Only a small portion of the fundamental beam, reflected from the front face of a dove prism, was incident on the quartz platelet. This produced a reference second harmonic (Miller, 1964). A dove prism was used instead of a glass slide so as to eliminate possible interference effects. Interference effects in the reflected beam can be caused by reflections from both the front and rear susrfaces of the glass slide. A Corning CS-2-64 red filter was used before the quartz to supress any ultraviolet frequencies that might have been present in the dye laser beam.

The major portion of the dye laser beam passed through the dove prism, a Corning CS-2-64 filter and onto the sample to be studied. Second harmonic light generated from the sample was then measured either by reflection or transmission. The reflection geometry is shown in Figure 2.2.

It is necessary to use selective optical filters to isolate the weak second harmonic light from that of the more intense fundamental. Estimating 10^{15} to 10^{17} photons in the fundamental dye laser beam and 10^{-12} second harmonic conversion efficiency, it is readily seen that the optical filter one must use needs to absorb 10^{17} fundamental photons while transmitting 10^{3} (or less) second harmonic photons. In addition, due to the high intensity of the fundamental light, this filter should not exibit "optical bleaching".

A 2" long cell of aqueous solution of copper sulfate transmits less than 10^{-17} from .694 to 1.02μ and was used as the optical filter (see Appendix B for filters for other wavelength ranges). This cell was made from bakalite tubing. Its windows were of fused quartz two inches in diameter. These windows afford good transmission of ultraviolet light necessary for the measurement of the second harmonic. Since the liquid used in these filters is quite corrosive, no metal was used in their construction. Care was used in selecting the glue necessary to bind the supersil and the bakalite. No optical bleaching of the $CuSO_4$ was ever observed.

To provide further optical isolation a 1/4 meter Jarrell-Ash spectrometer was used after the $CuSO_4$ cell in both the sample and quartz beams.

2.6 Photon Detection and Display

Second harmonic radiation reached the phototubes through the exit holes of the spectrometers. The phototubes used were EMI 9635 QD photomultipliers. These tubes had a somewhat modified S-20 like response. The quantum efficiency of these tubes is about 30% at .38μ but drops off rapidly at wavelengths longer than .5μ. The quantum efficiency is approximately 1% at .6μ. The quantum efficiency remains high towards the ultraviolet (better than 20% to 1800 A).

Both EMI 9635 QD have a 5 cm quartz (Spectrosil) end window and 13 venetian blind CsSb dynodes. The "test ticket" for both tubes indicates an overall sensitivity of 2000 A/L at 1120 volts, a cathode sensitivity of 60 A/L and a dark current of about 1 nanoampere.

In order to increase the dynamic range, the phototubes were operated at 900 VDC. The gain at this voltage was found to be approximately $3X10^6$.

Two precautions were taken to reduce the dark noise; i) maintaining the photomultipliers at room temperture and, ii) magnetic masking of the cathode surface.

It was observed that the current flowing through the dynode chain and the electronics within the photomultiplier housing caused heating. This increased the dark current. To solve the heating problem, the tube was purged with nitrogen at room temperture.

The second harmonic radiation impinges on only a small area in the center of the photocathode. The thermionic electrons are generated uniformly over the entire photocathode. To spatially filter the thermionic electrons, a magnetic defocusing technique is used (Knight, Kohanazahed, and Legyel, 1968). The magnetic field was produced by two axially poled toroidal ferrite magnets (EMI#MFA) placed close to the photocathode surface (3/8"). The magnetic field produced is normal to the photocathode surface near the center of the surface and is highly divergent near the circumference. Electrons emitted near the center of the cathode travel relatively unhindered to the first dynode. However, the electrons emitted outside the central area have little probability of reaching the first dynode.

The close proximity of the toroid to the photocathode (at

-900 V) demands that the torriod be raised to this potential also. A brass washer-like spacer raised to -900 V was placed between the toroid and the photocathode.

The photomultiplier dynode chain was wired as is shown in Figure 2.3. This chain was designed for high current pulse applications as is seen by the capacitors and larger resistors in the last 3 dynode stages. The capacitors maintain a constant voltage drop throughout the pulse duration. The larger resistors were used to minimize space charge effects caused by the large number of secendary electrons between the last few dynodes.

The output voltage of the photomultiplier tubes (50Ω terminated) could be displayed on a dual trace oscilliscope. The transient event could then be captured on polaroid film. Noting that second harmonic signals are weak, a large number of such pictures would have to be taken to obtain a true signal level. One recalls that the signal to noise ratio (S/N) for a photomultiplier is:

$$S/N = \sqrt{n}$$

where n is the total number of photoelectrons emitted from the photocathode. In this work, the minimum acceptable S/N was about 5. For most data points, the data was accumulated until a S/N ratio of better than 50 was obtained. This would have necessitated using large amounts of film and an extraordinary amount of time for data reduction, particularly if 50-100 individual pulses were necessary to obtain good S/N.

To remove accumulative errors caused by measuring polaroid pictures and to preserve the authors sanity a "pulse amplitude encoder" was designed and built here at Yale (see Appendix C). This unit replaced both the dual trace oscilloscope and the need to record transient events on polaroid film.

The output of both photomultiplier tubes was connected to a capacitor whose value was determined by both the gain and linearity of the phototubes. The voltage across this capacitor was proportional to the integrated light intensity. The "pulse amplitude encoder" sampled and measured the voltage across this capacitor. To decrease dark current noise, the capacitors were only allowed to charge when the second harmonic radiations were expected to arrive at the photocathodes. These capacitor voltages were converted from an analog to a digital form and then displayed on nixie tube readouts. The digital results could also be accumulated in a small semiconductor memory. Each new digital result was then automatically added to the previous results. After a sufficient number of accumulated photoelectrons (typically $2.5X10^4$), the results from both the sample and reference were recorded. Their ratio represents the strength of the second harmonic of the sample relative to quartz. Using a known standard in the sample channel then calabrated the quartz reference channel.

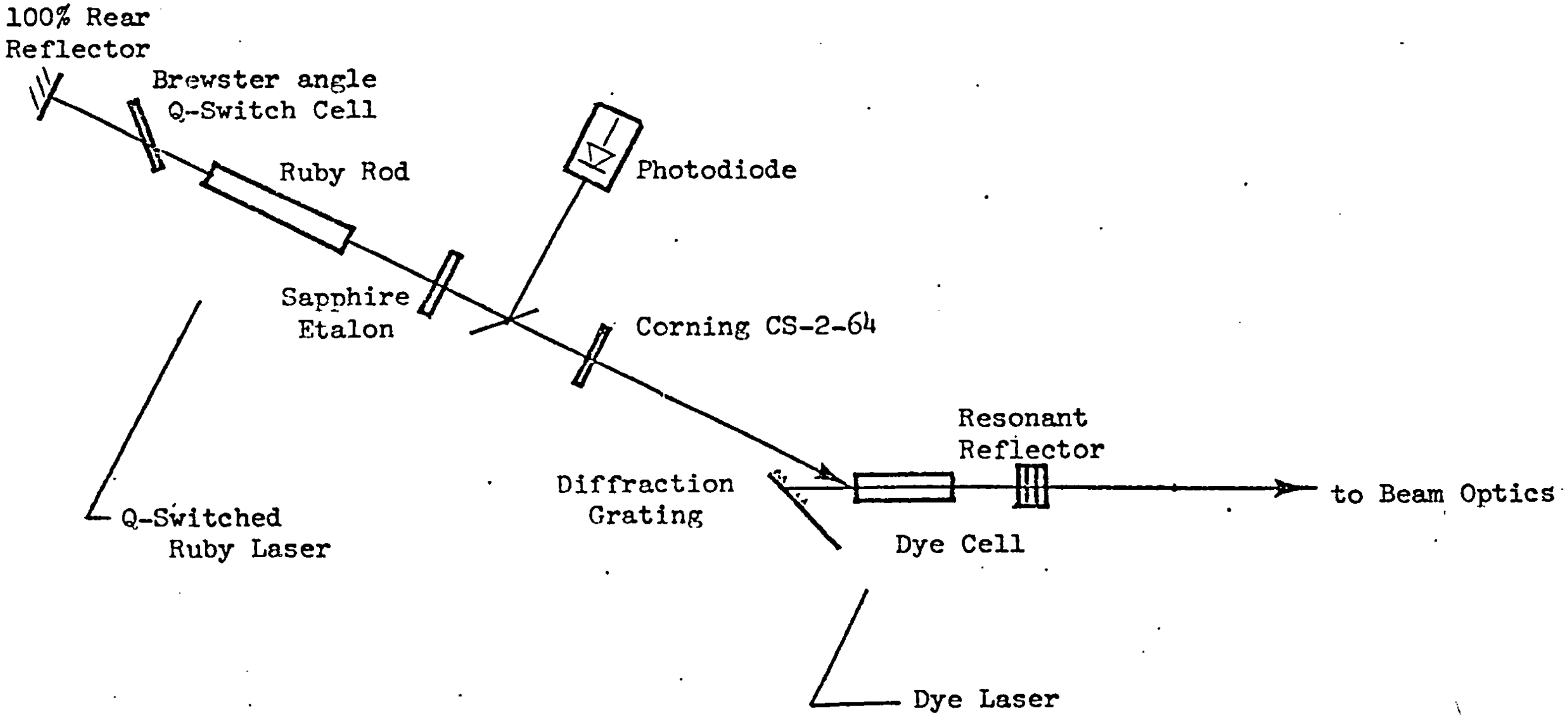

Figure 2.1

The Ruby and Dye Laser System

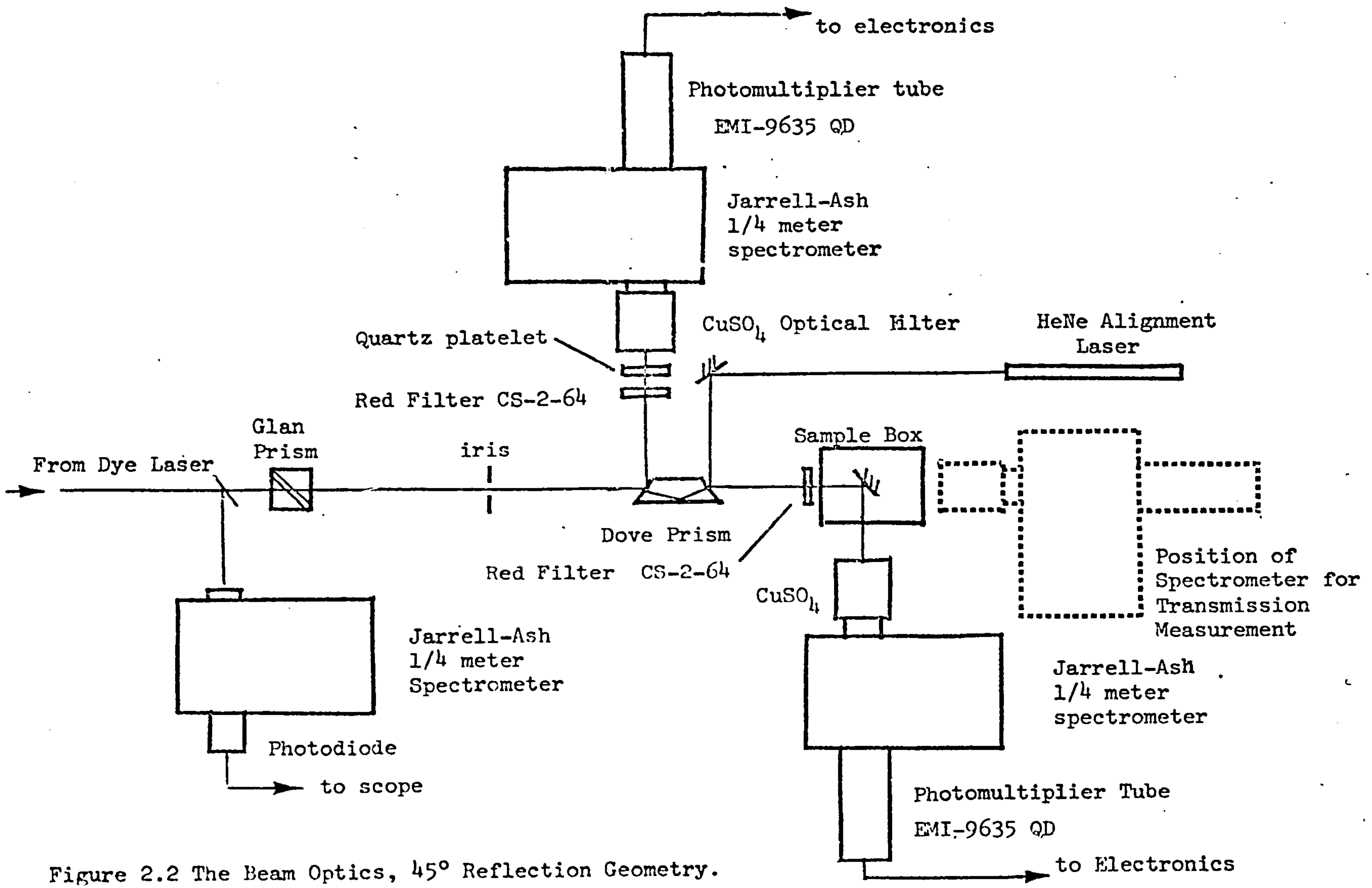

Figure 2.2 The Beam Optics, 45° Reflection Geometry.

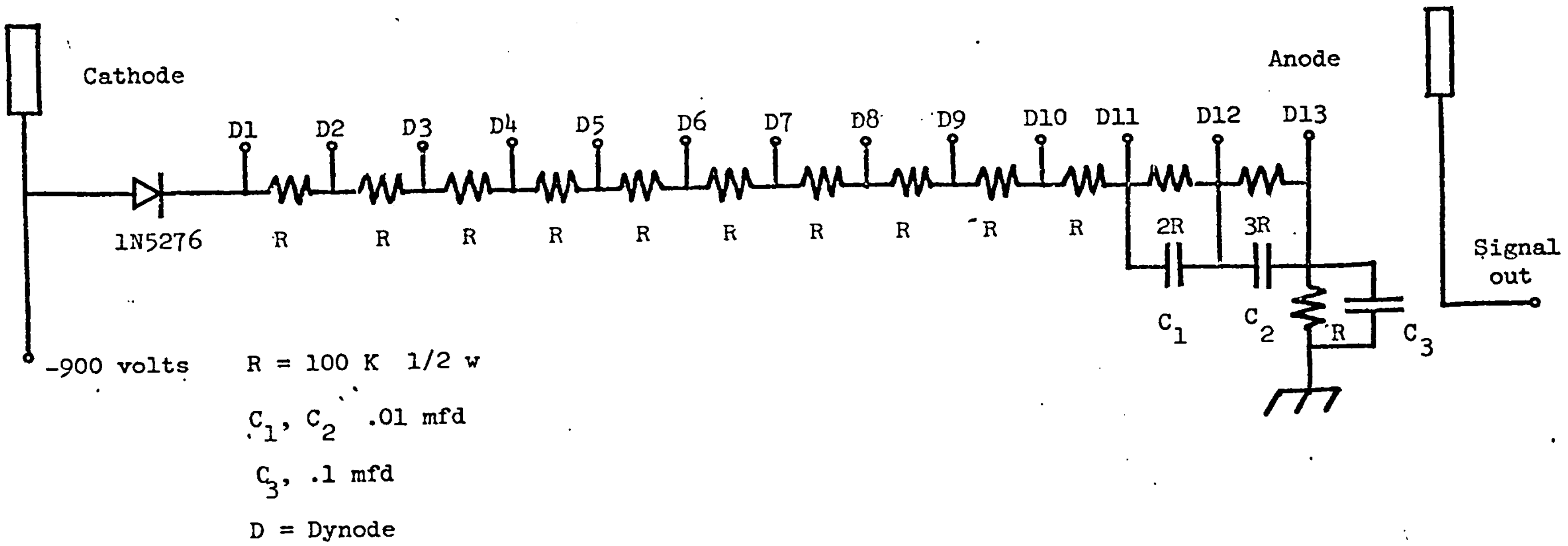

Figure 2.3

EMI-9635 QD PMT Cathode-Dynodes-Anode Wiring Diagram

Chapter 3

Dispersion of the Nonlinear Susceptibility Modulus of Semiconductors with the Zinc-Blende Structure

3.1 Introduction

In 1962 it was predicted (Bloembergen and Pershan, 1962) that second harmonic light is generated in the reflected direction from a piezoelectric crystal. Experimental verification came in 1963 (Ducuing and Bloembergen, 1963). Several experiments than followed (Bloembergen and Ducuing, 1963; Chang and Bloembergen, 1966) which verified the postulates of nonlinear reflection as set forth by Bloembergen and Pershan.

Experiments measuring the second harmonic intensity in the reflected direction provided a convenient and more precise way to determine the nonlinear susceptibility modulus $|\chi^{NL}|$. For crystals in the absorbing range, it was observed (Bloembergen, Chang, Ducuing and Lallemand, 1964) that the error in the measurement of $|\chi^{NL}|$ by a transmission experiment was much larger than the corresponding error from a reflection measurement. This was due to the larger influence played by the linear absorption in the transmission experiments than in the reflection experiments.

The early reflection experiments not only confirmed the theory of Bloembergen and Pershan but also verified that the reflected second harmonic obeyed the bulk crystal symmetry (see Section 3.5).

The measurement, by reflection, of $|\chi^{NL}|$ belonging to several zinc-blende semiconductors at several discrete frequencies was first reported in 1965 (Chang, Ducuing and Bloembergen, 1965). Nine different discrete frequencies were used and spanned 1.17 to 2.34 eV. The lowest photon energy being generated by a Nd doped glass laser, while the highest by doubling the Nd laser frequency with a KDP crystal. Intermediate frequencies were produced by a ruby laser and stimulated Raman lines from various organic fluids.

This chapter describes the measurement of $|\chi^{NL}|$ from 1.21 to 1.7 eV for five zinc-blende materials GaAs, InAs, InSb, InP and ZnTe. The dye laser provided the tunable source (see Chapter 2). Consequently, a more comprehensive sweep of photon energies could be obtained than could be obtained in the earlier experiment. Beam focusing and diverging effects, sources of error (see Section 3.5 and 3.6) when using stimulated Raman radiation, were not present in this work. Thus the values of the nonlinear susceptibility modulus $\left|\chi^{NL}\right|$ obtained in this work were believed to be more precise than those already reported (Chang, Ducuing and Bloembergen, 1965).

3.2 The Nonlinear Dielectric Tensor

Before discussing the laws of reflection and the experimental procedure for the zinc-blende measurements one must specify exactly what quantities we are measuring.

It has been mentioned (see Chapter 1) that the generalized nonlinear dielectric tensor contains 27 components which then, through the use of the piezoelectric contraction, reduce to 18. Any further reduction of the number of components must be achieved by considering the specific crystal symmetry involved. The tensor to describe second harmonic generation is the same as for piezoelectric tensors (Yariv, 1967).

The zinc-blende crystals all belong to the point group $\bar{4}3m$. Therefore symmetry considerations would predict only three tensor components χ_{14}, χ_{25}, and χ_{36}.

$$\chi^{NL} = \begin{bmatrix} \cdot & \cdot & \cdot & \chi_{14} & \cdot & \cdot \\ \cdot & \cdot & \cdot & \cdot & \chi_{25} & \cdot \\ \cdot & \cdot & \cdot & \cdot & \cdot & \chi_{36} \end{bmatrix}$$

with $\chi_{14} = \chi_{25} = \chi_{36}$.

These tensor components give rise to three components of nonlinear polarization:

eq. 3.1
$$\begin{aligned} P_x^{NLS}(2\omega) &= \chi_{14}\, E_y(\omega)\, E_z(\omega) \\ P_y^{NLS}(2\omega) &= \chi_{25}\, E_x(\omega)\, E_z(\omega) \\ P_z^{NLS}(2\omega) &= \chi_{36}\, E_x(\omega)\, E_y(\omega) \quad . \end{aligned}$$

where $E_x(\omega)$, $E_y(\omega)$, $E_z(\omega)$ are the electric fields of the fundamental radiation along the x, y, and z crystalline axes, respectively.

Thus fundamental radiation polarized along x, y, or z would ideally give rise to no second harmonic generation. This is a form of a "selection rule" for the zinc-blende materials. In the experiments described in this chapter, incident light was always polarized along a $(1\bar{1}0)$ axis thus giving rise to a nonlinear polarization along a (001) axis.

3.3 The Theory of the Nonlinear Susceptibility Dispersion

Early work in the treatment of the nonlinear optical susceptibility started with an application of second order perturbation theory (Armstrong, Bloembergen, Ducuing and Pershan, 1962; Loudon, 1962; and Butcher & McLean, 1963). The perturbation hamiltonian was assumed to take on the form:

eq. 3.2
$$\mathcal{H} = \sum_{\substack{\text{All}\\ \text{electrons}\\ k}}' \left(-\frac{e}{mc} A_k \cdot p_k + \frac{e^2}{2mc} A_k \cdot A_k \right)$$

where A_k was the vector potential of the applied field. Then the expectation value of the electron current density was calculated:

eq. 3.3 $$\sum_{\substack{\text{electrons}\\ k}} (\rho V_k)_{gg} = \sum_{k} \langle g \mid \frac{e}{m} p_k - \frac{e^2}{mc} A_k \mid g \rangle$$

where $|g\rangle$ was the perturbed ground state wavefunction.

The terms containing the second harmonic time dependence were then extracted. The results were used to evaluate the second order polarization of localized electrons which were then related to the nonlinear polarization source term P^{NLS} (see Section 3.4). The P^{NLS} is the driving term necessary to produce macroscopic inhomogeneous plane waves.

Kelly (Kelly, 1963 A,B) expanded this concept with the assumption that the electromagnetic wave at the fundamental frequency interacts with Bloch electrons. The nonlocal character of the Bloch electrons was taken into account and the frequency dependent part of the nonlinear response was evaluated for the three band model. Kelly also noted that the product of matrix elements in his expression for the nonlinear susceptibility would vanish if parity were a good quantum number.

Kelly's expression could be reduced (Bloembergen, Chang, and Ducuing, 1966) to the following form:

eq. 3.4 $$\chi_{14}^{NL.} = A \lim_{\mathrm{Im}\,\omega \to 0} \sum_{nn'} \int d^3k \; f(E_n, k) \left[\frac{\overset{(1)}{Q}_{n'n}(k)}{\omega^2 - \omega_{n'n}^2} + \frac{\overset{(2)}{Q}_{n'n}(k)}{4\omega^2 - \omega_{n'n}} \right]$$

where:
$$Q^{(1)}_{n'n} = \sum_{n''} \mathrm{Im}\left(p_{nn'}(k)\, p_{n'n''}(k)\, p_{n''n}(k)\right) \frac{\omega_{n''n} - 2\omega_{n'n}}{(\omega_{n'n} + \omega_{n''n})(\omega_{n'n} - 2\omega_{n''n})}$$

$$Q^{(2)}_{nn'} = 4\sum_{n''} \mathrm{Im}\left(p_{nn'}(k)\, p_{n'n''}(k)\, p_{n''n}(k)\right) \frac{1}{\omega_{n'n} - 2\omega_{n''n}}$$

and
$$p_{nn'}(K) = \int_{uc} d^3r\, u^{*}_{nk}(r)\, i\hbar\nabla\, u_{nk}(r)$$

The $\omega_{nn'}$ refer to differences in energy between the n and n' bands. $f(E_n,k)$ is the Fermi-Dirac distribution function.

It was noted (Chang, Ducuing, and Bloembergen, 1965) that an enhancement in χ^{NL} may occur near critical points in the joint density of states $\nabla(\omega_n - \omega_{n'}) = 0$ at ω or 2ω. This kind of enhancement also occurs in the linear susceptibility. It was noted that the momentum matrix elements in the linear susceptibility were inherently different from those in the nonlinear expression. The expression for the linear susceptibility is (Chang, Ducuing and Bloembergen, 1965):

eq. 3.5
$$\chi^{L}(2\omega) = B \lim_{\mathrm{Im}\,\omega \to 0} \sum_{n'n} \int d^3k\, \frac{f(E_n,k)\, |p_{nn'}(k)|^2}{\omega_{nn'}\,(4\omega^2 - \omega^2_{nn'})}$$

The $p_{nn'}(k)^{2}$ are slowly varing functions of k (Brust, 1964). A study of the nonlinear susceptibility dispersion would determine whether the $p_{nn'}(k)p_{n'n''}(k)p_{n''n}(k)$ were likewise so. It might not be expected since each $p_{nn'}(k)$ can have its own sign and phase for various points in the Brillouin zone.

An attempt at the calculation of the nonlinear susceptibility dispersion (Bell, 1969) was made by assuming the triple product of p(k) was constant, The results indicated that although the momentum matrix products were assumed constant, the nonlinear susceptibility could "behave quite differently" from the linear susceptibility. This was attributed to contributions of opposite signs from the imaginary part of the p(k) matrix elements at different points in the Brillouin zone (see Section 3.6).

In a more recent paper Bell (Bell, 1971) has fitted the experimental data of this work (Parsons and Chang, 1971) for InAs (see Section 3.6). A set of three bands, approximated with a model which has been used sucessfully in calculations of the linear susceptibility, were chosen to provide the interband transitions. The momentum matrix element product was again chosen to be constant. A sucessful agreement with experiment was achieved with InAs. In this paper Bell also calculated the dispersion of Miller's δ.

Miller's δ ,mentioned in Chapter 1, is defined as:

eq. 3.6
$$\delta_{ijk} = \frac{\chi^{NL}_{ijk}}{\chi^{L}_{ii}(2\omega)\,\chi^{L}_{jj}(\omega)\,\chi_{kk}(\omega)}$$

where $\chi^{L}(\omega)$ and $\chi^{L}(2\omega)$ are the linear susceptibilities at ω and 2ω, respectively. It was found to have a weaker frequency dependence than the nonlinear susceptibility itself.

Recently other theoretical contributions have been made which are relevant in the nonabsorbing region (Levine, 1969,70; Phillips and Van Vechten, 1969). These contributions use the dielectric-theory of electronegativity (Phillips, 1968 A,B). Calculations of the nonlinear susceptibility were done on a number of zinc-blende and wurtzite semiconductors.

The calculation of Phillips and Van Vechten describes the nonlinear susceptibility in terms of bonding and antibonding wave-functions. It predicts ratios for three nonlinear susceptibilities in wurtzite semiconductors (see Chapters 4 and 5) as well as the magnitude of χ^{NL} in zinc-blende materials. It should be emphasized though that these calculations were applicable only when ω and 2ω are not absorbed in the semiconductor.

The calculation of Levine used a localized-bond picture. A geometric factor was used to provide the correction factors necessary for differently structured semiconductors. The factor was identical in concept to the one used by Robinson (Robinson, 1968) when he discussed ratios among various nonlinear susceptibilities in wurtzite and zinc-blende semiconductors. (see Chapters 4 and 5).

3.4 The Laws of Reflection and Transmission in Zinc-Blende and ADP

In order to link $|\chi^{NL}|$ to the observed second harmonic intensity, the laws of reflection at the boundary of an isotropic nonmagnetic medium must be examined. This has been treated throughly by Bloembergen and Pershan.

When intense light impinges on the surface of a media which lacks inversion symmetry, a polarization at twice the original frequency develops. This macroscopic nonlinear polarization then drives the medium at the second harmonic. The general wave equation at this new frequency for a nonmagnetic isotropic material is:

eq. 3.7 $$\nabla\times(\nabla\times\bar{E}(2\omega)) - \frac{(2\omega)^2}{c^2}\epsilon(2\omega)\,\bar{E}(2\omega) = 4\pi\left(\frac{2\omega}{c}\right)^2\bar{P}^{NLS}$$

where $$\bar{P}^{NLS}(2\omega) = \chi^{NL}\,\bar{E}_0(\omega)\,\bar{E}_0(\omega)$$

and $\bar{E}_0(\omega)$ is the electric field of the incident light inside the medium and $\bar{P}^{NLS}(2\omega)$ was defined in equation 3.1.

The general solution to equation 3.7 consists of the general solution to the homogeneous equation and a particular solution to the inhomogeneous equation. These solutions must satisfy the boundary conditions of the problem. The boundary conditions are, from electromagnetics, that both the tangential components of $E(2\omega)$ and $H(2\omega)$ be continous across the boundary. To satisfy this an electromagnetic wave at the second harmonic must propagate outside the medium. Bloembergen and Pershan point out that this wave exists even though the crystal is strongly absorbing at the fundamental and/or the second harmonic. An early experiment (Ducuing and Bloembergen, 1963) showed that this was indeed the case and that the nonlinear polarization emanated from the bulk of the crystal. Bulk symmetry properties were observed. This ruled out the possibility that the observations were totally surface dependent and had nothing to do with the bulk of the medium.

For all zinc-blende crystals reported in this work the crystallographic orientation was chosen as is pictured in Figure 3.1.

The electric field reflected at the second harmonic frequency for the orientation shown in Figure 3.1 is (Bloembergen and Pershan, 1962):

eq. 3.8
$$\bar{E}_R(2\omega) = \frac{4\pi |P^{NLS}(2\omega)| \sin\theta_S \sin\theta_T \sin(\alpha + \theta_T + \theta_S)}{\sin\theta_R \sin(\theta_T + \theta_S) \sin(\theta_T + \theta_R) \cos(\theta_T - \theta_R)}$$

where: $P^{NLS}(2\omega)$ is the quantity described in equation 3.1

θ_R is the angle of incidence of the fundamental beam

$$\sin\theta_S = \frac{1}{\sqrt{\epsilon(\omega)}} \sin\theta_R$$

$$\sin\theta_T = \frac{1}{\sqrt{\epsilon(2\omega)}} \sin\theta_R$$

and α is the angle between the direction of propagation of the linear fundamental refracted beam and the $\bar{P}^{NLS}(2\omega)$.

The second harmonic radiates in the plane of reflection.

At 45° angle of incidence used in all the experiments with the zinc-blende in this work the formula reduces to:

eq. 3.9 $$E_R(2\omega) = \frac{16\sqrt{2}\sqrt{2\epsilon_2 - 1}\;|\chi_{14}^{ZB}|\;\pi\;E^2(\omega)}{\left(\sqrt{2\epsilon_2 - 1} + \sqrt{2\epsilon_1 - 1}\right)\left(\sqrt{2\epsilon_1 - 1} + 1\right)^2\left(\sqrt{2\epsilon_2 - 1} + 1\right)^2}$$

where ϵ_1 is the complex dielectric constant at the fundamental frequency and ϵ_2 is the complex dielectric constant at the second harmonic. $E(\omega)$ is the electric field of the fundamental wave outside the medium.

If one now compares the reflected second harmonic intensity generated from the zinc-blende material to that of some known standard the relative value of $|\chi_{14}|$ can be converted to an absolute value.

In order to obtain a absolute value of the nonlinear susceptibility of a zinc blende material a standard of ADP was used.

When measuring the nonlinear coefficient of a transparent crystal such as ADP, it is not advisable to use the reflection technique. The much larger second harmonic built up within the bulk due to possible phase matching, may be reflected from its rear surface. This may interfere with the reflected second harmonic generated from the front surface of the crystal. This could lead to a large error in the intensity measurement. ADP is a transparent crystal and thus its second harmonic was measured by transmission.

The technique of accomplishing this will now be discussed.

ADP is a uniaxial crystal with 42m symmetry. This requires that the nonlinear dielectric tensor have three elements:

$$\chi^{NL} = \begin{bmatrix} \cdot & \cdot & \cdot & \chi_{14} & \cdot & \cdot \\ \cdot & \cdot & \cdot & \cdot & \chi_{25} & \cdot \\ \cdot & \cdot & \cdot & \cdot & \cdot & \chi_{36} \end{bmatrix}$$

and $\chi_{14} = \chi_{25}$.

Kleinman's conjecture (Kleinman, 1962) also requires that $\chi_{25} = \chi_{36}$.

The orientation for second harmonic generation chosen is shown in Figure 3.2. The nonlinear polarization is also horizontal as it was for the zinc-blende materials. This orientation was chosen so that the differences in transmission due to polarization effects in the 1/4 meter spectrometer need not be of concern.

Measurement of the second harmonic intensity from ADP was accomplished by the "Maker Fringe" technique (Jerphagnon and Kurtz, 1970). Bloembergen and Pershan have derived the general form for the transmitted intensity of the second harmonic light from a plane parallel plate such as the ADP crystal used. The equation describes the "Maker Fringes" that occur as the effective crystal thickness is varied by tilting the crystal plate. The intensity of the second harmonic is found to oscillate as a function of thickness. This is due to the interference between the inhomogeneous and homogeneous harmonic waves.

This tilting also causes a decrease in the intensity of the second harmonic due to linear Fresnel corrections.

For near normal incidence, Bloembergen and Pershan's formula for the transmitted intensity from a nonlinear plate can be reduced to:

eq. 3.10 $$E_T^{ADP}(2\omega) = \frac{4\pi[P^{NLS}(2\omega)](n_o+1)}{(n_e-n_o)(n_e+n_o)}$$

where n_e is the extraordinary index of refraction of ADP at 2ω, n_o is the ordinary index of refraction at ω, and $P^{NLS}(2\omega)$ is the nonlinear source polarization. For the orientation shown in Figure 3.2 it is defined by:

eq. 3.11 $$P^{NLS}(2\omega) = \frac{\chi_{36}^{ADP} E_o^2(\omega)}{2}$$

where $E_o(\omega)$ is the electric field <u>inside</u> the media. Adding the necessary linear Fresnel losses to Bloembergen and Pershan's formula one obtains:

eq 3.12 $$E_T(2\omega) = \frac{8\pi\chi_{36}^{ADP} E^2(\omega)}{(n_e^2-n_o^2)(n_o+1)}$$

where $E(\omega)$ is the incident electric field <u>outside</u> the medium.

The second harmonic intensity is then:

eq 3.13 $$I_T^{ADP}(2\omega) = E_T(2\omega)\,E_T^*(2\omega)$$

The ADP second harmonic intensity was measured by tilting the

ADP about its "c" axis. Interference patterns between the homogeneous and inhomogeneous waves were obtained (Jerphagnon and Kurtz, 1970). The envelope maximum of an interference pattern was taken as $I_T^{ADP}(2\omega)$.

Error can be introduced from the following three main sources: i) the ADP surfaces are not parallel; ii) surface defects on the ADP; and iii) beam divergence in the laser. The ADP sample used was parallel to 10 seconds and the surface was flat to $\lambda/4$. Due to the hydroscopic property of the crystal, it was preserved in a dessicant so as to minimize surface deterioration. Errors due to the surface quality were small. Beam divergence (or convergence) will diminish the peak to valley ratio of the interference pattern. This causes an error in the measurement of $I_T^{ADP}(2\omega)$. Since all the intensity minima approached zero in this work, small beam divergence is inferred. Consequently errors introduced in the ADP intensity measurement due to a nonparallel laser beam were small.

Clearly the Maker fringe technique requires care. Many second harmonic intensity data points as a function of the tilt angle, must be taken to reproduce the interference pattern. In contrast, the zinc-blende material required only one intensity data point.

3.5 Zinc-Blende Experimental Procedure.

3.5.1 The Crystal Surface and its Preparation

It has been discussed that the second harmonic intensity obtained by reflection is linked to the bulk symmetry of the crystal. In order to insure this several precautions were taken.

The crystals were polished as per our instructions with 1μ Linde C, 0.3μ Linde A and 0.1μ Linde B abrasives in that order. This gradual polishing decreased the surface damage depth.

To further remove this damage layer, all crystals were mildly etched. The common etchants were used (Gatos and Lavine, 1963). See Appendix D for the etching solutions and the etching procedure in detail. It should be noted that the amount of etching should be quite small. The surface, if allowed to etch too long, would become "orange peel". This would, while removing the damage layer, produce waves and ripples in the surface which would cause the reflected light to become spatially diffused. Thus the finite aperture of the spectrometer and the uncertainty in the angle of incidence would both lead to a decrease in the intensity of the second harmonic. If however, the crystals were not etched at all, it was discovered that the second harmonic intensity would also be less than its "true" value. It had been reported (Chang and Bloembergen, 1966) that testing the "selection rules" of the reflected second harmonic, the amount of surface damage could be estimated. Fundamental light would be polarized parallel to a (110) axis (allowed) and the second harmonic observed in a (001) direction. This signal would then be compared to the second harmonic emitted when the fundamental was polarized on a (100) axis (forbidden). An arbitrary decision was made that if the allowed to forbidden harmonic intensity ratio was at least 20, one could assume that the effect of the damage layer was small. One was then observing an intensity related to the bulk material.

In order to check further into this rule, it was decided to monitor the second harmonic at 4100 Å as a function of etching time. A sample of GaAs was used. It was observed that the allowed intensity increased with increasing etch time, although the intensity ratio (allowed/forbidden) was better than 20:1 in all cases. The "optimum" etch time (with an allowed/forbidden of 40:1) was somewhat ill defined since the allowed signal leveled off (as a function of etch time) then stayed fixed until the surface became visibly over etched (orange peel). A general decrease in the second harmonic was then observed due to the spatial diffusivity of the beam.

This etch dependency, while perhaps affecting the absolute magnitudes of the intensities, seemed to preserve peaks or structure in the nonlinear susceptibility. This gives one confidence that although the absolute magnitudes of the nonlinear susceptibility may be somewhat in error, their dispersion is certainly being represented.

While an intensity ratio criterion of 40:1 (allowed/forbidden) could be strictly adhered to as a measure of the surface damage, this was not always achievable in practice. Due to the weak signals, sometimes even in the allowed polarization, it was hard to ascertain this ratio. A criterion of >20:1 was used without exception in this work.

3.5.2 The Comparison of GaAs and ADP

Now that the explicit expressions have been obtained connecting the second harmonic intensity generated from both ADP (eq. 3.13) and zinc-blende (eq. 3.9) material, a comparison between the two nonlinear susceptibilities can be made. The modulus of their ratio $\frac{|\chi_{14}^{ZB}|}{|\chi_{36}^{ADP}|}$ can be expressed as:

eq. 3.14
$$\frac{|\chi_{14}^{ZB}|}{|\chi_{36}^{ADP}|} = Y(\epsilon_1, \epsilon_2, n_e, n_o)\sqrt{\frac{I_R^{ZB}(2\omega)}{I_T^{ADP}(2\omega)}}$$

where $Y(\epsilon_1, \epsilon_2, n_e, n_o)$ is given by:

eq. 3.15
$$Y(\epsilon_1, \epsilon_2, n_e, n_o) = \frac{\left(\sqrt{2\epsilon_2-1}+\sqrt{2\epsilon_1-1}\right)\left(\sqrt{2\epsilon_2-1}+1\right)^2\left(\sqrt{2\epsilon_1-1}+1\right)^2}{(n_e^2-n_o^2)(n_o+1)\sqrt{2}\sqrt{2\epsilon_2-1}}$$

as obtained from equations 3.13 and 3.9. ϵ_1, ϵ_2, n_e, and n_o were defined before. $I^{ADP}(2\omega)$ was the transmitted harmonic intensity generated from ADP and $I_R^{ZB}(2\omega)$ was the reflected harmonic intensity generated from the zinc-blende material.

To measure these two intensities, the same spectrometer, photomultiplier, and copper sulfate filter were moved as a unit from the reflection geometry to the transmission geometry (see Figure 2.2). The intensity ratios $\frac{I_R^{ZB}(2\omega)}{I_T^{ADP}(2\omega)}$ obtained in this way were all reproducible to within 5-10%. Care must be used in aligning the dye laser beam with respect to the spectrometer in both geometries.

The factor $Y(\epsilon_1, \epsilon_2, n_e, n_o)$ shown in equation 3.15 was calculated for many zinc-blende crystals by use of a PDP-10 computer. The program provided for, among other things, automatic interpolation of the input dielectric constants. Thus the absolute value of $Y(\epsilon_1, \epsilon_2, n_e, n_o)$ could be calculated at all photon energies of interest (see Appendix E). The $Y(\epsilon_1, \epsilon_2, n_e, n_o)$ are plotted in Figures 3.8 to 3.12.

Clearly, uncertainty in ϵ_1 and ϵ_2 of the various semiconductors (particularly in the region of sharp structure) represents a major source of error in $Y(\epsilon_1, \epsilon_2, n_e, n_o)$ and consequently in the nonlinear susceptibility ratio. For this reason the measured second harmonic intensity ratio for each of the semiconductors is plotted also in Figures 3.8 to 3.12 in the event that more accurate linear dielectric constant becomes available.

The linear dielectric constant data in the wavelength range of interest was obtained from a listing by Seraphin and Bennett) (Seraphin and Bennett, 1967). Plots of the dielectric constants at both the fundamental and second harmonic energies are shown in Figures 3.3 to 3.7. The ADP index of refraction data was obtained from Zernike (Zernike, 1964).

Due to the amount of time consumed and the difficulty in obtaining intensity measurements from the ADP, only the nonlinear susceptibility modulus for GaAs was calibrated to ADP. All other semiconductor measurements were then done by comparison to GaAs. The conversion factor for other zinc-blende (ZB) nonlinear susceptibilities to that of ADP was:

eq. 3.16
$$\frac{|\chi_{14}^{ZB}|}{|\chi_{36}^{ADP}|} = \frac{Y_{ZB}}{Y_{GaAs}} \frac{|\chi_{14}^{GaAs}|}{|\chi_{36}^{ADP}|} \sqrt{\frac{I_R^{ZB}(2\omega)}{I_R^{GaAs}(2\omega)}}$$

where
$$Y_{ZB} = \frac{\left(\sqrt{2\epsilon_2-1}+\sqrt{2\epsilon_1-1}\right)\left(\sqrt{2\epsilon_1-1}+1\right)^2\left(\sqrt{2\epsilon_2-1}+1\right)^2}{2\sqrt{2}\,\sqrt{2\epsilon_2-1}\,(n_o+1)(n_e^2-n_o^2)}$$

and ϵ_1 and ϵ_2 are the complex linear dielectric constants of the zinc-blende material to be measured.

By comparison to GaAs it should be noted that no errors arose from inaccuracies in the GaAs linear dielectric constants. Errors due to the GaAs dielectric constants were canceled in $\frac{|\chi_{14}^{GaAs}|}{|\chi_{36}^{ADP}|}$.

These were the only Fresnel factors, both linear and nonlinear, necessary for the calculation of the nonlinear susceptibility for zinc-blende materials. The results of these measurements will now be presented.

3.6 The Discussion of Experimental Results

The results of the measurements of the nonlinear susceptibility modulus dispersion ratio $\frac{|\chi_{14}|}{|\chi_{36}^{ADP}|}$ for the five zinc-blende type semiconductors are shown in Figures 3.13 to 3.17 for ZnTe, InP InAs, InSb, and GaAs respectively. The magnitudes of the nonlinear susceptibility for all the compounds were normalized with respect to ADP. The nonlinear susceptibility of ADP was assumed constant over the photon energies inspected. The abscissa of the graphs represents the photon energy of the fundamental beam. There are two ordinate axes. One represents the ratio of the modulus of the nonlinear susceptibility of the zinc-blende material to that of ADP. The other represents Miller's δ . The necessary linear dielectric constant data for the computation of Miller's δ was obtained from Figures 3.3 to 3.7.

At first hand the results indicate that there is indeed structure in the modulus of the nonlinear susceptibility as was first noted in 1965 (Chang, Ducuing and Bloembergen, 1965). Comparing the 1965 results to the results of this chapter, we see some discrepancy. This can be attributed to the poor beam divergency in their experiment. As was discussed in Section 3.4, large errors arise in the ADP signal when the beam is not parallel.

Now the new results will be examined to see if additional structure in the nonlinear susceptibility dispersion exists that is not in the linear susceptibility dispersion.

3.6.1 The Nonlinear Susceptibility Dispersion of ZnTe.

In ZnTe (see Figure 3.13) a dramatic increase is observed in the modulus of the nonlinear susceptibility as the absorption of the harmonic photons increases. The fundamental beam is not absorbed in this photon energy region but the absorption of the second harmonic beam increases more than an order of magnitude. (see Figure 3.3). The absorption maximum corresponds to a critical point in the joint density of states at the Λ point of the Brillouin zone (E_1 peak is at 3.6 eV). Consequently only the second term in equation 3.4 dominates.

Miller's δ is suprisingly constant. While it is observed that the nonlinear susceptibility increases almost a factor 5, the Miller's δ increases only a factor 2. This is consistant with Bell's calculation (Bell, 1971) in which he shows that less structure should be observed in Miller's δ than in the nonlinear susceptibility itself.

3.6.2 The Nonlinear Susceptibility Dispersion of InP.

In InP (see Figure 3.14) one also observes an increase in the modulus of the nonlinear susceptibility as the second harmonic energy increases into the absorption region. The fundamental is not absorbed (see Figure 3.4). At 3.2 eV there is a critical point in the joint density of states corresponding to the Λ point in the Brillouin zone (E_1 peak). This critical point is the same one that exists in the second term of equation 3.4. Again this term dominates the expression for the nonlinear susceptibility at 1.6 eV. In addition the nonlinear susceptibility exhibits a peak at about 1.31 eV. This peak might be due to transitions at the fundamental absorption edge (E_o is at 1.34 eV). These have been observed in the linear reflection data (Cardona, 1965). No structure in the $|\chi^{NL}|$ can be attributed to the $E_o+\Delta$ spin orbit split energy (1.43 eV).

Miller's δ shows some variation over the photon energy range pictured. It should be noted that although the nonlinear susceptibilities at 1.3 and 1.6 eV are quite different, the Miller's δ for the two energies are about the same. Miller's δ for the photon energy 1.4 eV is quite small compared to the other two points (1.3 and 1.6 eV). One could postulate that the reason for this is a cancellation of terms in equation 3.4. This could arise from the simultaneous resonance of the first and second terms of equation 3.4. This could also explain the lack of structure at 1.43 eV. The first term of equation 3.4 would be resonant with the fundamental at 1.43 eV and the second term would then be resonant with the second harmonic at 2.9 eV. 2.9 eV is close to a critical point in the joint density of states at 3.12 eV known as the $E_1(1)$ point (Cardona,Shaklee, and Pollack, 1967). This partial cancellation could be the reason for the dip in Miller's δ or in other words, the lack of structure in the nonlinear susceptibility.

3.6.3 The Nonlinear Susceptibility Dispersion of InAs

In InAs (see Figure 3.15) one observes two peaks in the nonlinear susceptibility. In InAs the E_1 peak is at 2.5 eV. and its spin split counterpart at 2.78 eV (Cardona, Shaklee, and Pollack, 1967). It is thus theorized that the two peaks in the nonlinear susceptibility modulus are related to the resonances in the second harmonic with these two critical points. Here again only the second term in equation 3.4 predominates. Bell has (Bell, 1971) calculated the expected dispersion of the modulus of the nonlinear susceptibility and obtained satisfactory agreement with the experimental results.

For InAs Miller's δ seems fairly constant with only small changes in magnitude near the peaks. Bell has shown (Bell, 1971) that these might be expected.

3.6.4 The Nonlinear Susceptibility Dispersion of InSb

In the case of InSb (see Figure 3.16) two peaks are observed. There exists what is known as an $E_1+\Delta$ peak (Cardona, Shaklee and Pollack, 1967) at 2.38 eV. The nonlinear susceptibility modulus of InSb peaks near 1.2 eV, where the second harmonic is resonant to this $E_1+\Delta$ peak. Thus the second term in equation 3.4 dominates. In addition there is an unexplained peak at 1.38 eV. This does not correspond to any known transitions at either 1.38 or 2.76 eV although there is some fine structure near 2.8 eV in the electroreflectance data of Cardona et. al. (Cardona, Shaklee and Pollack, 1967)

Miller's δ for InSb is also shown. There is very little structure but there seems to be a general negative slope as a function of increasing photon energy.

3.6.5 The Nonlinear Susceptibility Dispersion of GaAs.

GaAs (see Figure 3.17) is a rather unique case. The fundamental can be resonant to the E_o transition at 1.43 eV <u>and</u> the second harmonic can be resonant to the $E_1(1)$ transition at 2.89 eV. This might lead to strange behavior of the nonlinear susceptibility. Both terms contribute to the nonlinear susceptibility and cancellation may occur. The absence of a peak in the $|\chi^{NL}|$ data may imply this cancellation. This lack of a peak also contributes to a drop in the value of Miller's δ near 1.4 eV. A peak in the $|\chi^{NL}|$ of GaAs occurs at about 1.3 eV. This could be due to a partial cancellation of the terms mentioned above.

Miller's δ is also shown in Figure 3.18. The reason for the dip has been just postulated. A large peak in δ is observed near 1.3 eV corresponding to the peak in the nonlinear susceptibility.

3.6.6 Concluding Remarks

For each of the above mentioned semiconductors, two facts may be concluded.

First, if one term dominates in equation 3.4 then we can coorelate the structure of χ^{NL} to a critical point in the joint density of states at either ω or 2ω. This was clearly seen in ZnTe, InP, and InAs.

Second, if both terms in equation 3.4 are of comparable amplitude then an interference effect between the two terms can occur. Since the linear susceptibility is not expressible by these terms, the dispersion of χ^{NL} can have different structure than that of the linear susceptibility. Thus, the division of the nonlinear susceptibilities by the linear susceptibilities will not lead to a constant - Miller's δ. In the wavelength region where both terms in equation 3.4 are important, dispersion of Miller's δ is to be expected.

The interference effect is interesting because new information can be obtained from it. As was mentioned in Section 3.3, the quantum mechanical expression for the nonlinear susceptibility (equation 3.4) contains a triple matrix element product. The linear susceptibility expression (equation 3.5) contains only a double matrix product. When both terms contribute to the value of the χ^{NL} expression, its magnitude is sensitive to the value of the triple matrix element product from each of the two terms. Therefore χ^{NL} could provide more information about the electronic band properties, particularly the electronic wavefunctions, than is available from linear susceptibility data alone.

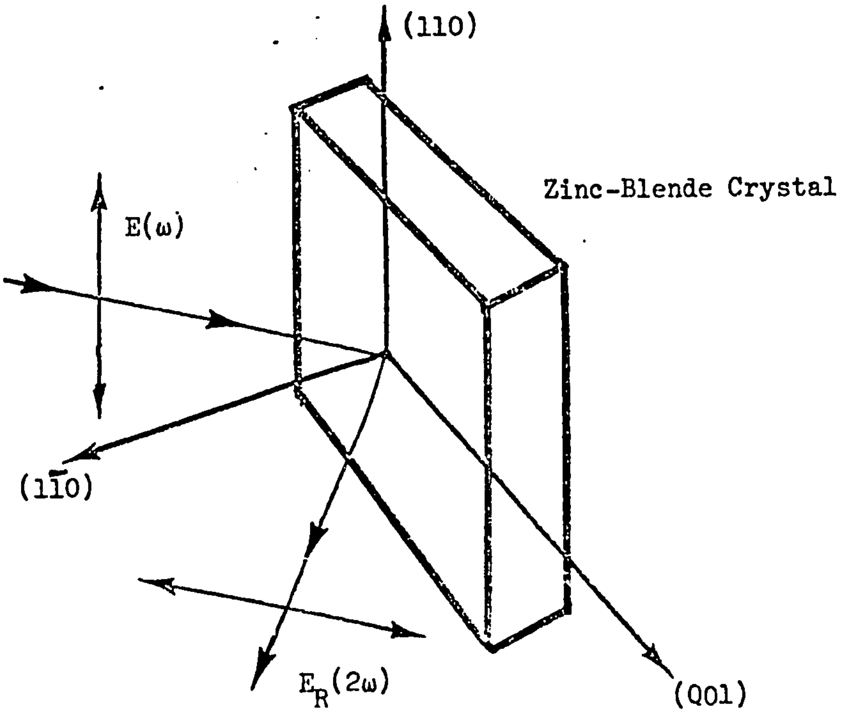

Figure 3.1

The Crystal Orientation Used for the Measurement of the Modulus of the Nonlinear Susceptibility of Zinc-Blende Materials

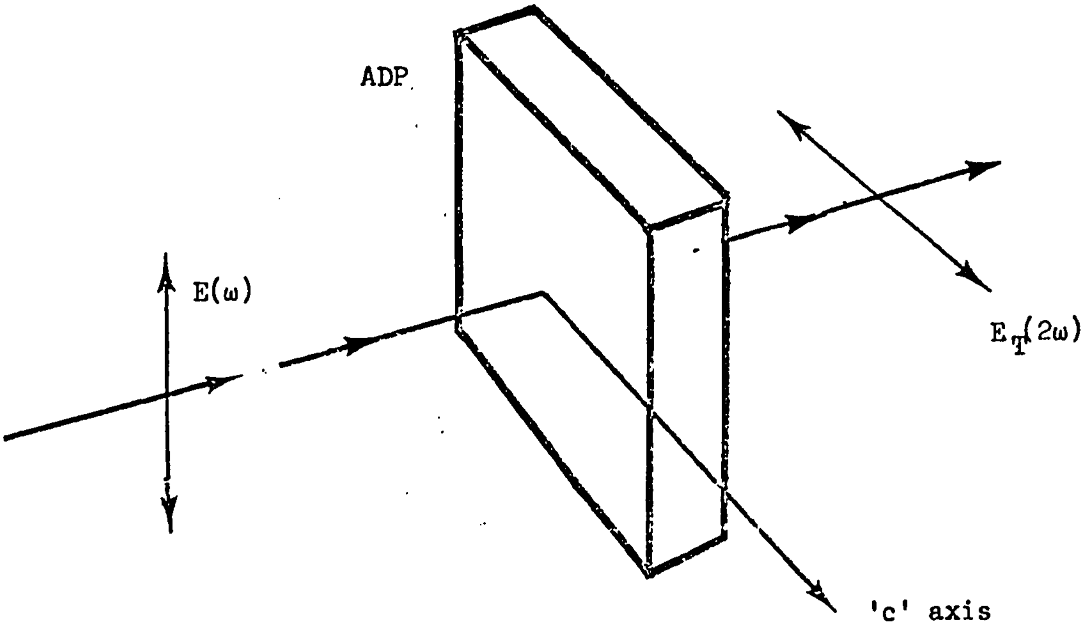

$E_T(2\omega)$ source is $P^{NLS}_{'c'}(2\omega) = \chi_{36}E_x(\omega)E_y(\omega)$

Figure 3.2

The Crystal Orientation and Electric Field Vectors of the ADP Standard.

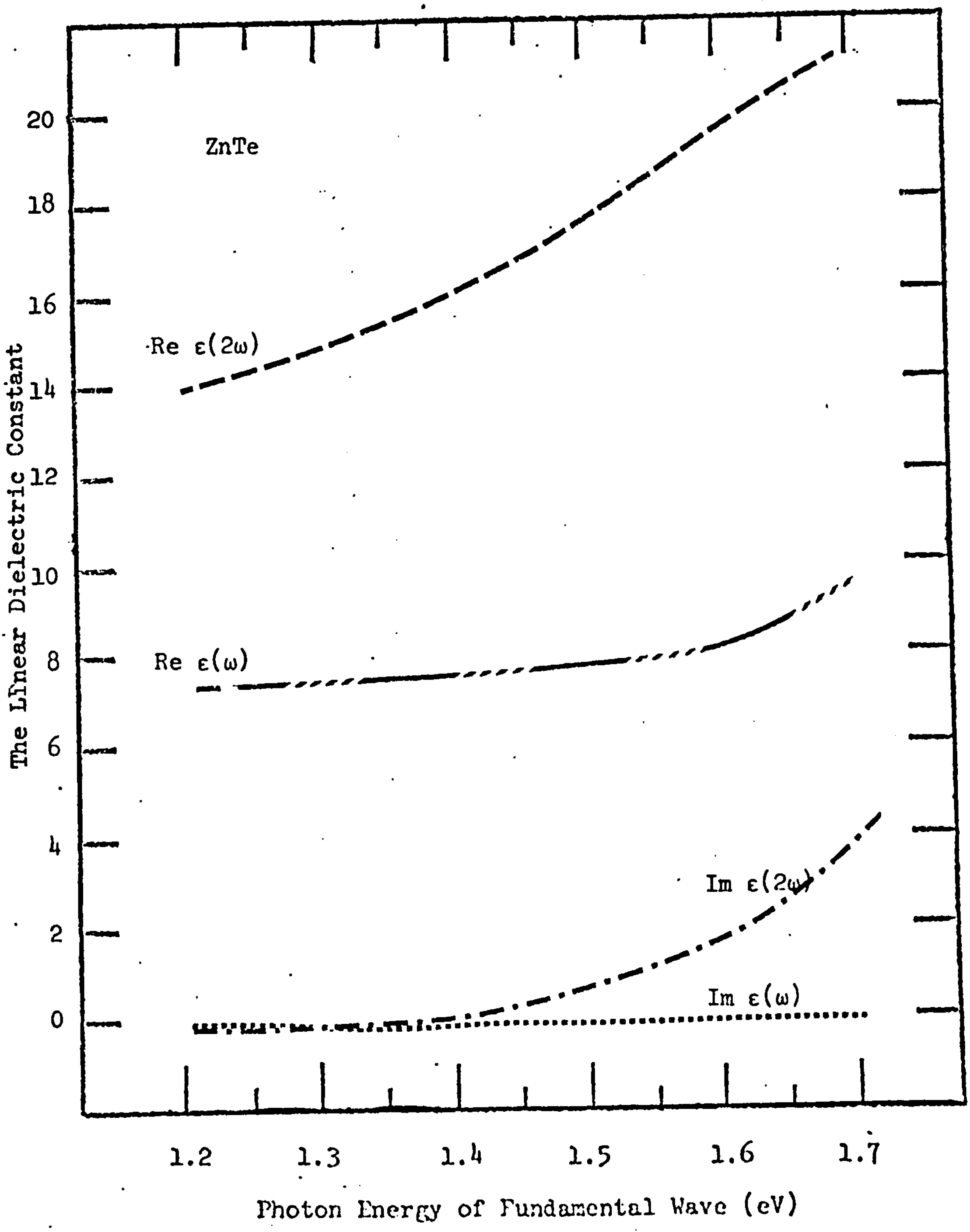

Figure 3.3

The Real and Imaginary Parts of the Linear Dielectric Constants of ZnTe at the Fundamental and Second Harmonic Frequencies.

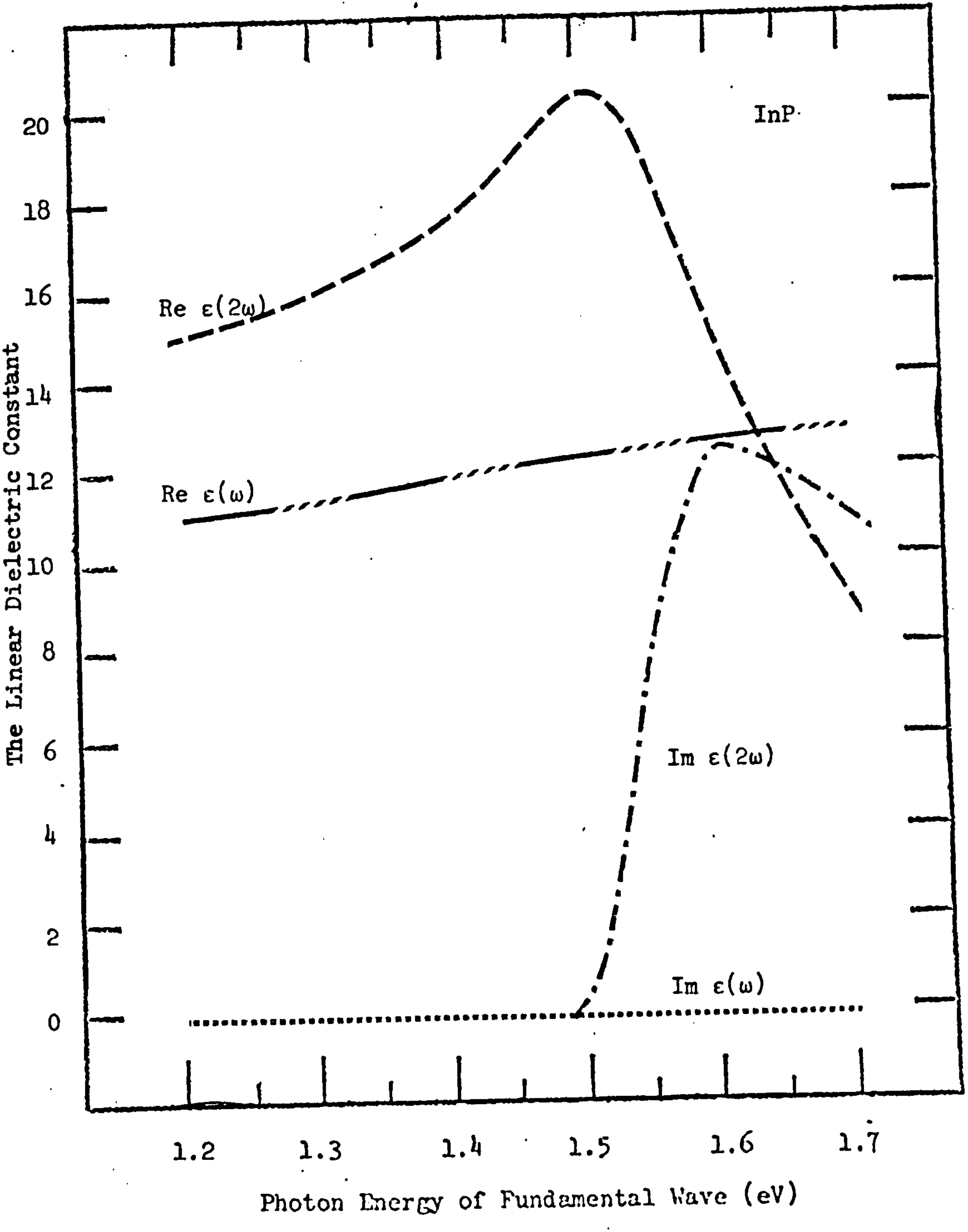

Figure 3.4

The Real and Imaginary Parts of the Linear Dielectric Constants of InP at the Fundamental and Second Harmonic Frequencies.

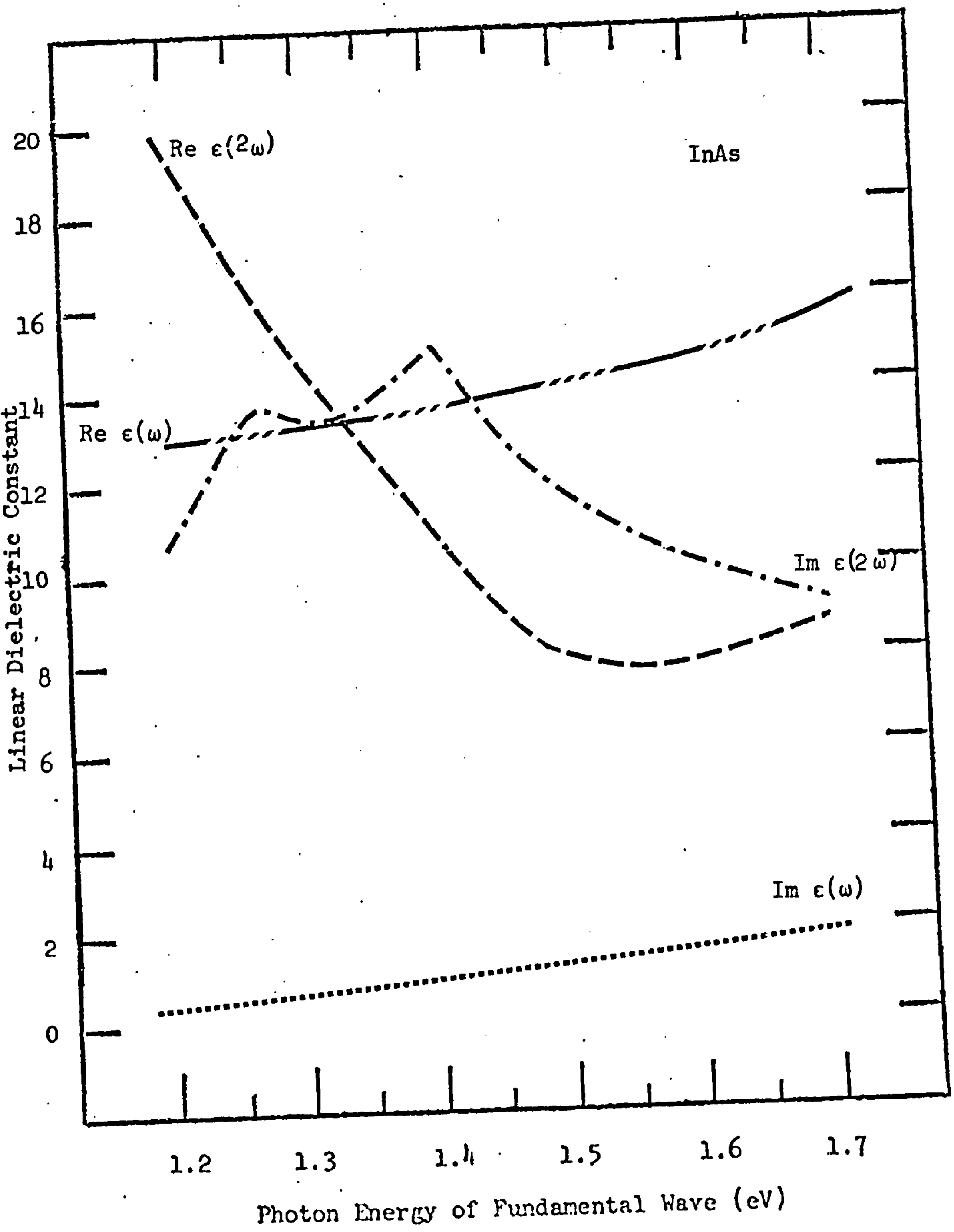

Figure 3.5

The Real and the Imaginary Parts of the Dielectric Constants of InAs at the Fundamental and Second Harmonic Frequencies.

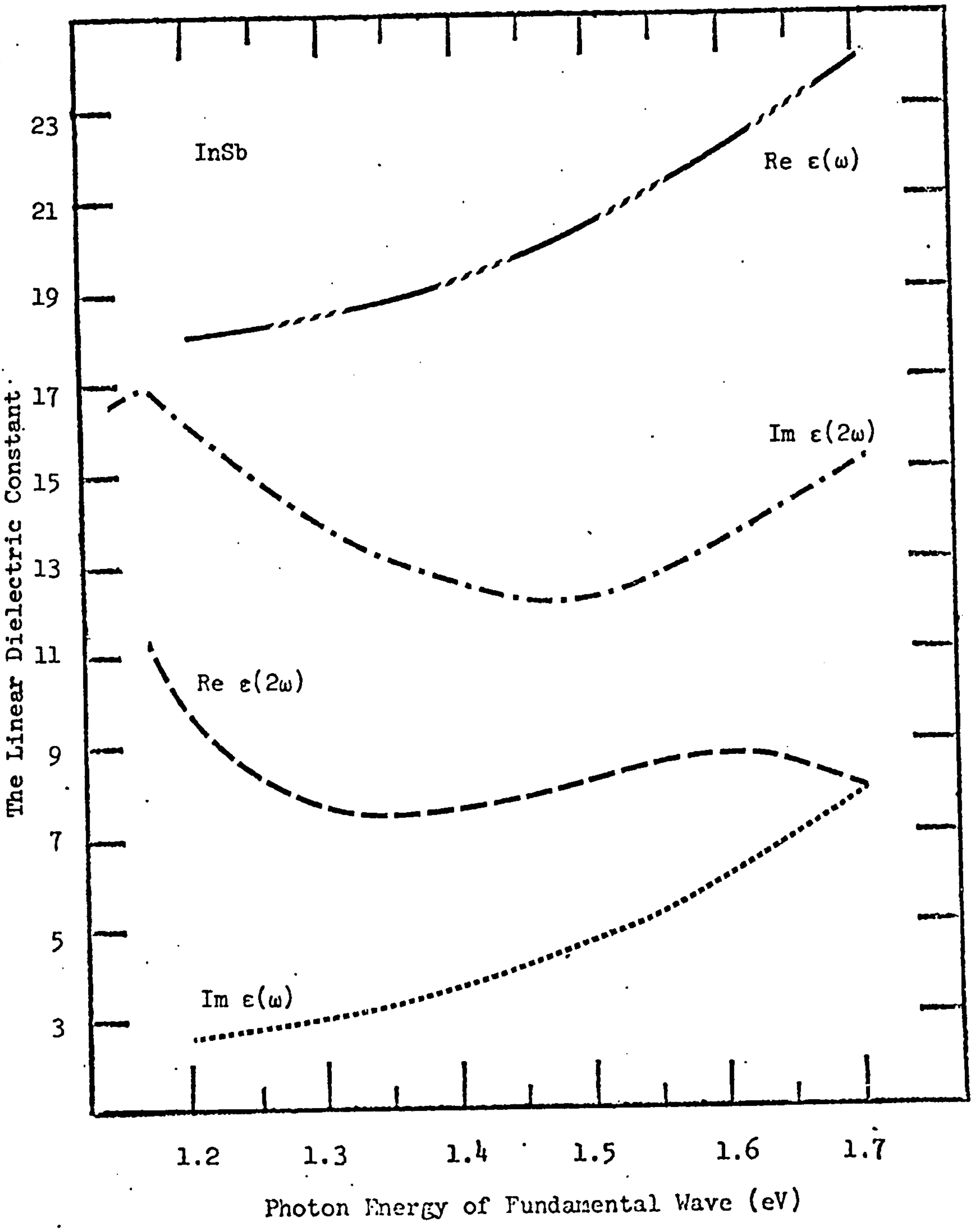

Figure 3.6

The Real and Imaginary Parts of the Linear Dielectric Constants of InSb at the Fundamental and Second Harmonic Frequencies.

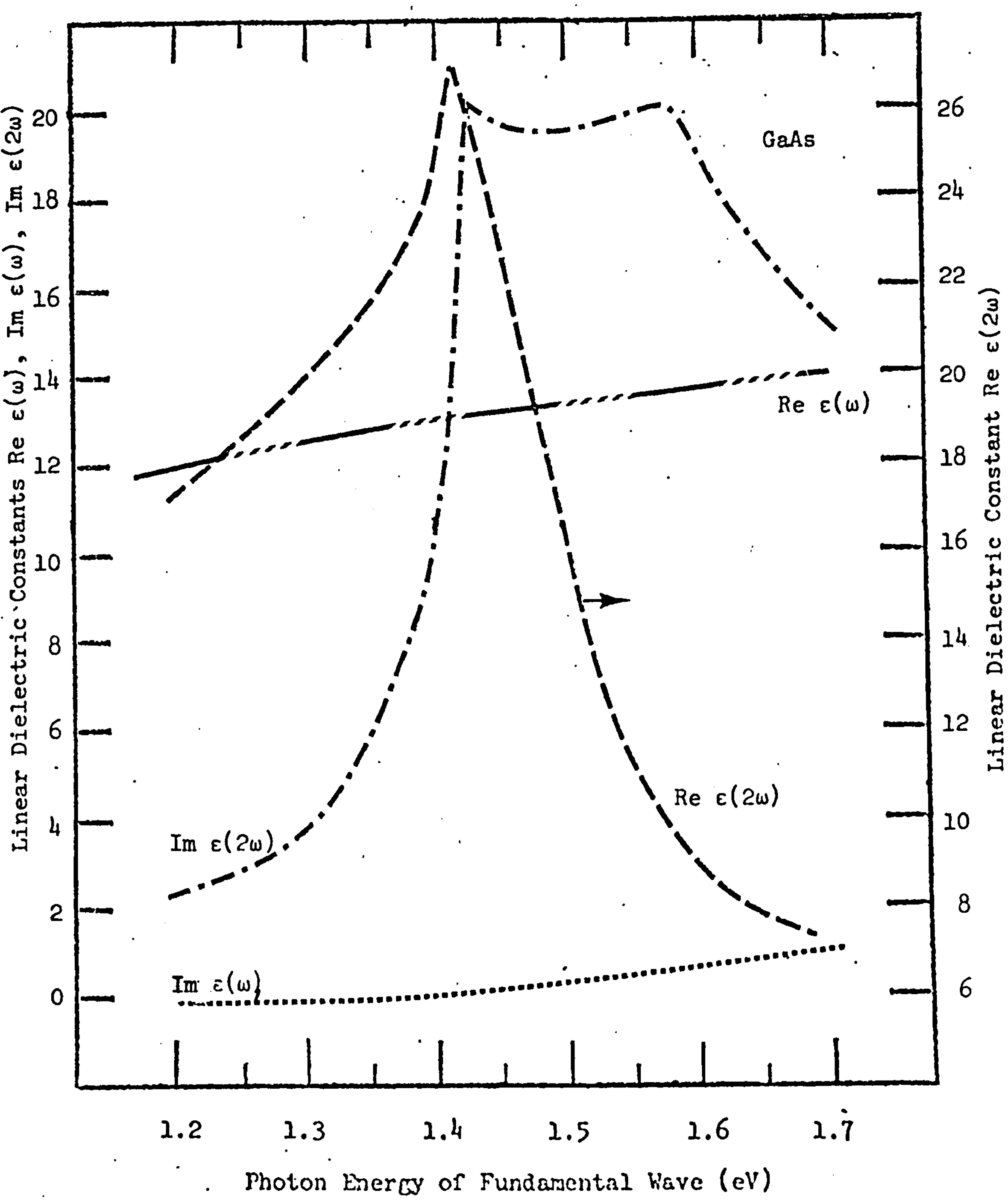

Figure 3.7

The Real and the Imaginary Parts of the Linear Dielectric Constants of GaAs at the Fundamental and Second Harmonic Frequencies.

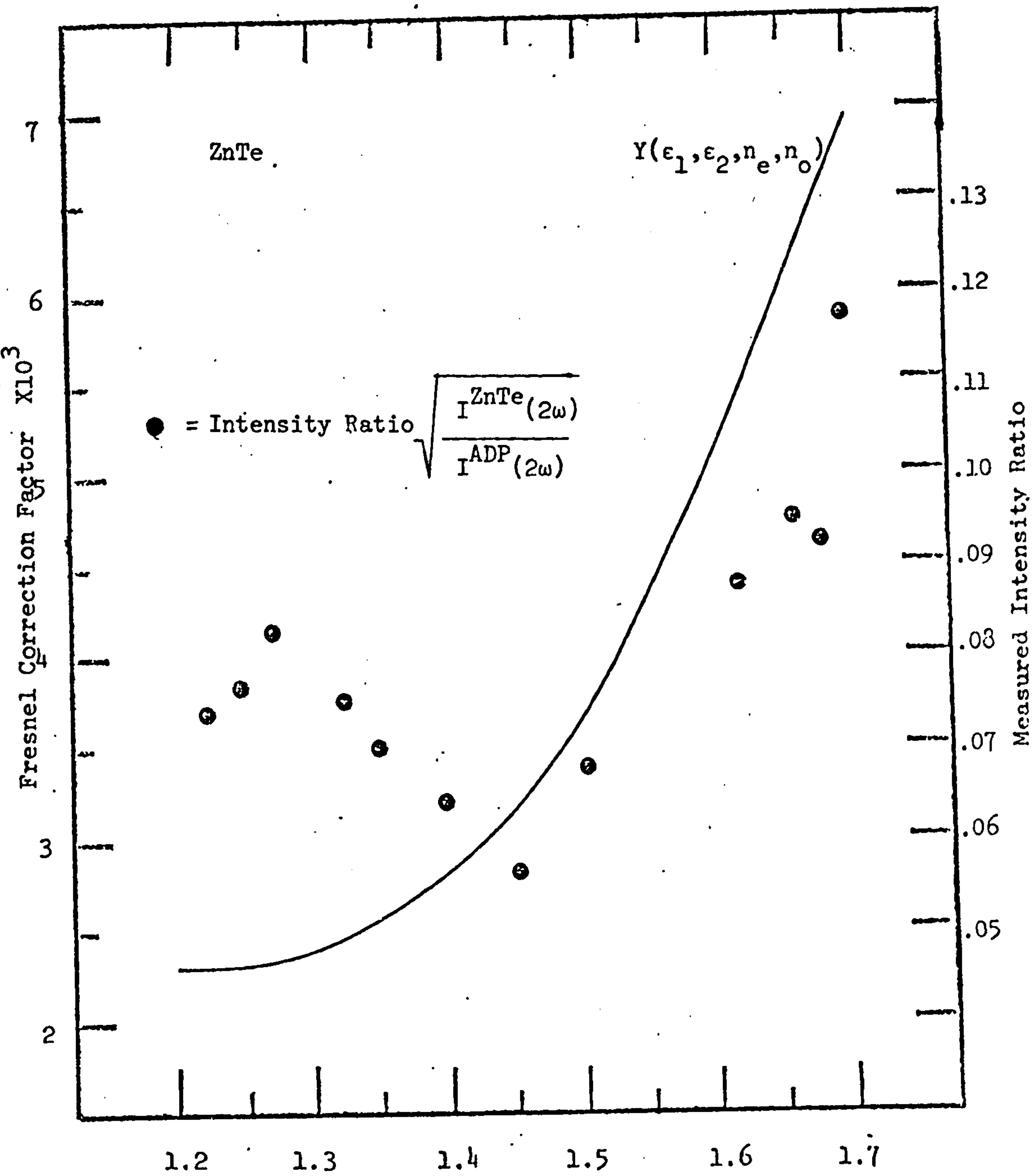

Figure 3.8

The Fresnel Correction Factor (see text) and the Measured Intensity Ratio as a Function of Photon Energy, ZnTe.

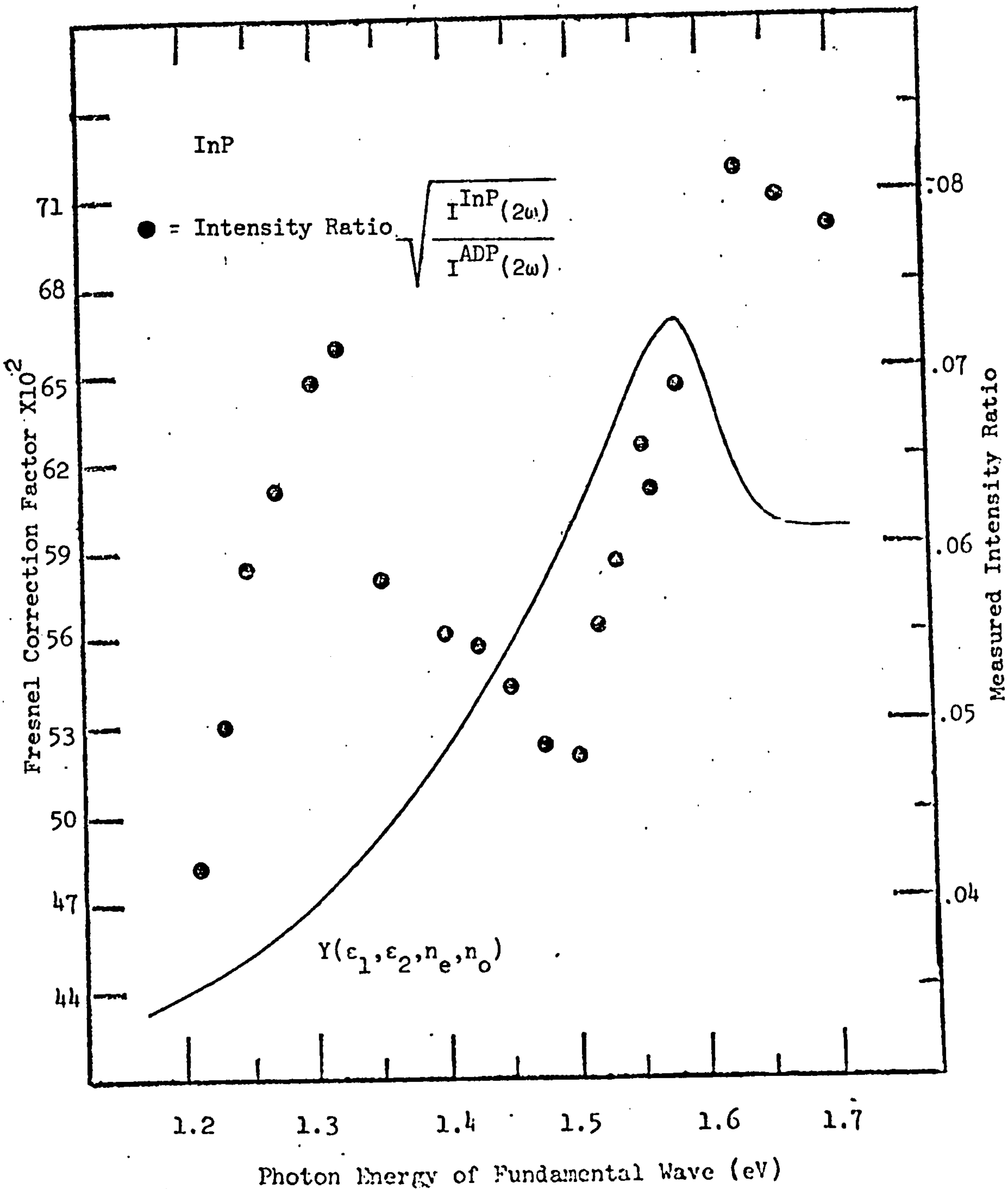

Figure 3.9

The Fresnel Correction Factor (see text) and the Measured Intensity Ratio as a Function of Photon Energy, InP.

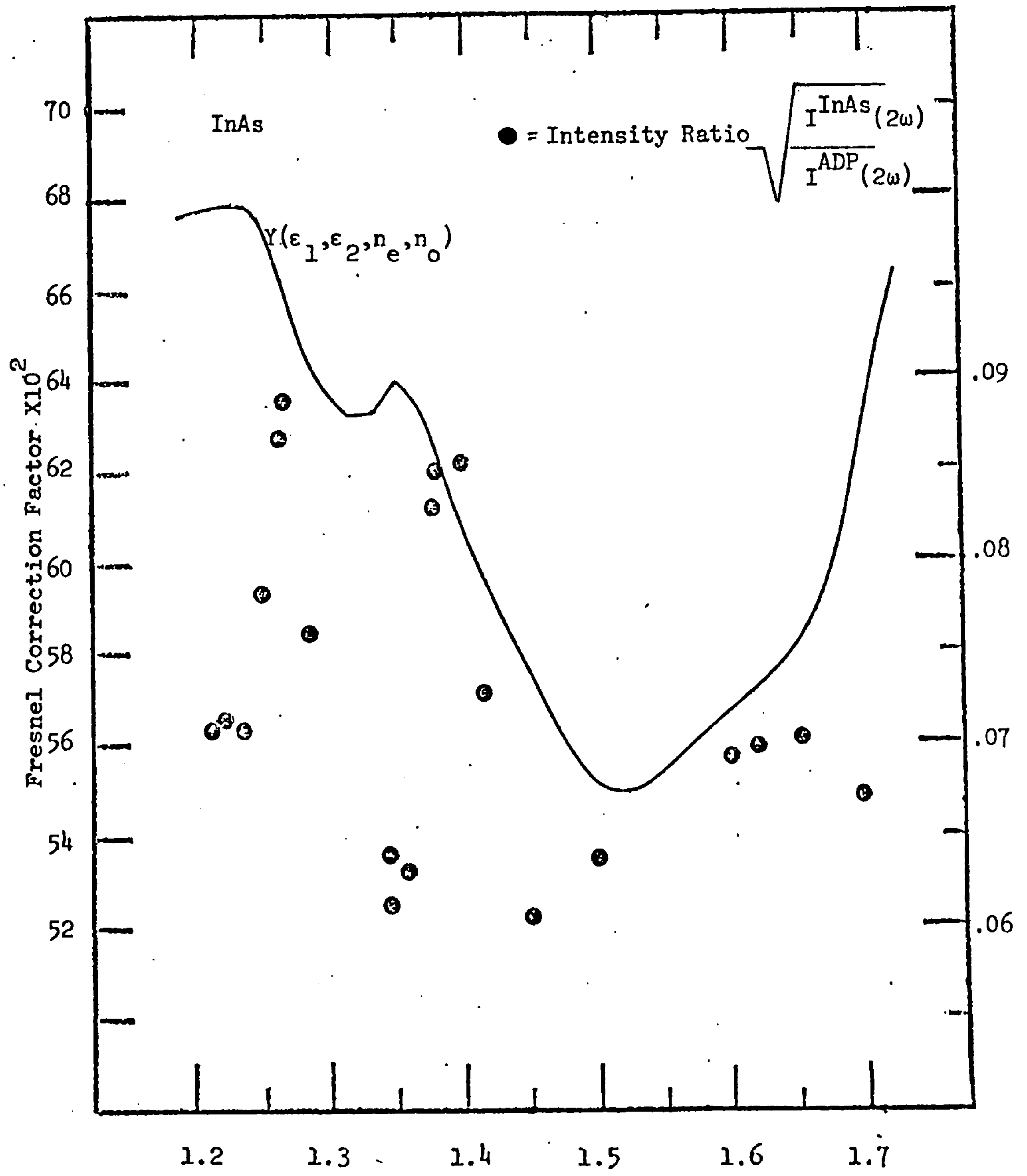

Figure 3.10

The Fresnel Correction Factor (see text) and the Measured Intensity Ratio as a Function of Photon Energy, InAs.

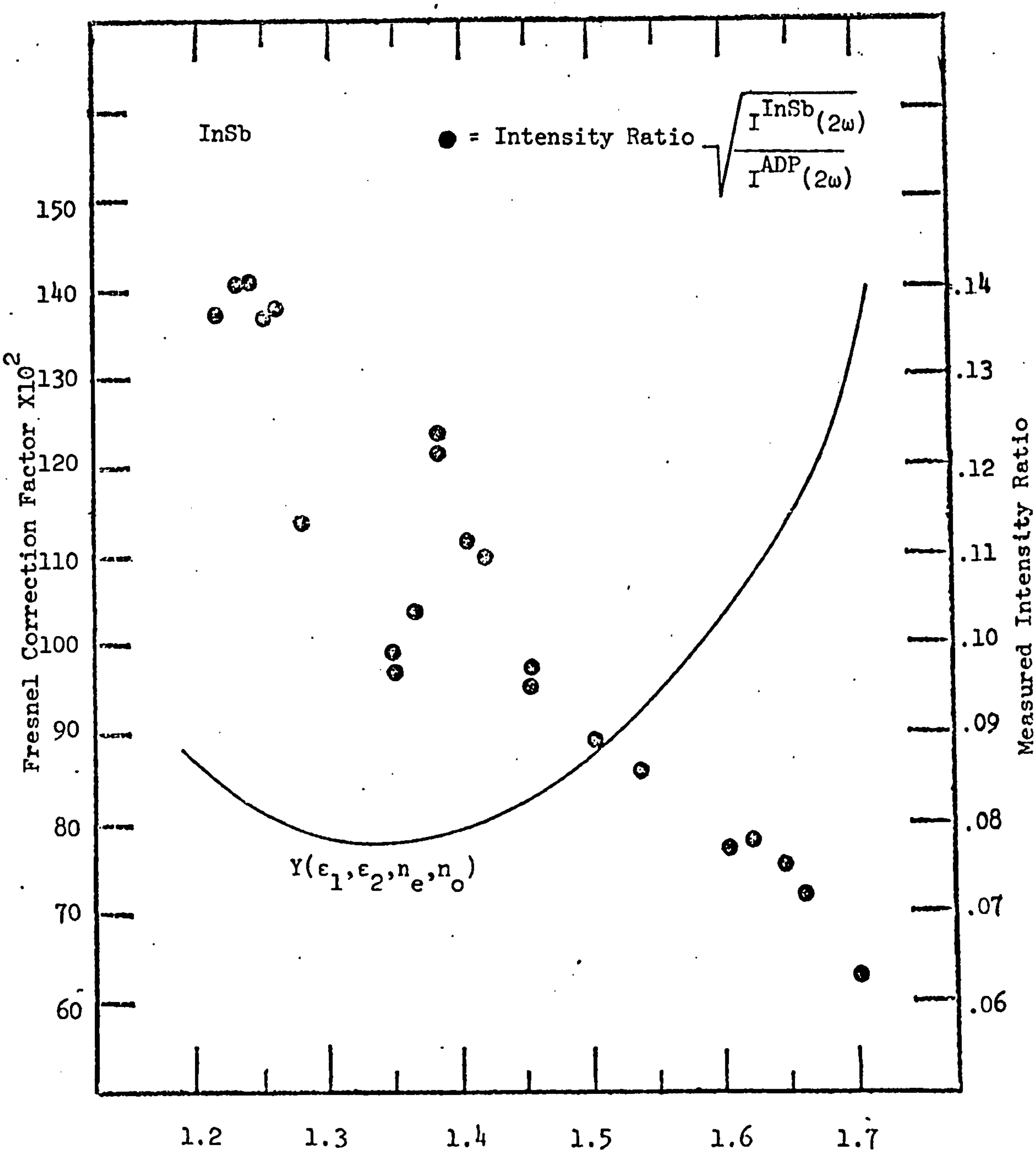

Figure 3.11

The Fresnel Correction Factor (see text) and the Measured Intensity Ratio as a Function of Photon Energy, InSb.

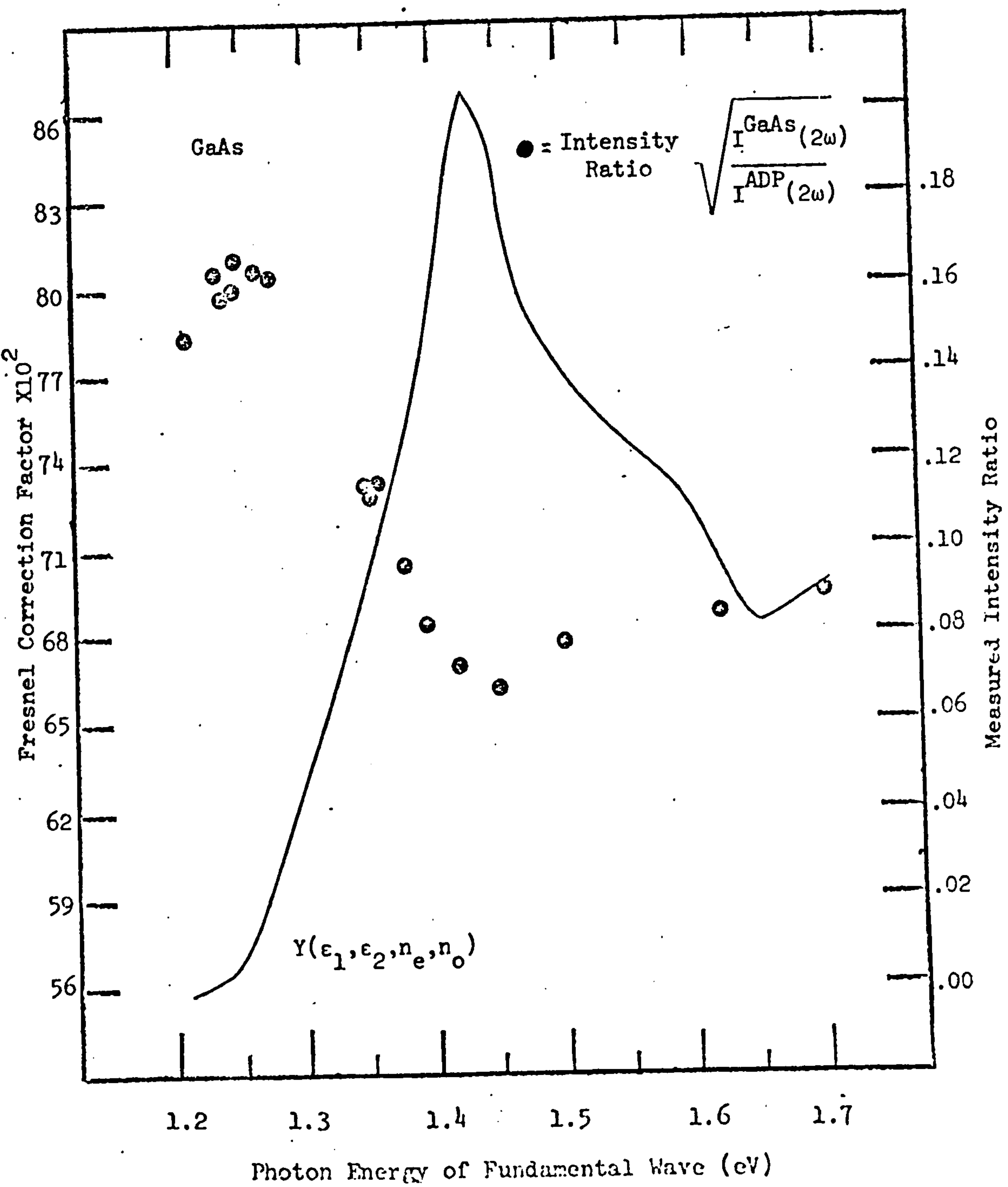

Figure 3.12

The Fresnel Correction Factor (see text) and the Measured Intensity Ratio as a Function of Photon Energy, GaAs.

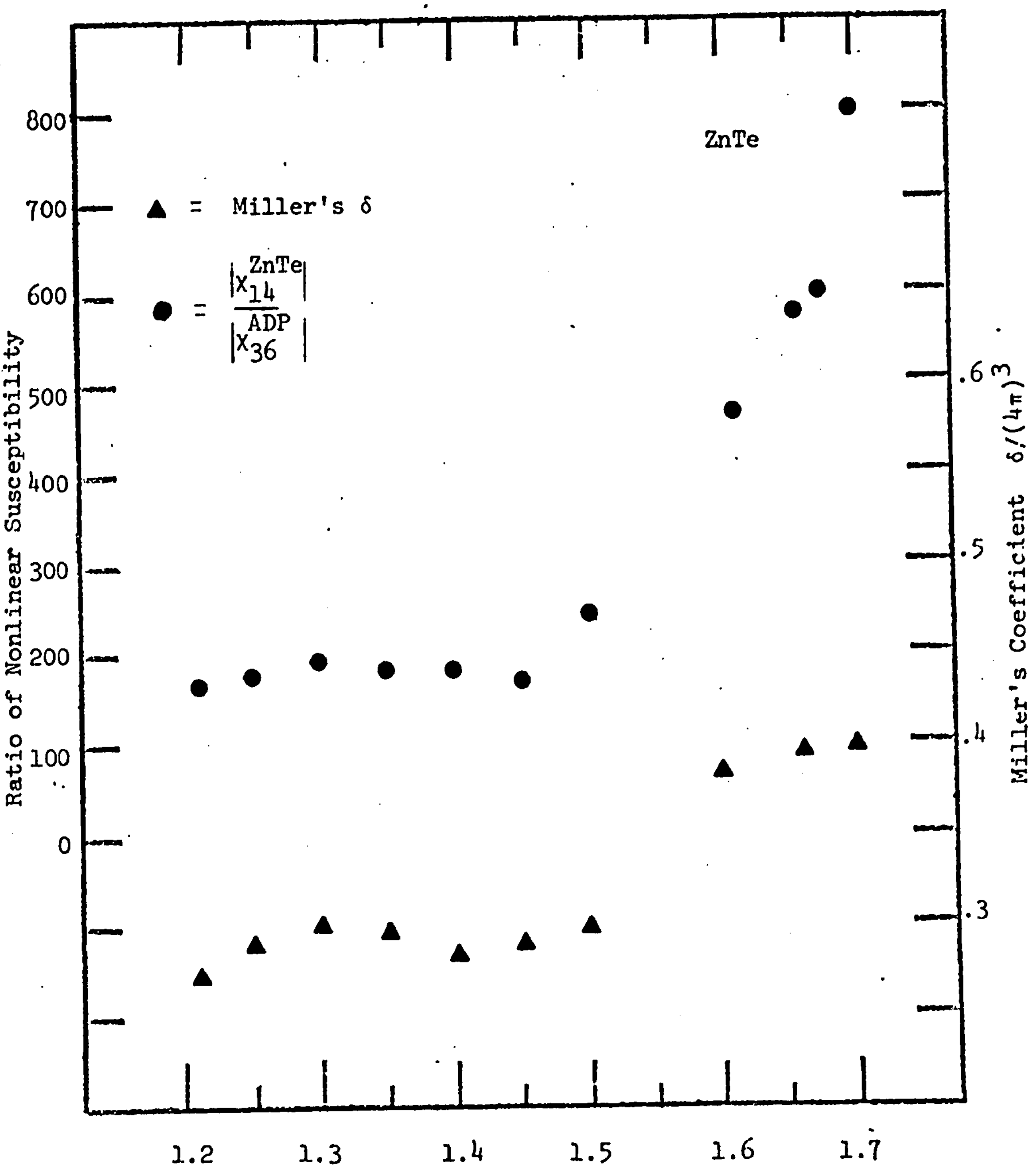

Figure 3.13

The Modulus of the Nonlinear Susceptibility of ZnTe,as a Function of Photon Energy of the Fundamental Wave. Miller's δ is also shown in units of 3X10^{-9} esu.

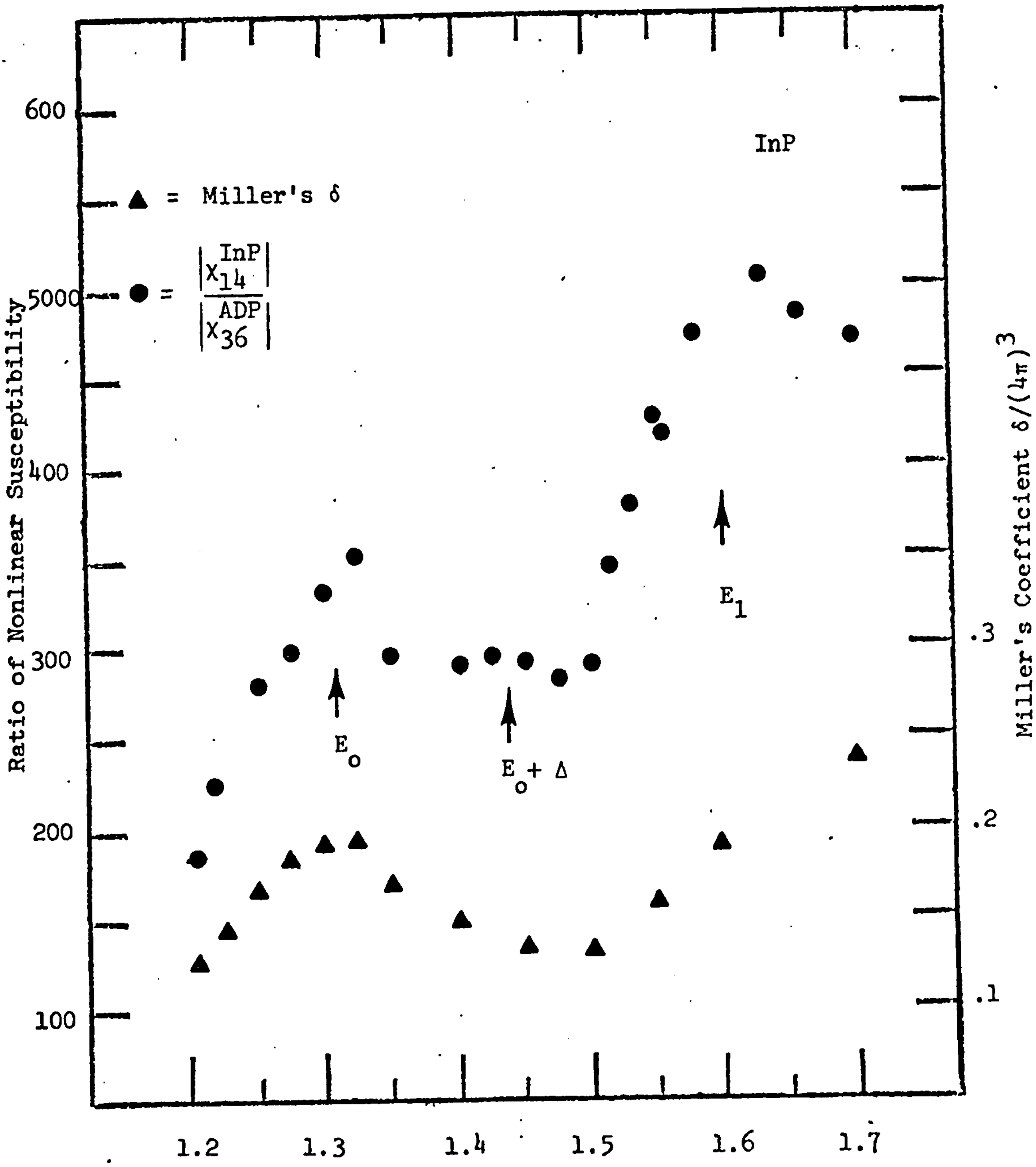

Figure 3.14

The Modulus of the Nonlinear Susceptibility of InP as a Function of Photon Energy of the Fundamental Wave. Miller's δis also shown in units of $3X10^{-9}$ esu.

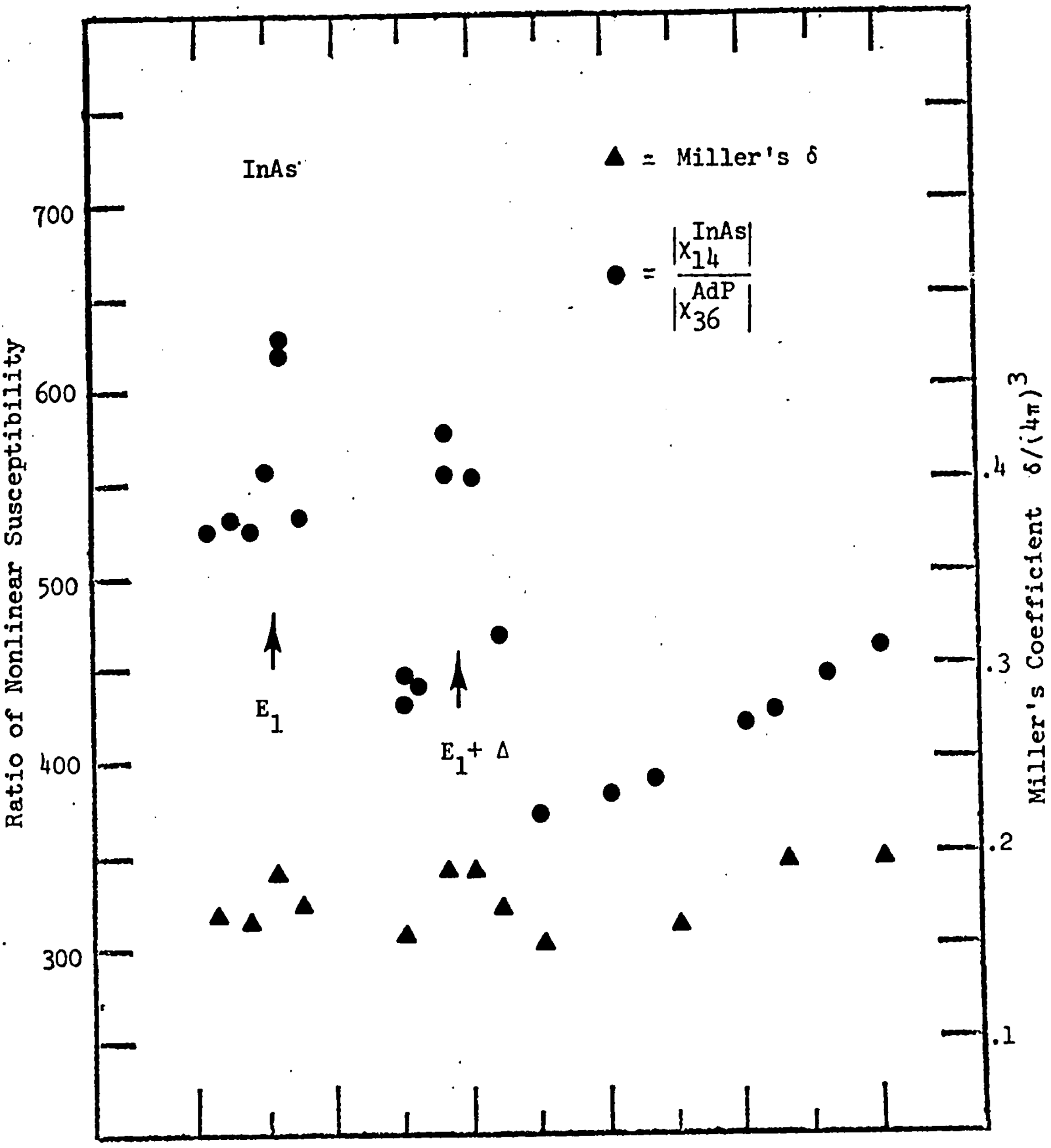

Figure 3.15

The Modulus of the Nonlinear Susceptibility of InAs as a Function of Photon Energy of the Fundamental Wave. Miller's δ is also shown in units of $3X10^{-9}$ esu.

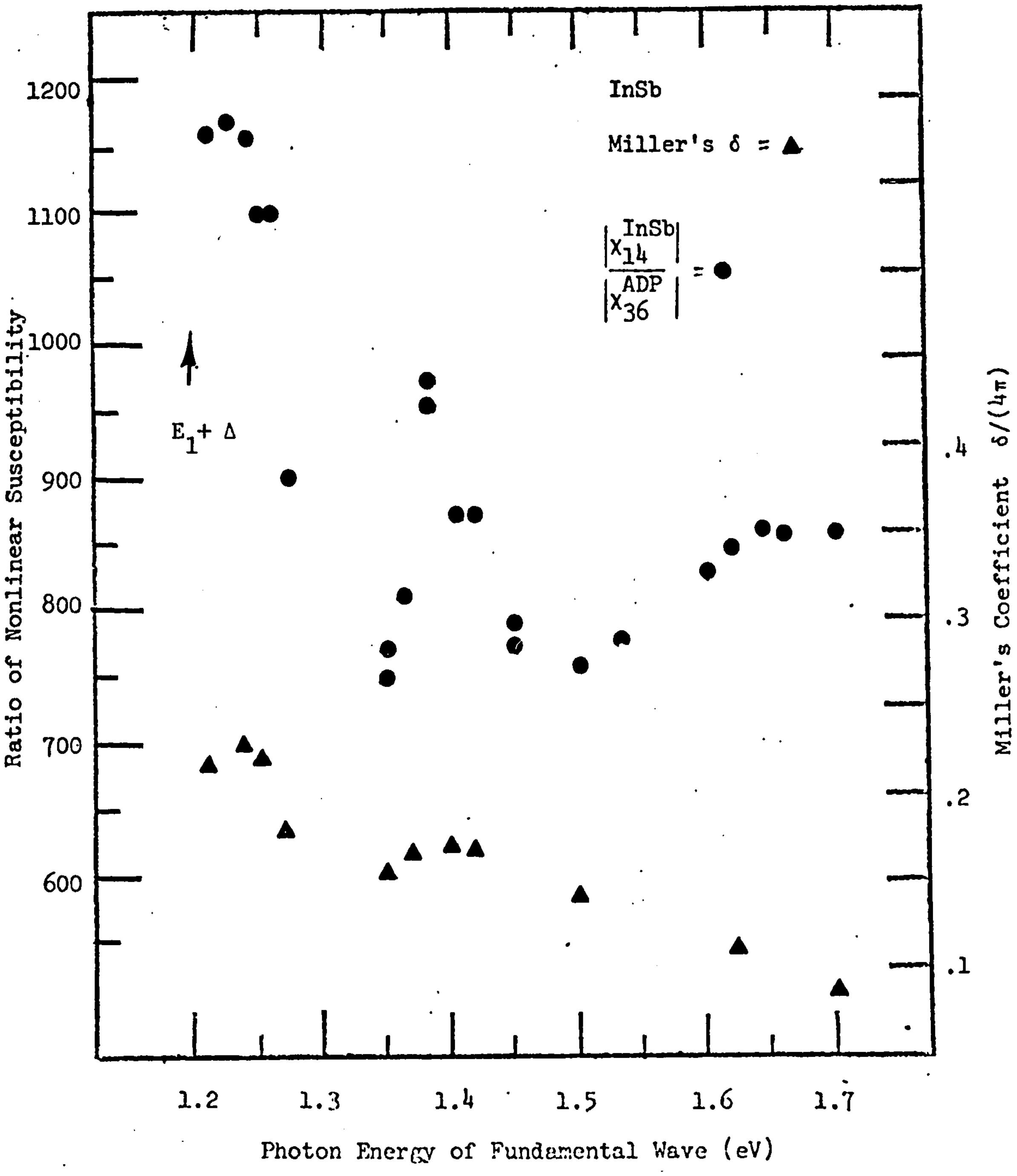

Figure 3.16

The Modulus of the Nonlinear Susceptibility of InSb as a Function of Photon Energy of the Fundamental Wave. Miller's δ is also shown in units of $3X10^{-9}$ esu.

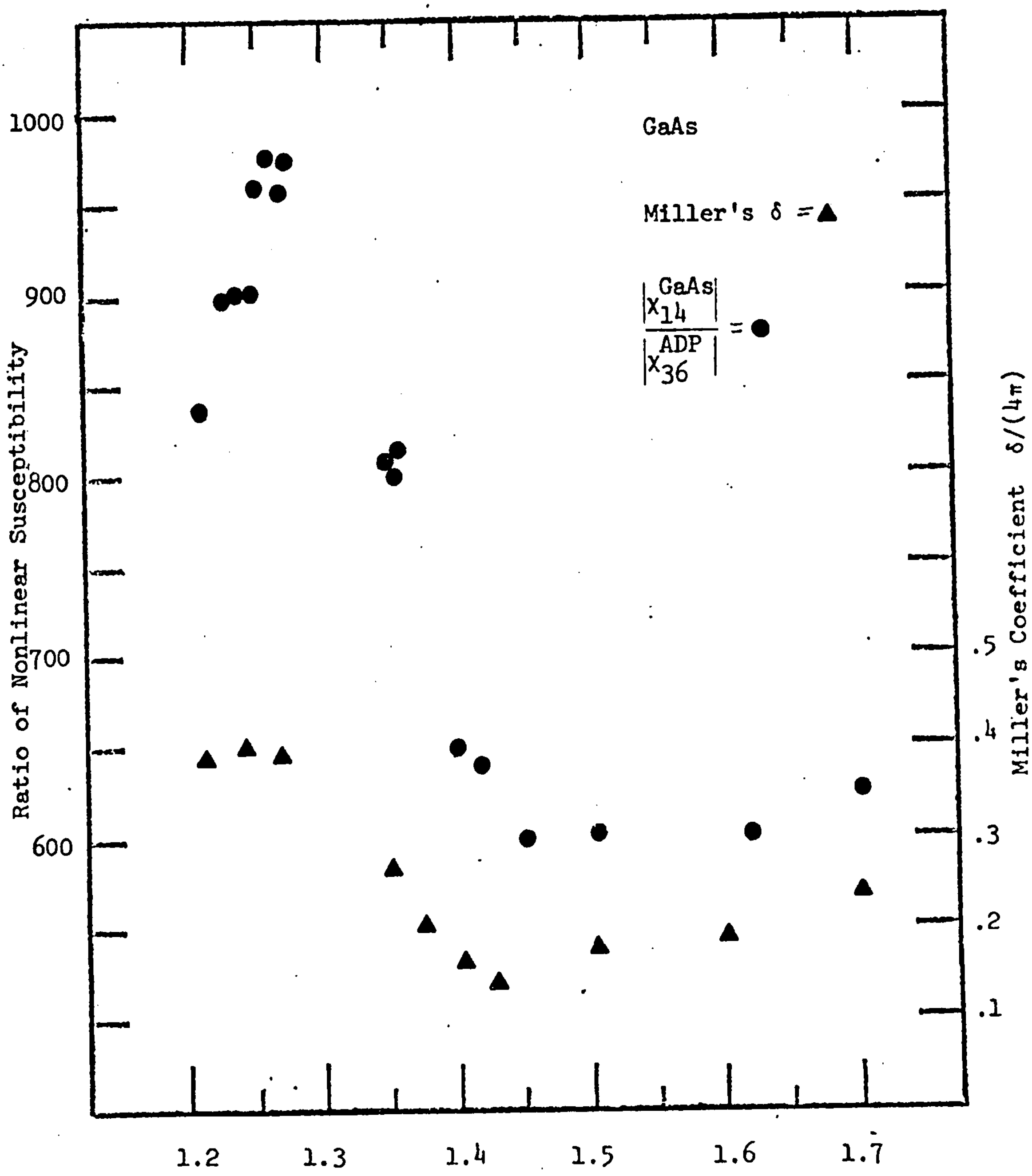

Figure 3.17

The Modulus of the Nonlinear Susceptibility of GaAs as a Function of Photon Energy of the Fundamental Wave. Miller's δ is also shown in units of $3X10^{-9}$ esu.

Chapter 4

The Dispersion of the Nonlinear Susceptibility Moduli for Semiconductors of the Wurtzite Structure

4.1 Introduction

In Chapter 3 the dispersion of the nonlinear susceptibility of various zinc-blende materials was studied. It was found that peaks or structure in the nonlinear susceptibility could be, in most cases identified with critical points in the joint density of states of the materials. In wurtzite structured materials we expect this also to be the case but one additional feature can be studied.

Wurtzite structured materials have 3 independent nonlinear susceptibility constants (See Sec. 4.2). Various authors (Robinson, 1968; Phillips and Van Vechten, 1969, Kleinman, 1962) have suggested that these optical nonlinear susceptibilities bear special relationships to one another not dictated by symmetry requirements. These special relationships are discussed more fully later in the chapter. It suffices to mention at this point that these special relationships rely on bond polarizabilities and their directions within a unit cell. A study of the dispersion of the independent nonlinear susceptibility would shed more light on the validity of these models. Furthermore these dispersion measurements may indicate how these relationships might be altered near an absorbing region of the material.

In this chapter equations describing the reflected harmonic intensity from a uniaxial crystal are described. The dispersion of the nonlinear susceptibility moduli for wurtzite CdS and CdSe is then studied. Particular attention is paid to the ratios among the independent nonlinear susceptibilities.

4.2 The Nonlinear Dielectric Tensor

Before discussing the laws of reflection and the experimental procedure for the wurtzite class semiconductors one must specify exactly what quantities we are measuring.

The 27 component nonlinear dielectric tensor (see Chapter 1) reduces to 18 independent components through the use of piezo-electric contraction. Further reduction of the number of tensor elements results by considering the specific crystal symmetry. The wurtzite crystals all belong to the point group 6mm. Symmetry considerations then predict 5 tensor components χ_{15}, χ_{24} , χ_{31} , χ_{32}, and χ_{33} (Yariv, 1967).

$$\chi^{NL} = \begin{vmatrix} \cdot & \cdot & \cdot & \cdot & \chi_{15} & \cdot \\ \cdot & \cdot & \cdot & \chi_{24} & \cdot & \cdot \\ \chi_{31} & \chi_{32} & \chi_{33} & \cdot & \cdot & \cdot \end{vmatrix}$$

with $\chi_{31} = \chi_{32}$

$\chi_{15} = \chi_{24}$

The resulting nonlinear source polarizations are:

eq. 4.1
$$P_x^{NLS}(2\omega) = 2\chi_{15} E_x(\omega) E_z(\omega)$$
$$P_y^{NLS}(2\omega) = 2\chi_{15} E_y(\omega) E_z(\omega)$$
$$P_z^{NLS}(2\omega) = \chi_{31} E_x^2(\omega) + \chi_{31} E_y^2(\omega) + \chi_{33} E_z^2(\omega)$$

where $E_i(\omega)$ is the electric vector in the direction i vibrating at a frequency ω within the material. $P^{NLS}(2\omega)$ is the nonlinear source polarization in the direction i vibrating at frequency 2ω.

$E_i(\omega)$ along any one of the crystal axes (001) does give rise to a $P^{NLS}(2\omega)$, as opposed to the zinc-blende materials which induce no $P^{NLS}(2\omega)$ for these directions. Now the use of polarization "selection rules" as a criterion for surface quality must be different.

The quantities we are measuring in this chapter will be χ_{15}, χ_{31} and χ_{33}.

4.3 Theory of the Nonlinear Susceptibility Dispersion, Wurtzite Materials.

The theoritical discussion made in Chapter 3 holds equally well for wurtzite structured materials. The effects of the joint density of states and of the matrix element variation throughout the Brillouin zone are of importance as before. The effect of excitons now plays a more important role in wurtzite semiconductors.

Wurtzite structure provides additional interest because it possesses three independent tensor elements χ_{15}, χ_{31}, and χ_{33}. Kleinman,based on a reversible thermodynamic argument, has suggested

(Kleinman, 1962) that there is an additional symmetry requirement for the tensor elements, provided that the material is transparent at $\hbar\omega$ and $2\hbar\omega$ (see Chapter 1). This result, for wurtzite materials, leads to $\chi_{15} = \chi_{31}$. It should be emphasized that this relationship should hold only if the medium is transparent at ω and 2ω .

More recently several authors (Robinson, 1968; Phillips and Van Vechten, 1969; and Levine, 1969,70) have calculated the nonlinear susceptibility of several wurtzite materials in the transparency region. Their calculations, which attribute the nonlinear susceptibility to the anharmonic motion of the "bond charge" between the atoms, predict another relationship among the nonlinear dielectric tensor elements. This additional relationship arose from the symmetry of the tetrahedral bonds (sp^3) that surround any $A^N B^{8-N}$ semiconductor. Their relationship makes $\frac{\chi_{33}}{\chi_{31}} = -2$. The minus sign is important. The bond charge argument also predicts $\chi_{15} = \chi_{31}$, agreeing with Kleinman's predictions. It should again be noted that these arguments hold only in the transparency region. It would be of interest to scrutinize these relationships in the absorbing region. Both CdS and CdSe permit interesting test cases for the various perdictions among the nonlinear tensor elements in the absorbing region. No experiments to date have been performed in this region.

The experimental work at 10.6 and 1.06μ (Miller, 1964;Miller and Nordland, 1970; Boyd, Buchler and Storz, 1971; Patel, 1966; Soref and Moos, 1964) has all verified $\frac{\chi_{33}}{\chi_{31}}$ = -2 for CdS and CdSe. Furthermore $\frac{\chi_{15}}{\chi_{31}}$ has been found to be 1 within experimental error. The experimental work to date on these materials has all been performed by transmission. The transmission technique inhibits accurate work from being performed in the absorption region as was explained in Chapter 3.

4.4 The Boundary Value Problem

4.4.1 Introduction

Before measurements can be made of $|\chi^{NL}|$ by reflection techniques the nonlinear optics laws for an uniaxial, nonmagnetic, piezoelectric crystal must be solved. The solution will also enable one to determine the relative signs of the nonlinear coefficients in the absorbing region (see Chapter 5 for details).

4.4.2 The Crystal Orientation

A crystal orientation must be chosen so as to enable us to determine the three nonlinear coefficients.

The crystal orientation for both CdS and CdSe is shown in Figure 4.1. An "a" axis was normal to the surface and the "c" axis was in the surface. By rotating the crystal about its "a" axis, one would be able to pick out various components of the nonlinear polarization.

The general nonlinear source polarization terms when $\overline{E}(\omega)$ is along the $\hat{y}$ direction (as it was for all the experiments) and the "c" axis is at an angle θ to the y axis (see Figure 4.1) can be written as:

eq. 4.2

$$P_x^{NLS}(2\omega,\theta) = 0$$

$$P_y^{NLS}(2\omega,\theta) = (\chi_{31}\cos\theta\sin^2\theta + \chi_{33}\cos^3\theta + 2\chi_{15}\sin^2\theta\cos\theta)\,\mathcal{E}^2(\omega)$$

$$P_z^{NLS}(2\omega,\theta) = (\chi_{31}\sin^3\theta + \chi_{33}\sin\theta\cos^2\theta - 2\chi_{15}\cos^2\theta\sin\theta)\,\mathcal{E}^2(\omega)$$

4.4.3 The Solution to the Boundary Value Problem

The general solution of the boundary value problem for the production of the second harmonic at the surface of a nonlinear nonmagnetic, uniaxial crystal was first attempted by Fischer (Fischer, 1967). Due to a poor choice of coordinates to represent the solution his result was useful only for a very specialized geometry which is not of interest to this work. The solution arrived at in this work is useful for all geometries of interest.

To begin with one must first solve the wave equation with a nonlinear source polarization. Then one must use the boundary conditions to match the solutions at the crystal surface. The reflected second harmonic electric vector can be written as:

eq. 4.3 $\bar{E}_R(r,t) = \bar{E}_R(2\omega)\, e^{i\frac{2\omega}{c}(\bar{n}_r(2\omega)\cdot\bar{r} - ct)}$.

where $n_r(2\omega)$ is called the propagation vector.

The wave equation in a nonlinear uniaxial crystal can be written as:

eq. 4.4 $\nabla\times(\nabla\times\bar{E}(r,t)) + \frac{1}{c^2}\frac{\partial^2}{\partial t^2}\epsilon(2\omega)\,\bar{E}(r,t) = -\frac{4\pi}{c}\frac{\partial^2}{\partial t^2}\underline{P}^{NLS}$

It is known (Bloembergen and Pershan, 1962) that the general solution consists of the solution of the homogeneous equation (free waves) plus one particular solution of the inhomogeneous equation (bound waves). The bound waves travel in phase (are bound with) the nonlinear source polarization.

In order to keep account of the various propagation velocities in an uniaxial crystal (ordinary and extraordinary) one must define three seperate interactions among the fundamental waves. If we define $\vec{E}_o(\omega)$ as the electric vector associated with an ordinary ray and $\bar{E}_{ao}(\omega)$ as the electric vector associated with an extraordinary ray the interactions are:

i) interactions between ordinary rays: $\bar{P}_1^{NLS}(2\omega) = \chi_{31}\bar{E}_o(\omega)\bar{E}_o(\omega)$.

ii) interactions between extra ordinary rays:

$$\bar{P}_2^{NLS}(2\omega) = \chi_{33}\bar{E}_{ao}(\omega)\bar{E}_{ao}(\omega).$$

and:

iii) interactions between ordinary and extraordinary rays:

$$\bar{P}_3^{NLS}(2\omega) = \chi_{15}\bar{E}_{ao}(\omega)\bar{E}_o(\omega).$$

Thus the $P^{NLS}(2\omega)$ in equation 4.4 is:

eq. 4.5 $$P^{NLS} = \sum_{\alpha=1,2,3} P_\alpha^{NLS}(2\omega)\, e^{i\left(\frac{2\omega}{c}\right)\left(\bar{n}_\alpha(2\omega)\cdot\bar{r} - ct\right)}$$

where $\bar{n}_1(2\omega) = \bar{n}_o(\omega)$

$\bar{n}_2(2\omega) = \bar{n}_{ao}(\omega)$

$\bar{n}_3(2\omega) = [\bar{n}_o(\omega) + \bar{n}_{ao}(\omega)]/2$

define the propagation vectors of the bound waves which are obtained from: $$\bar{P}^{NLS} = \chi^{NL}\bar{E}_i(\omega)\,\bar{E}_i(\omega)$$

where $E_i(\omega)$ is the electric field inside the nonlinear media.

The solution to 4.4 consists of, as was mentioned, the general solution of the homogeneous equation (free waves) and a particular solution of the inhomogeneous equation (bound waves).

The homogeneous solution is just the plane wave solution with the two waves, an ordinary wave and an extraordinary wave:

eq. 4.6 $$\bar{E}_{hom} = \left(\bar{e}_o(2\omega)\,E_o(2\omega)\,e^{i\frac{2\omega}{c}(n_o(2\omega)\cdot r} + \bar{e}_{ao}(2\omega)\,E_{ao}(2\omega)\,e^{i\frac{2\omega}{c}(n_{ao}(2\omega)\cdot r}\right)e^{i2\omega t}$$

where $\bar{e}_{ao}(2\omega)$ and $\bar{e}_o(2\omega)$ are the polarization vectors of the extraordinary and ordinary waves respectively.

The solution to the inhomogeneous equation is given by (Fischer, 1967):

eq. 4.7 $$\bar{E}_{inh} = \sum_{\alpha=1,2,3} (-1)\, \vec{P}_\alpha\, e^{i\frac{2\omega}{c}(\bar{n}_\alpha(2\omega)\cdot\bar{r} - ct)}$$

where $$\bar{P}_\alpha = 4\pi A^{-1} \bar{P}^{NLS}$$

and $$A = n_\alpha n_\alpha + \epsilon(2\omega) - n_\alpha^2 I$$

Electromagnetic theory predicts that the tangential component of both E and H be continuous across the boundary at all times. Invoking this and representing the reflected electric vector by two vectors which are normal to the direction of propagation of the second harmonic in the linear medium (Fischer's error, see Appendix F) yields the correct result:

eq. 4.8 $$\vec{E}_R(2\omega) = \frac{v_2(\bar{n}_r \times \bar{u}_1) - v_1(\bar{n}_r \times \bar{u}_2)}{-n_r\cdot(u_1 \times v_2)}$$

where

eq. 4.9
$$\bar{u}_1 = \bar{n}_o\cdot(\bar{e}_{ao} \times \bar{e}_o)(\bar{e}_{ao} \times \hat{q}) - \hat{q}\cdot(e_{ao} \times e_o)(e_{ao} \times n_r)$$
$$\bar{u}_2 = \bar{n}_{ao}\cdot(\bar{e}_{ao} \times \bar{e}_o)(\bar{e}_o \times \hat{q}) - q\cdot(e_{ao} \times e_o)(e_o \times n_r)$$

and where

eq. 4.10
$$v_1 = [\bar{e}_{ao}\cdot(\bar{n}_\alpha \times \bar{E}_{inh})][\hat{q}\cdot(\bar{e}_{ao} \times \bar{e}_o)] + [\bar{e}_{ao}\cdot(\bar{n}_o \times \bar{e}_o)][\bar{e}_{ac}\cdot(\hat{q} \times \bar{E}_{inh})]$$
$$v_2 = [\bar{n}_{ao}\cdot(\bar{e}_{ao} \times \bar{e}_o)][\bar{e}_o\cdot(\hat{q} \times \bar{E}_{inh})] - [\bar{e}_o\cdot(\bar{n}_\alpha \times \bar{E}_{inh})][\hat{q}\cdot(\bar{e}_{ac} \times \bar{e}_o)]$$

where: $\bar{n}_\alpha$ is the propagation vector of the bound wave.

$\bar{n}_o$ is the propagation vector of the ordinary wave.

$\bar{n}_{ao}$ is the propagation vector of the extraordinary wave.

$\hat{q}$ is an inward normal of the crystal face.

and: $\vec{e}_{ao}$ and $\vec{e}_o$ are the polarization vectors.

While equations 4.8 through 4.10 appear at first glance to be rather unsightly they are nevertheless straightfoward. With the aid of a computer (Digital Equipment PDP-10) a program was written which did all the scalar and vector products when the appropriate input data was given.

This appropriate input data consisted of: i) the relavant dielectric constants for CdS and CdSe (Cardona and Harbeke, 1965); ii) the angle of incidence of the fundamental frequency light; and iii) the angle the "c" axis made with the E(ω). For the details see Appendix E.

The program output was of the form:

eq 4.11 $$\bar{E}_k^{(i)} = a_1^{(i)}(\theta)\chi_{31} + a_2^{(i)}(\theta)\chi_{33} + a_3^{(i)}(\theta)\chi_{15}$$

where each of the constants $\vec{a}_i(\theta)$ was computed from 4.8 to 4.10. The three constants related to each of the nonlinear susceptibility coefficients were seperately calculated.

The linear dielectric constants for CdS and CdSe were plotted in Figures 4.2 to 4.5.

4.5 The Experimental Procedure

4.5.1 Introduction

The procedure for measuring the nonlinear susceptibility moduli of CdS and CdSe consisted of two parts. The motivation behind this two part analysis lies in the ability to seperately measure the three nonlinear coefficients upon rotation of the crystal about its face normal.

First $|\chi_{33}|$ and $|\chi_{31}|$ were measured seperately with respect to GaAs at 45° angle of incidence. Second $|\chi_{33}|$, $|\chi_{31}|$, and $|\chi_{15}|$ were measured with respect to each other at 14° angle of incidence. One obtains $\frac{|\chi_{15}|}{|\chi_{31}|}$ and $\frac{|\chi_{33}|}{|\chi_{31}|}$. The ratio $\frac{|\chi_{33}|}{|\chi_{31}|}$ was also obtained in the first part and thus served as a self-consistancy check of our nonlinear reflection equations and of our measurement accuracy.

One would like to refer the moduli of the nonlinear susceptibility of the wurtzite materials to the nonlinear susceptibility of ADP. To accomplish this a 45° incidence geometry was chosen. The second harmonic intensity from the wurtzite semiconductors was compared with that from GaAs. Then using appropriate Fresnel factors one can relate the nonlinear susceptibility of the wurtzite to that of ADP. It should be noted, that the uncertainty in the linear dielectric constants of GaAs cancel out in this procedure, since the initial measurements on GaAs with ADP were also made with the GaAs at 45° angle of incidence.

The 45° geometry does not permit one to measure $|\chi_{15}|$ independently. The reflected second harmonic would have contributions from the

$|\chi_{33}|$ and $|\chi_{31}|$ terms. If the angle of incidence were decreased to 0° then the contributions from $|\chi_{31}|$ and $|\chi_{33}|$ would be at right angles to that from the $|\chi_{15}|$ term. An optical analyzer could isolate just the $|\chi_{15}|$ contribution. Due to the difficulty in obtaining a true 0° incidence geometry a compromise was made. A 14° angle of incidence geometry was used (calculations indicated that a $< 3\%$ error would be introduced by using 14° instead of 0°).

4.5.2 The Preparation of the Crystal Surface

In order to insure that the reflected harmonic intensity was associated to the bulk properties, precautions like those described in Chapter 3, were taken.

The crystals were polished as per our instructions with 1μ Linde C, 0.3μ Linde A, and 0.1μ Linde B abrasives in that order.

To remove surface damage layers both CdS and CdSe were mildly etched (see Appendix D). The etching rates of these crystals were found to be long in comparison to those of the zinc-blende materials. After etching, the crystals were checked for their polarization "selection rules" (See Sec. 4.5.3). Ratios of the allowed to forbidden signals were greater than 20:1.

4.5.3 The 45° Experiment, Measurement of $|\chi_{33}|$ and $|\chi_{31}|$.

The measurement of $|\chi_{33}|$ and $|\chi_{31}|$ for CdS and CdSe was performed in a manner not unlike the measurements of the zinc-blende materials. The electric vector of the fundamental beam was vertically polarized and made parallel to "c" or perpendicular to "c" depending whether $|\chi_{33}|$ or $|\chi_{31}|$ was measured. The second harmonic then emerged vertically for the $|\chi_{33}|$ measurement and horizontally for the $|\chi_{31}|$ measurement.

The formula relating $|\chi_{33}|$ to that of ADP, using GaAs as an intermediate reference, is given by:

eq. 4.12 $$\frac{|\chi_{33}^{W}|}{|\chi_{36}^{ADP}|} = \frac{Y_{33}}{Y_{GaAs}} \frac{|\chi_{14}^{GaAs}|}{|\chi_{36}^{ADP}|} \sqrt{\frac{I_{V}^{W}(2\omega)}{I^{GaAs}(2\omega)}}$$

where $$Y_{33} = \frac{6\pi}{(n_e^2 - n_o^2)(n_c + 1)\, a_2^{(y)}(0)}$$

and $I_{V}^{W}(2\omega)$ is the harmonic intensity with vertical polarization from the wurtzite material.

The formula relating $|\chi_{31}|$ to that of ADP is given by:

eq. 4.13 $$\frac{|\chi_{31}^{W}|}{|\chi_{36}^{ADP}|} = \frac{Y_{31}}{Y_{GaAs}} \frac{|\chi_{14}^{GaAs}|}{|\chi_{36}^{ADP}|} \sqrt{\frac{I_{h}^{W}(2\omega)}{I^{GaAs}(2\omega)}}$$

where $$Y_{31} = \frac{8\pi}{(n_e^2 - n_o^2)(n_c+1)\, a_1^{(2)}(\theta c)\sqrt{2}}$$

and $I_{h}^{W}(2\omega)$ is the harmonic intensity with horizontal polarization from the wurtzite material.

The Fresnel factors for vertically light incident at 45° are plotted with "c" horizontal (Y_{31}) and with "c" vertical (Y_{33}). For CdS and CdSe these factors are shown in Figures 4.6 to 4.9.

The fact that the reflected harmonic signal from GaAs is horizontally polarized, while that associated with $|\chi_{33}|$ in CdS or CdSe is vertically polarized , adds one experimental complication. The Jarrell Ash spectrometer must be calibrated so as to include the transmission ratio of vertically to horizontally polarized inputs. This complication is not present when measuring $|\chi_{31}|$ since the reflected harmonic is polarized in the same direction (horizontal) as that of GaAs.

The harmonic intensity from CdS relative to that from ADP is shown in Figures 4.6 and 4.7. Figures 4.8 and 4.9 are for CdSe.

4.5.4 The 14° Experiment; Measurement of the Ratio $\frac{|\chi_{33}|}{|\chi_{31}|}$ and $\frac{|\chi_{15}|}{|\chi_{31}|}$.

It was mentioned in the introduction to this section that near normal incidence geometry was necessary for the measurement of the nonlinear susceptibility coefficient $|\chi_{15}|$. That is it was necessary to chose an experimental geometry in which $|\chi_{15}|$ could be measured alone. This could be accomplished if all other harmonic contributions were polarized perpendicularly to that of $|\chi_{15}|$. Then an analyzer could be used to reject the orthogonal components. Using 14° geometry, less than 3% of the other harmonic contributions were along the same polarization direction as $|\chi_{15}|$ (see calculation in Figure 4.10).

The harmonic intensity from each wurtzite material was measured with the crystal and the analyzer in three different positions. These were: 1) the "c" axis vertical and the analyzer vertical: χ_{31}, $I_v^W(2\omega)$; 2) the "c" axis horizontal and the analyzer horizontal: χ_{33}, $I_h^W(2\omega)$; 3) the "c" axis at 45° and the analyzer at 45°: χ_{15}, $I_{45}^W(2\omega)$. The transmission of the spectromenter with 45° polarized input light was again calibrated with respect to the horizontally polarized input.

The necessary Fresnel factors were derived from equations 4.8 through 4.10. Calculation was done with the aid of the computer program. With reference to equation 4.11 one writes:

eq. 4.14
$$\frac{|\chi_{33}|}{|\chi_{31}|} = \frac{a_1^{(2)}(90)}{a_2^{(2)}(c)} \sqrt{\frac{I_v^w(2\omega)}{I_h^w(2\omega)}}$$

and

eq. 4.15
$$\frac{|\chi_{15}|}{|\chi_{31}|} = \frac{a_1^{(2)}(90)}{a_3^{(2)}(45)} \sqrt{\frac{I_{45}^w(2\omega)}{I_h^w(2\omega)}}$$

where the $a_i(\theta)$ are the same constants as in equation 4.11.

Using the above equations one then solved for the nonlinear susceptibility ratios $\frac{|\chi_{33}|}{|\chi_{31}|}$ and $\frac{|\chi_{15}|}{|\chi_{31}|}$.

4.6 The Discussion of the Experimental Results.

4.6.1 Introduction

The results of the measurements of $|\chi_{33}|$ and $|\chi_{31}|$ for CdS and CdSe compared to $|\chi_{36}^{ADP}|$ are shown in Figures 4.11 and 4.13 respectively. The abscissa of the graphs represents the photon energy of the of the fundamental frequency wave. The ordinate axis represents the ratios of the nonlinear susceptibility modulus of the wurtzite material to that of the ADP.

Shown in Figures 4.12 and 4.14 are the computed values of Miller's δ . The nonlinear susceptibility values used were from Figures 4.11 and 4.13. The linear dielectric constants were taken from Figures 4.2 to 4.5.

The results will now be examined in detail.

4.6.2 The Nonlinear Susceptibility Dispersion of CdS

In CdS (Figure 4.11) there exists a peak in $|\chi_{33}|$ and $|\chi_{31}|$ as the harmonic photon energy is coincident with the exciton energy (2.5 eV). Since the fundamental frequency is not absorbed, this peak corresponds to a resonance of the second harmonic energy with the exciton energy.

Beyond the exciton region a general increase in the nonlinear susceptibility coefficients can be seen. This enhancement is due to $2\hbar\omega$ approaching the E_1 transition energies (5 eV and 5.5 eV) and to $\hbar\omega$ approaching the exciton energy.

The dispersion of the nonlinear susceptibility ratios $\frac{|\chi_{33}|}{|\chi_{31}|}$ and $\frac{|\chi_{15}|}{|\chi_{31}|}$ are shown in Figure 4.15. The first ratio was measured in both 45° and 14° geometries. The agreement between the two two seperate measurements was excellent.

The ratio $\frac{|\chi_{33}|}{|\chi_{31}|}$ has dispersion. As was mentioned in Section 4.3 several authors have postulated that $\frac{|\chi_{33}|}{|\chi_{31}|} = 2$ in transparency region of the crystal. When $2\hbar\omega$ is below the exciton energy, the postulate appears to hold. When the second harmonic is coincident with the exciton energy the ratio peaks. Beyond the exciton energy $\frac{|\chi_{33}|}{|\chi_{31}|}$ falls to about 1.6. Recall that the predictions of Levine, Robinson, and Phillips and Van Vechten hold only in the transparency region. Geometric arguments, based on the distribution of bond charge, predicted the ratios $\frac{|\chi_{33}|}{|\chi_{31}|} = 2$ and $\frac{|\chi_{15}|}{|\chi_{31}|} = 1$. If other contributions to the nonlinear susceptibility became important as $2\hbar\omega$ approached the exciton energy, then deviations from $\frac{|\chi_{33}|}{|\chi_{31}|} = 2$ might exist. This would be particularly true if such other contributions were not tetrahedrally coordinated in a manner like the bond charge.

The $\frac{|\chi_{15}|}{|\chi_{31}|}$ nonlinear susceptibility ratio does not deviate significantly from 1 but is constant throughout the photon energy range studied. Near 1.25 eV, where absorption occurs in the second harmonic, nothing happens to the ratio $\frac{|\chi_{15}|}{|\chi_{31}|}$. The reason for this is not altogether clear since both Kleinman's and Robinson's arguments should hold only in the transparent region of the crystal. Clearly much theoretical analysis must be done before anything quantative can be said.

4.6.3 The Nonlinear Susceptibility Dispersion of CdSe.

In CdSe (Figure 4.13) there is no discernible structure in $|\chi_{33}|$ or $|\chi_{31}|$. This is not unexpected, since $2\hbar\omega$ is above the exciton energy (1.9 eV) but below the E_1(A) peak (4.2 eV). Between these energies there exists no other critical points of the joint density of states. Only a general increase in the nonlinear susceptibility is observed as $2\hbar\omega$ is increased.

Miller's δ are shown in Figure 4.14. Again they exhibit less structure than the nonlinear susceptibilities. There is a general increase near 1.7 eV.

The ratios $\frac{|\chi_{33}|}{|\chi_{31}|}$ and $\frac{|\chi_{15}|}{|\chi_{31}|}$ are shown in Figure 4.16. Again $\frac{|\chi_{33}|}{|\chi_{31}|} < 2$ above the exciton lines. The ratio increases towards 2 with higher photon energies. Again the ratio $\frac{|\chi_{15}|}{|\chi_{31}|}$ is 1 within experimental error for all photon energies investigated.

There are larger errors in these measurements because the incident intensities were kept low in order to prevent surface damage to CdSe, which had a very low power damage threshold.

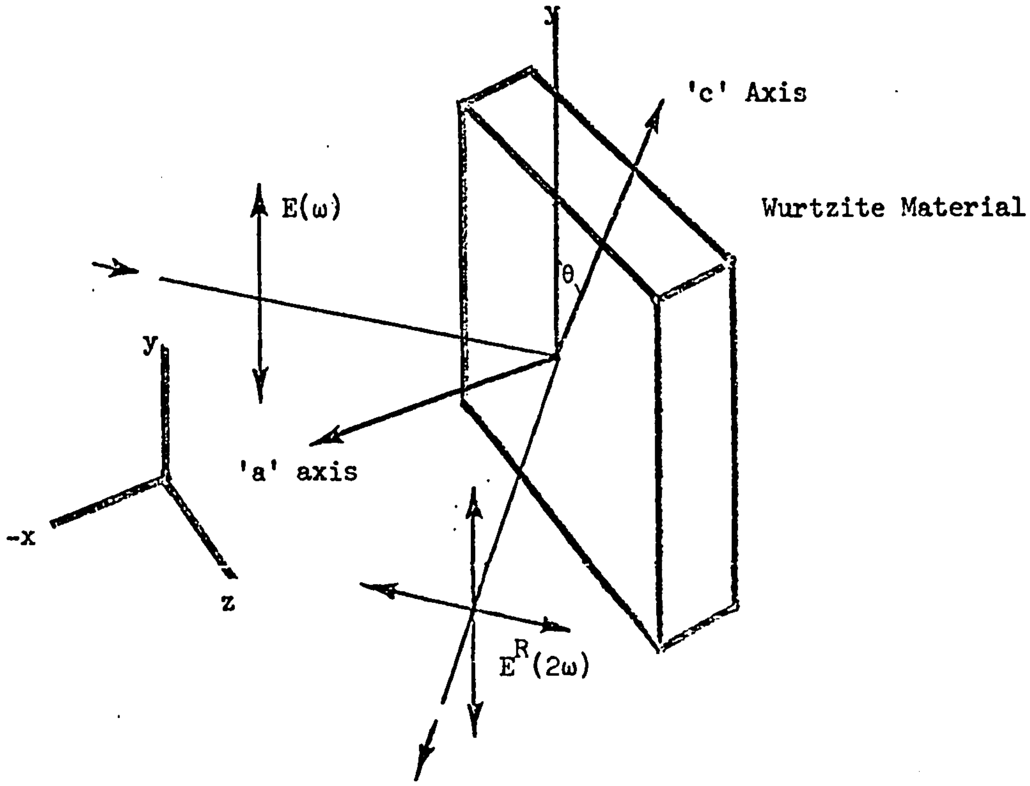

Figure 4.1

Crystal Orientation of the
Wurtzite Materials

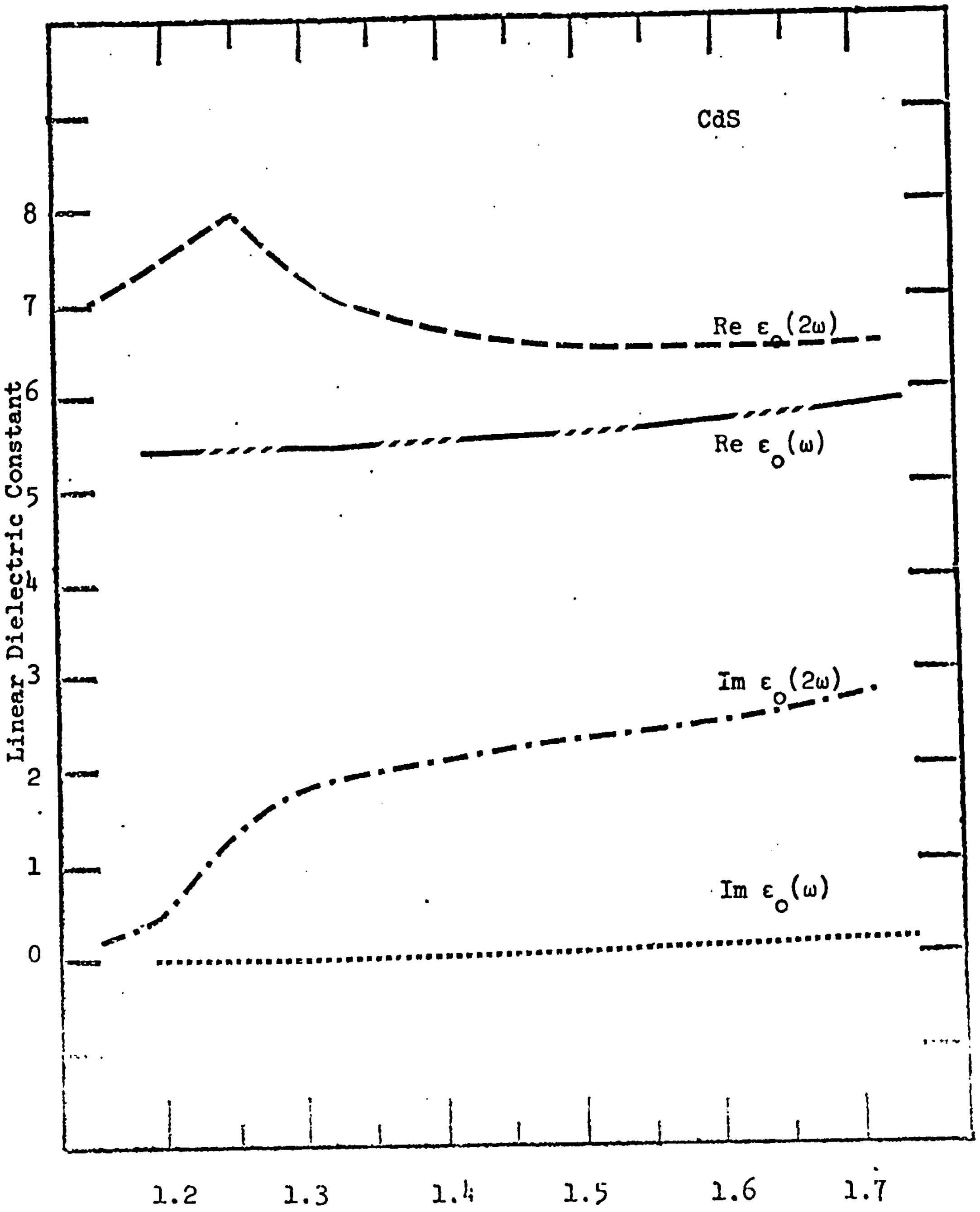

Figure 4.2

The Real and Imaginary Parts of the Ordinary Dielectric Constants of CdS at the Fundamental and Second Harmonic Frequencies.

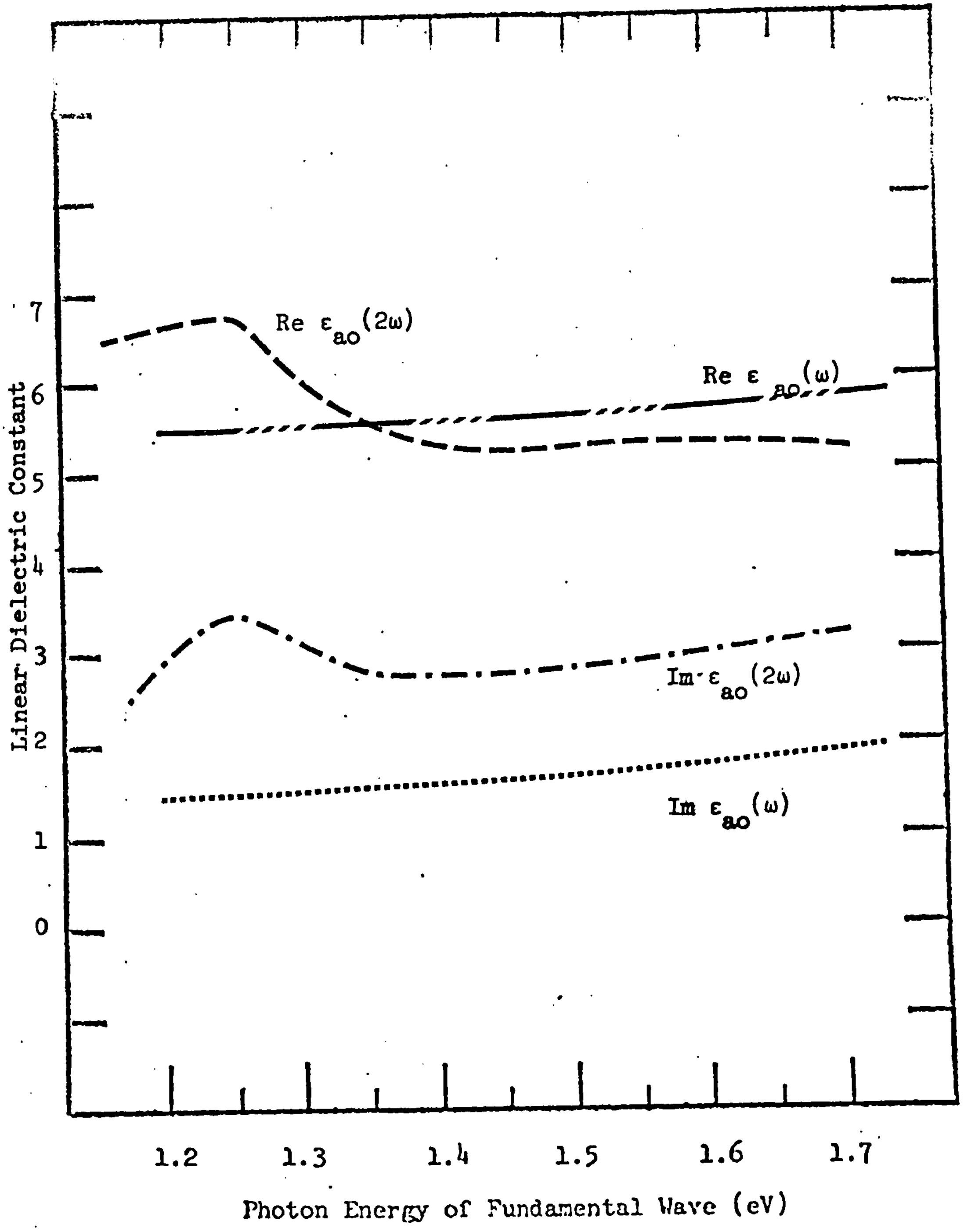

Figure 4.3

The Real and Imaginary Parts of the Extraordinary Dielectric Constants of CdS at the Fundamental and Second Harmonic Frequencies.

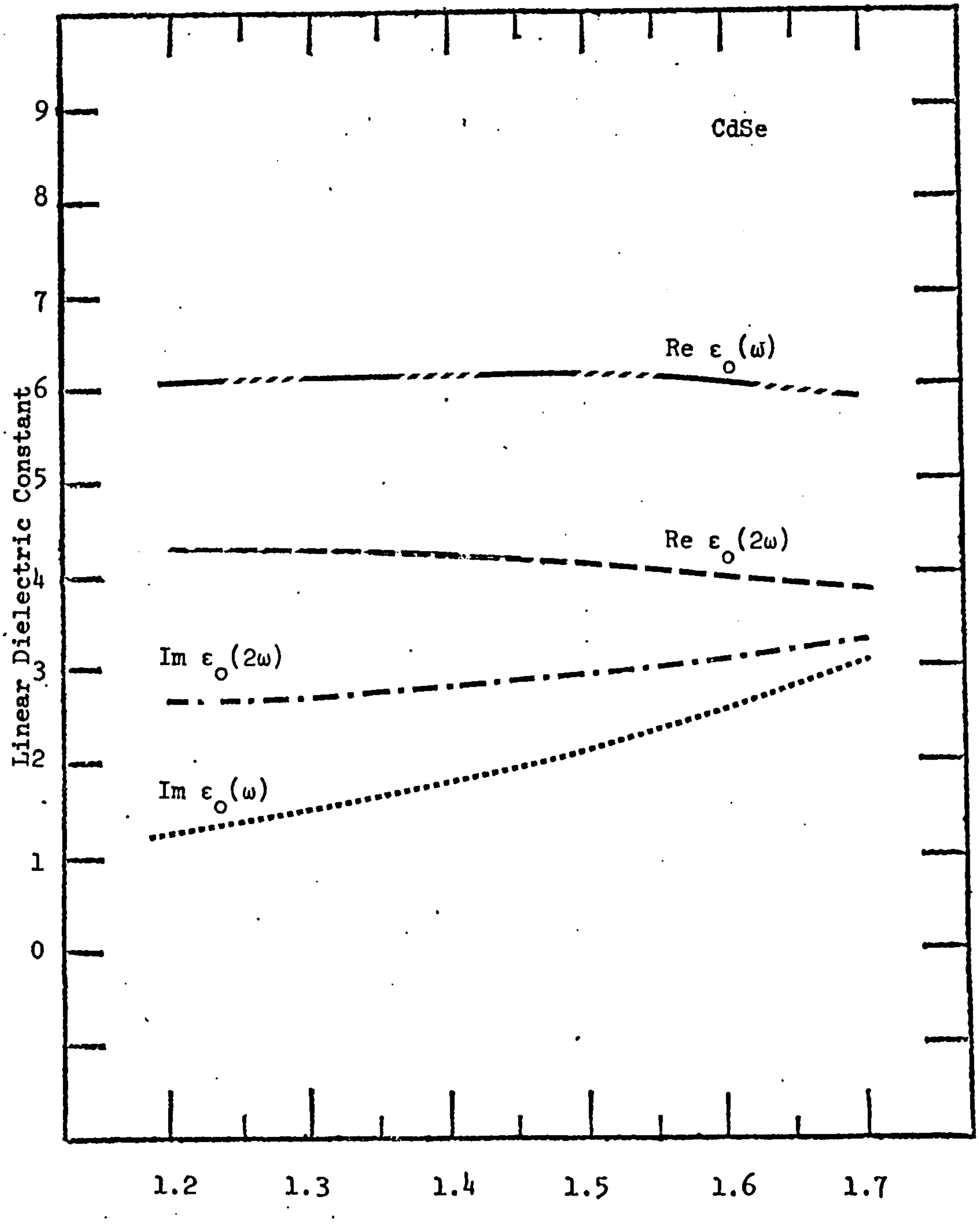

Figure 4.4

The Real and Imaginary Part of the Ordinary Dielectric Constant of CdSe at the Fundamental and Second Harmonic Frequencies

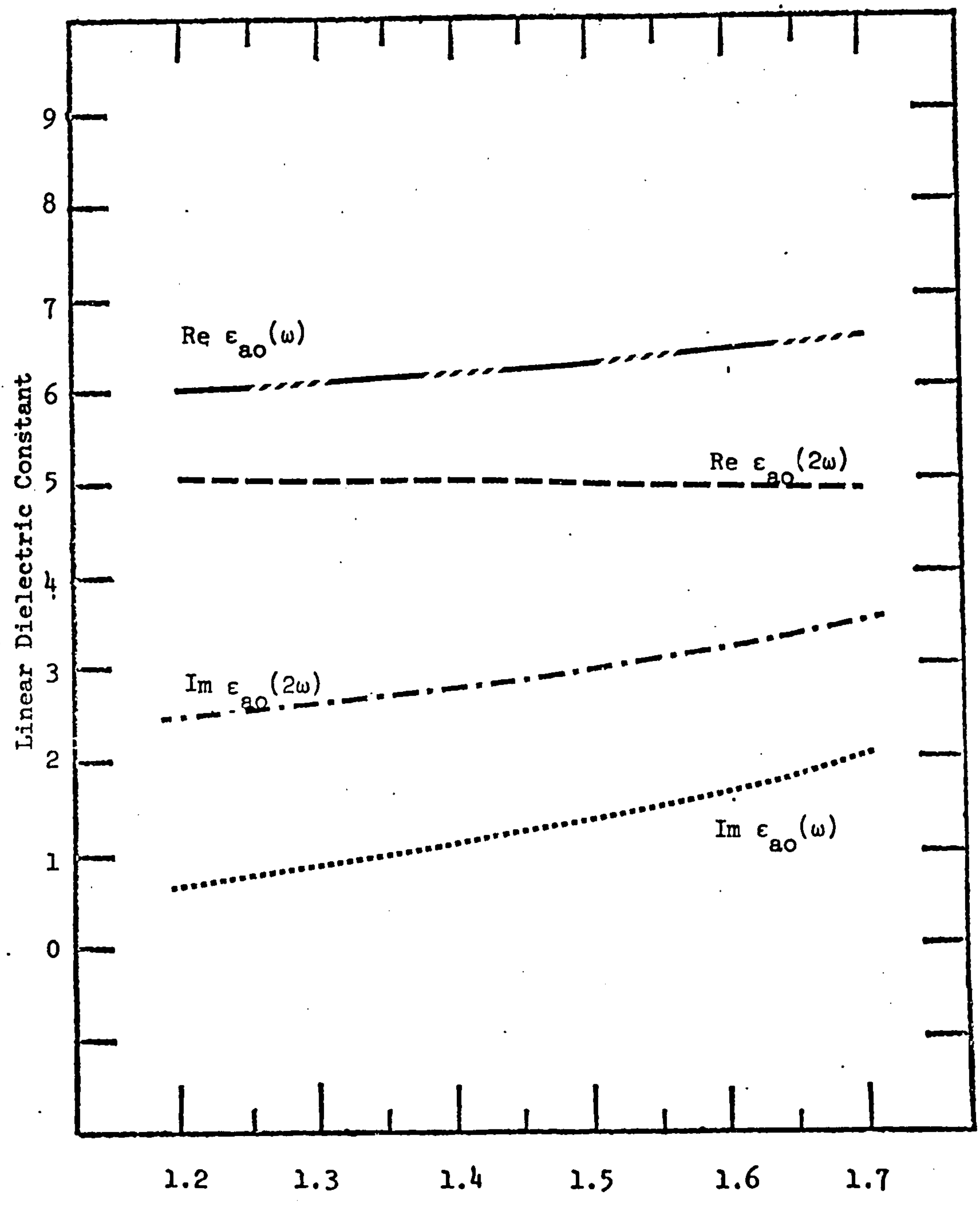

Figure 4.5

The Real and Imaginary Parts of the Extraordinary Dielectric Constants of CdSe at the Fundamental and Second Harmonic Frequencies

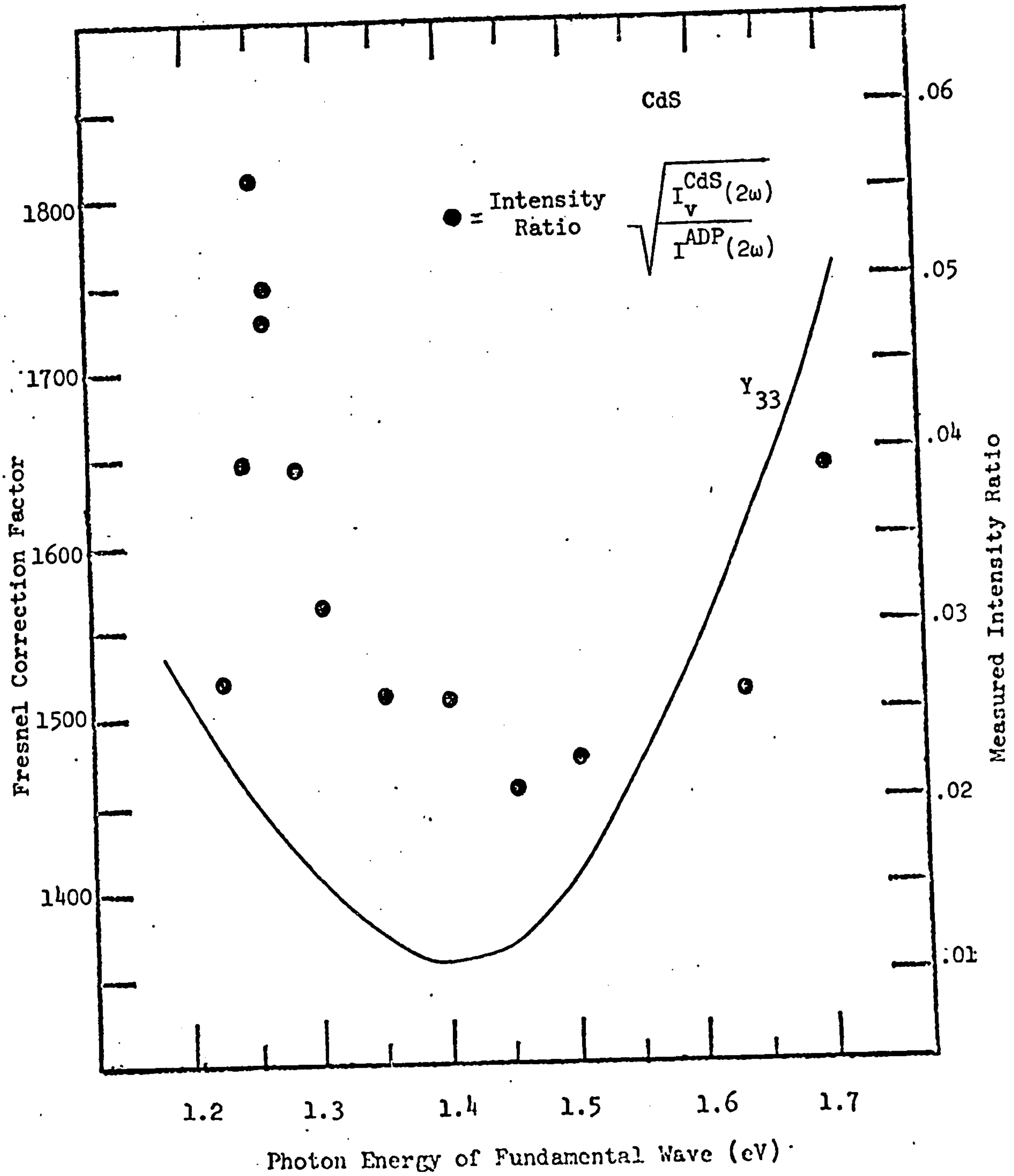

Figure 4.6

The Fresnel Correction Factor and the Measured Intensity Ratio for χ_{33} as a Function of Photon Energy of the Fundamental Wave. CdS

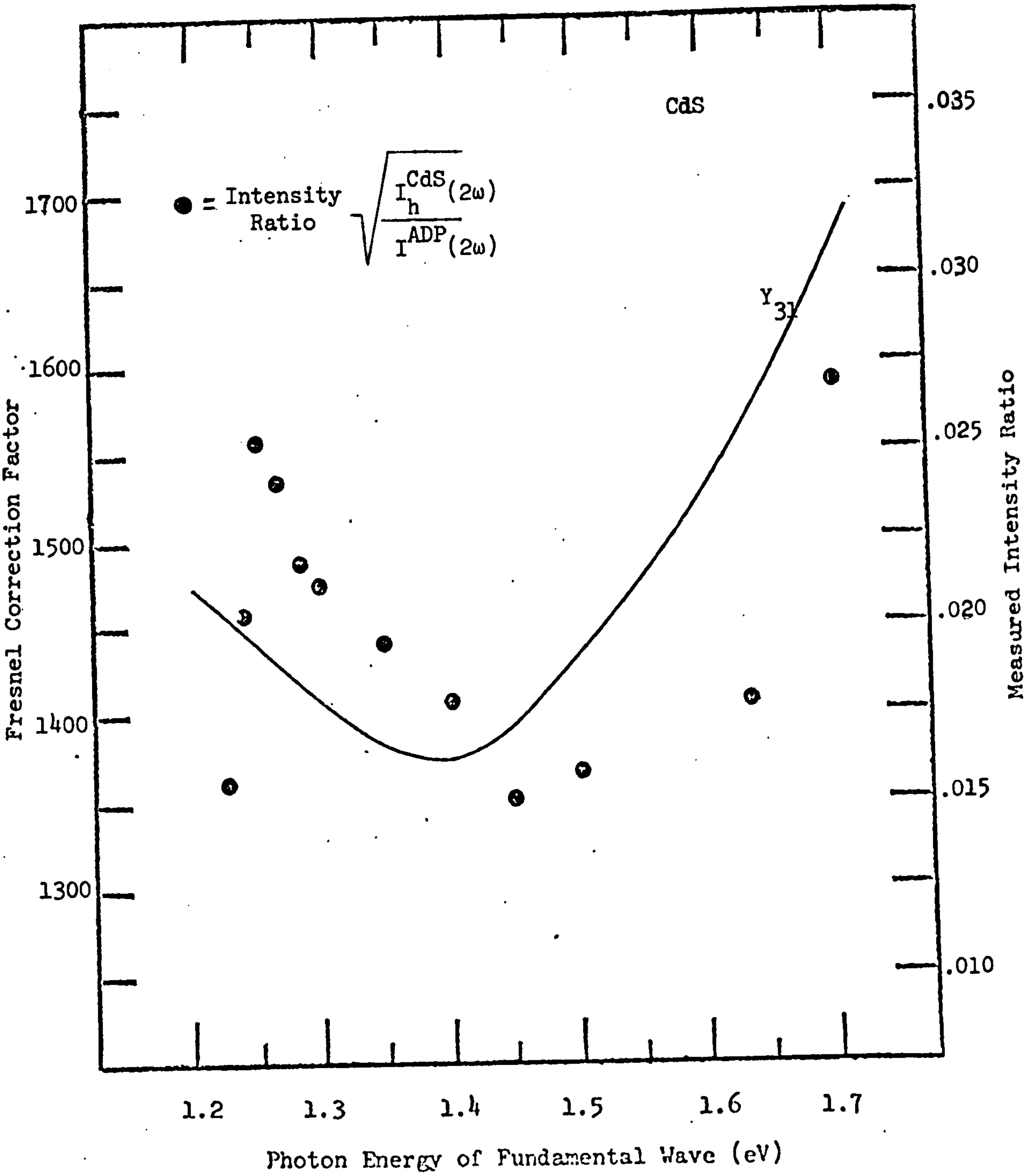

Figure 4.7

The Fresnel Correction Factor and the Measured Intensity Ratio for χ_{31} as a Function of Photon Energy of the Fundamental Wave CdS.

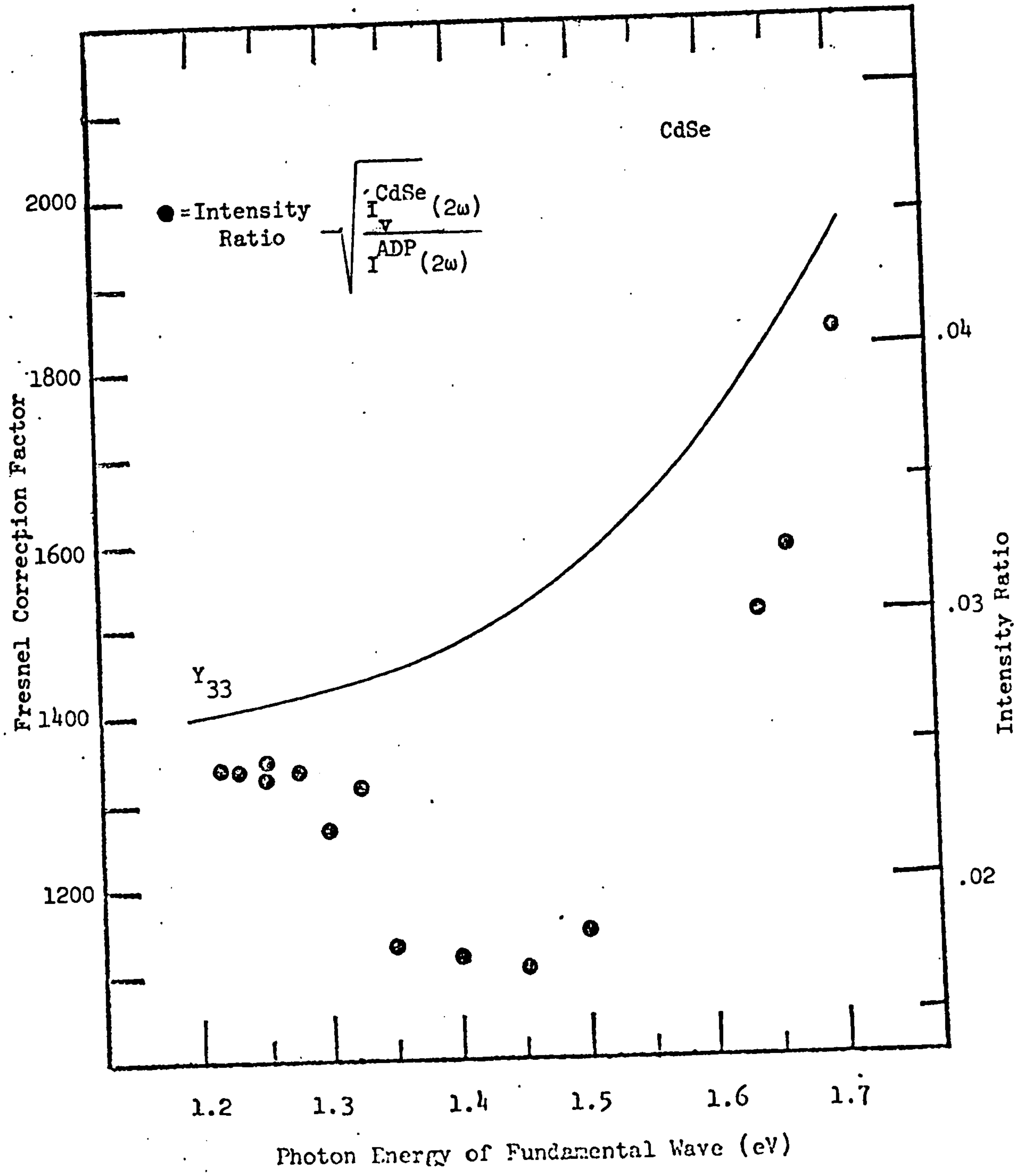

Figure 4.8

The Fresnel Correction Factor and the Measured Intensity Ratio for χ_{33} as a Function of Photon Energy of the Fundamental Wave CdSe

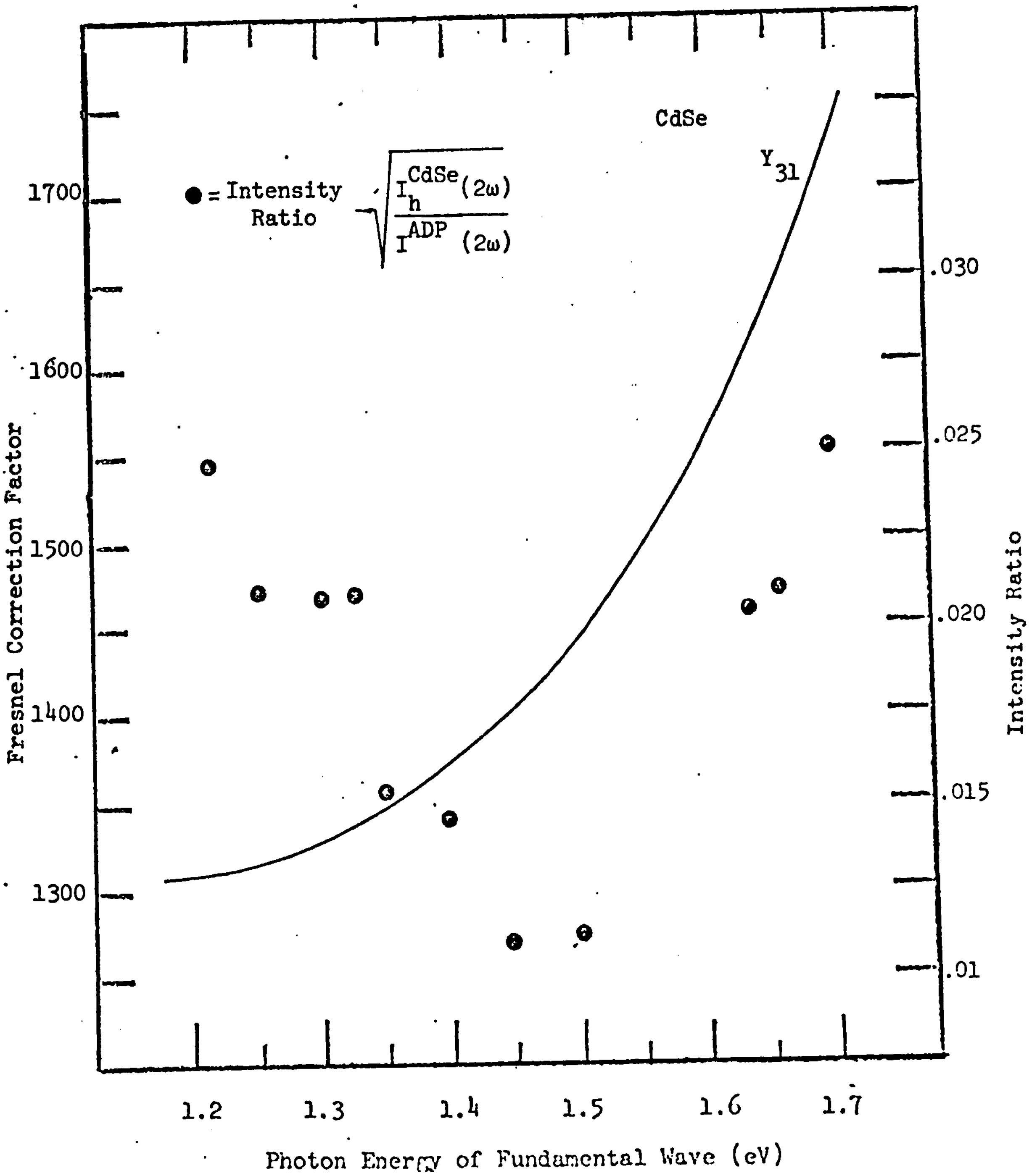

Figure 4.9

The Fresnel Correction Factor and the Measured Intensity Ratio for X_{31} as a Function of Photon Energy of the Fundamental Wave

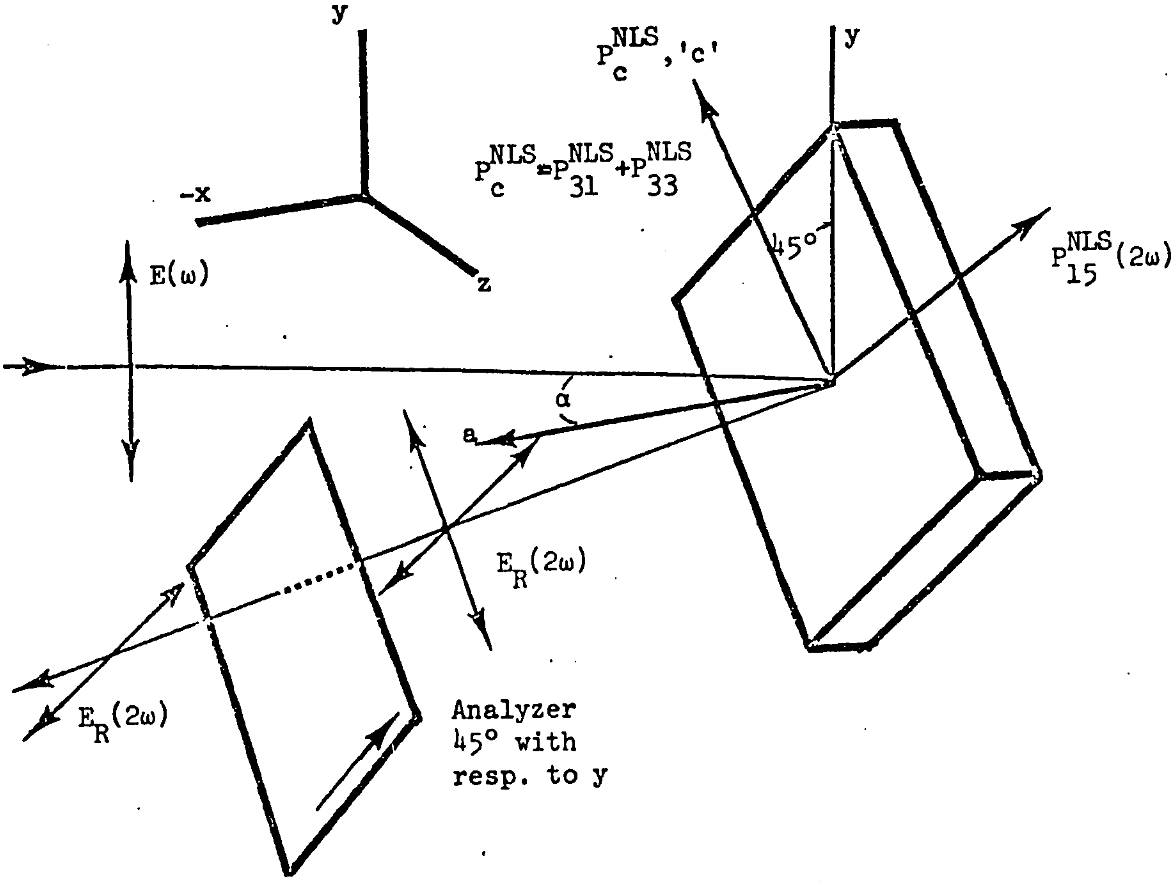

The error in the measurement of $P_{15}^{NLS}(2\omega)$ from $P_c^{NLS}(2\omega)$ when the 'c' axis is 45° with respect to the vertical and α is the angle of incidence is

$$e = \frac{(\cos^2\alpha - 1)\,|P_c^{NLS}|}{(2 - \sin^2\alpha)\,|P_{15}^{NLS}|}$$

$$\text{if } \alpha = 14° \text{ and } \left|P_c^{NLS}\right| = \left|P_{15}^{NLS}\right|$$

$$e = .029$$

Figure 4.10

The Experimental Crystal Orientation for the Measurement of the Modulus of the Nonlinear Susceptibility, χ_{15} for 6mm Materials.

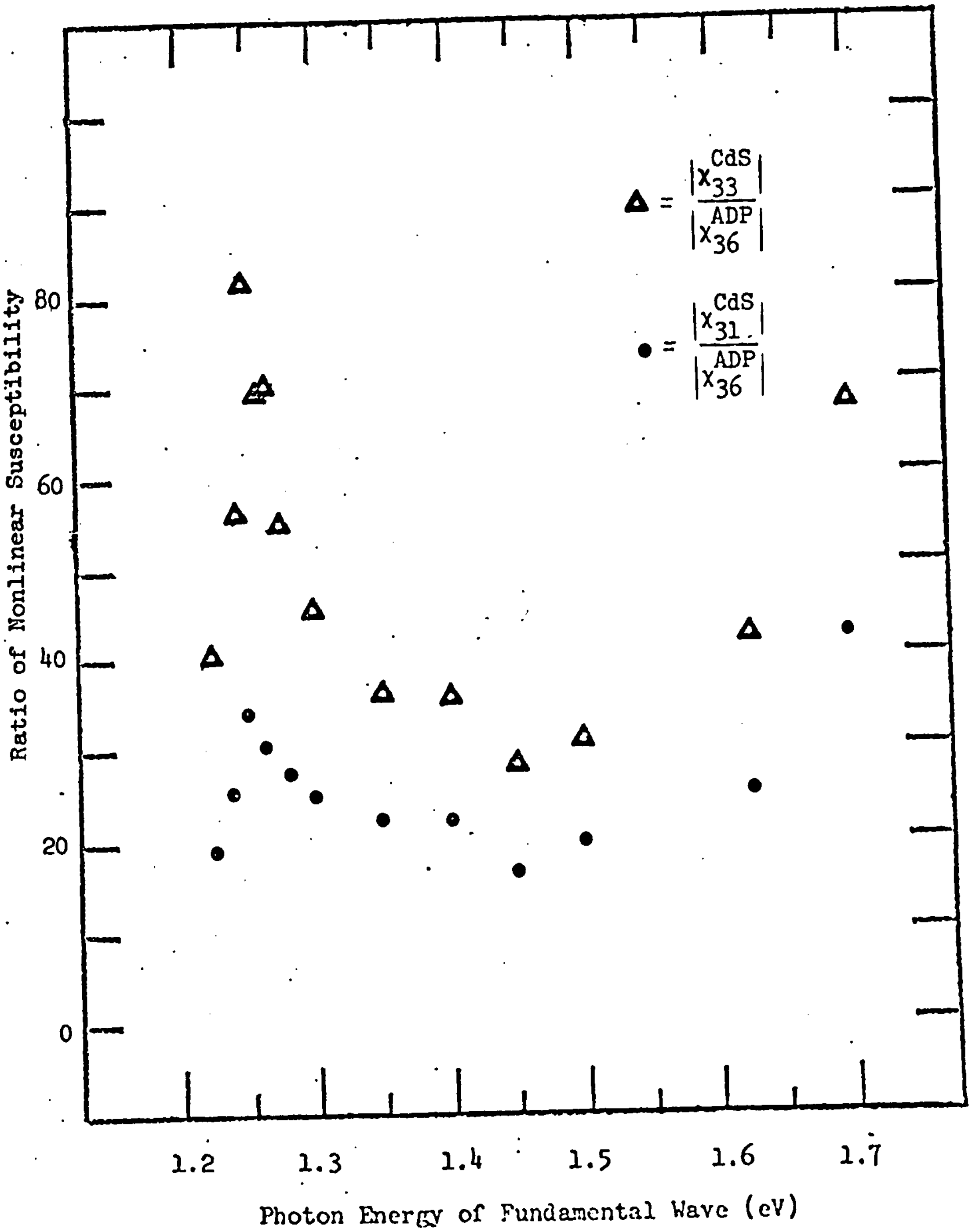

Figure 4.11

The Moduli of the Nonlinear Susceptibility for CdS as a Function of the Photon Energy of the Fundamental Wave

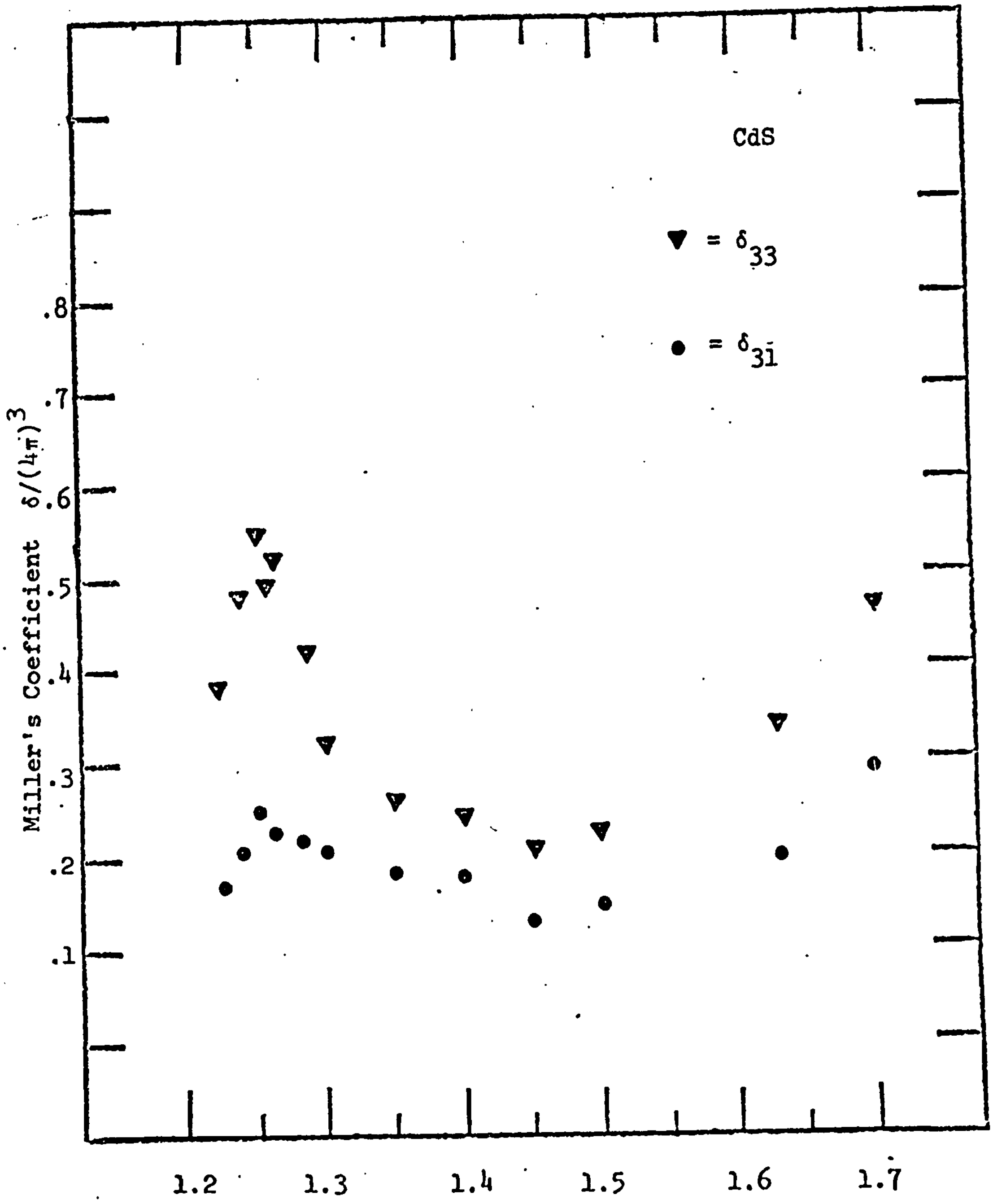

Figure 4.12

Miller's δ_{33} and δ_{31} as a Function of Photon Energy of the Fundamental Wave, CdS (in units of $3\text{X}10^{-9}$ esu)

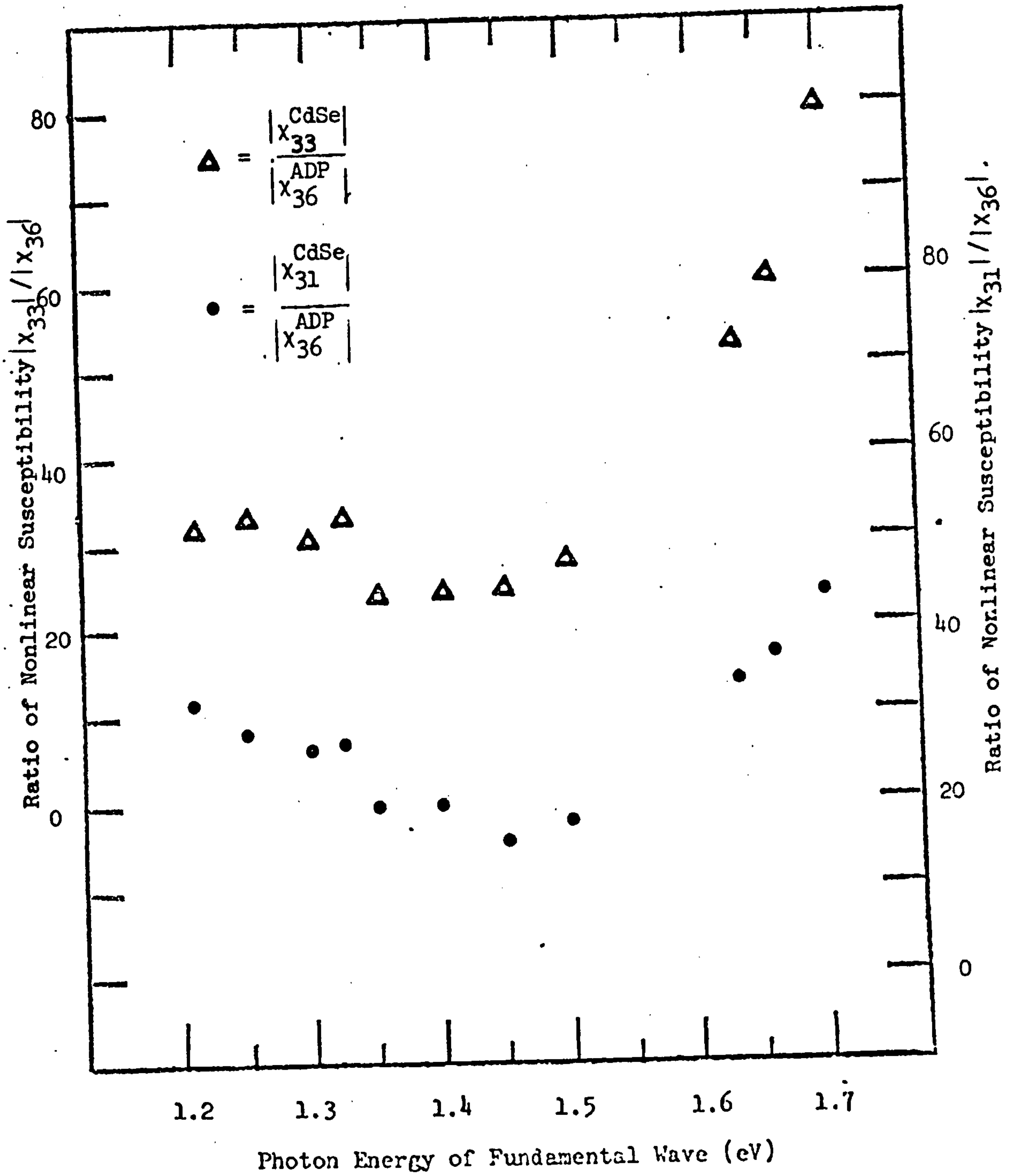

Figure 4.13

The Moduli of the Nonlinear Susceptibility for CdSe as a Function of Photon Energy of the Fundamental Wave.

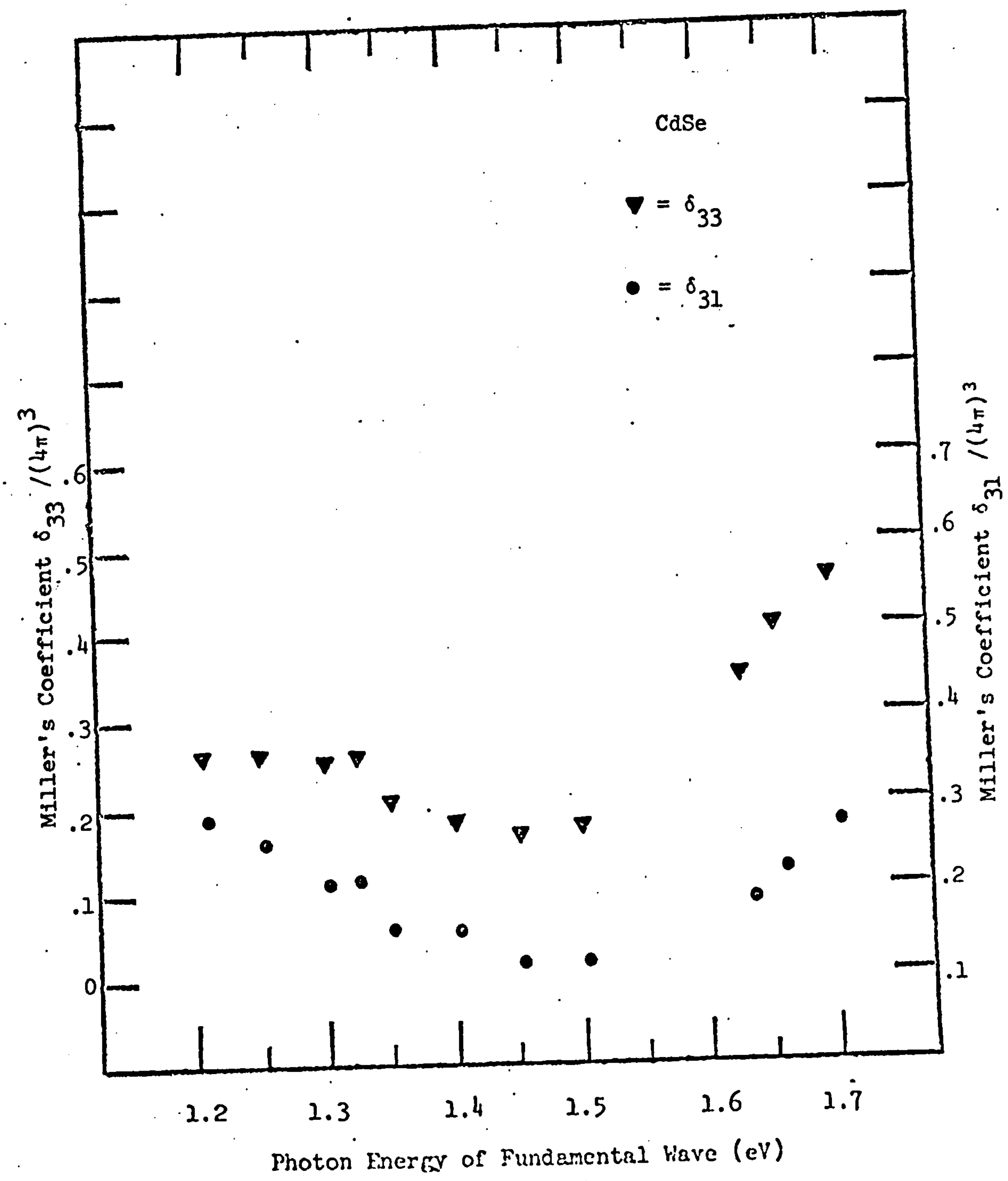

Figure 4.14

Miller's δ_{33} and δ_{31} as a Function of Photon Energy of the Fundamental Wave, CdSe.

(in units of $3X10^{-9}$ esu.)

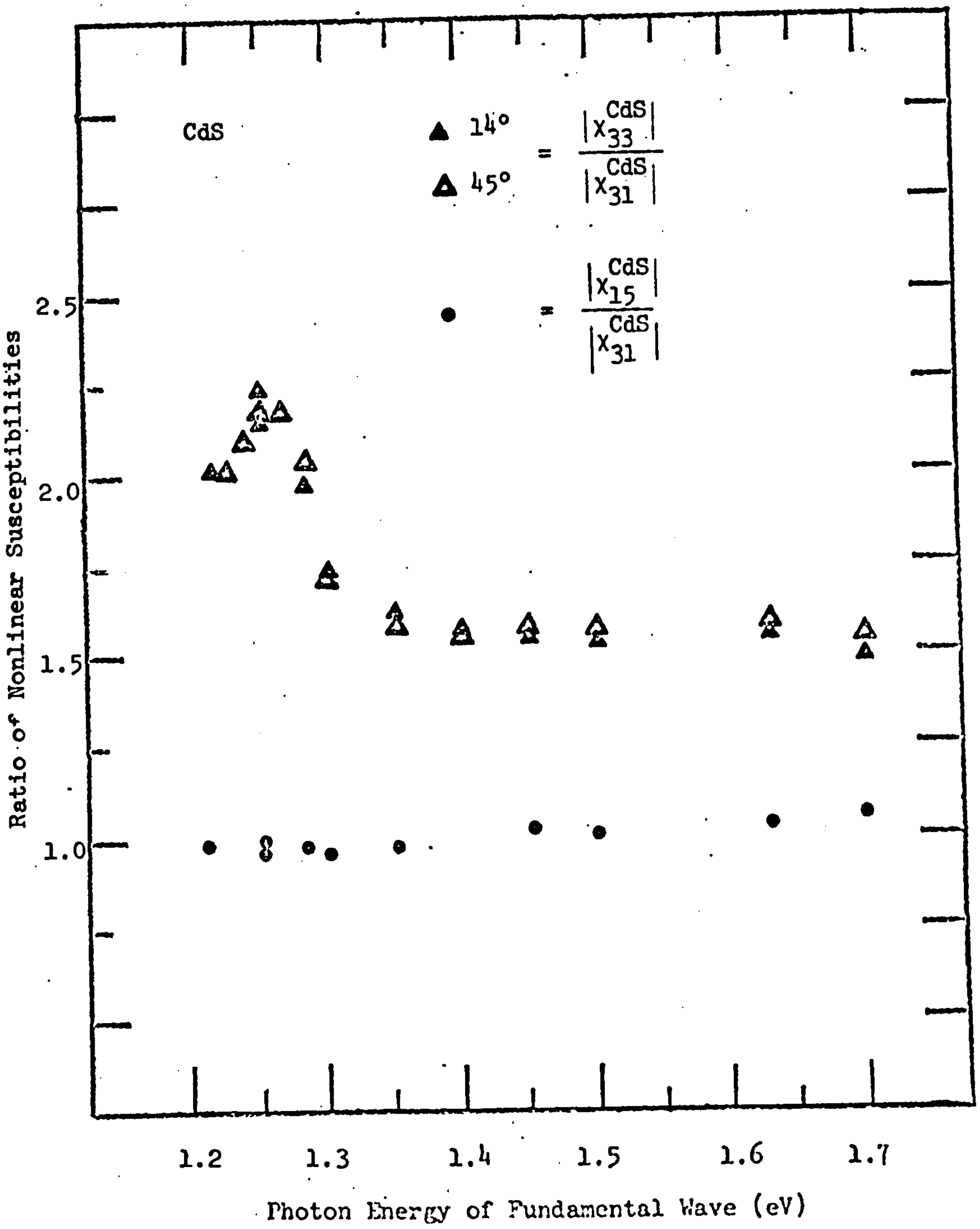

Figure 4.15

Ratio of the Moduli of the Nonlinear Susceptibilities of CdS as a Function of the Photon Energy of the Fundamental Wave.

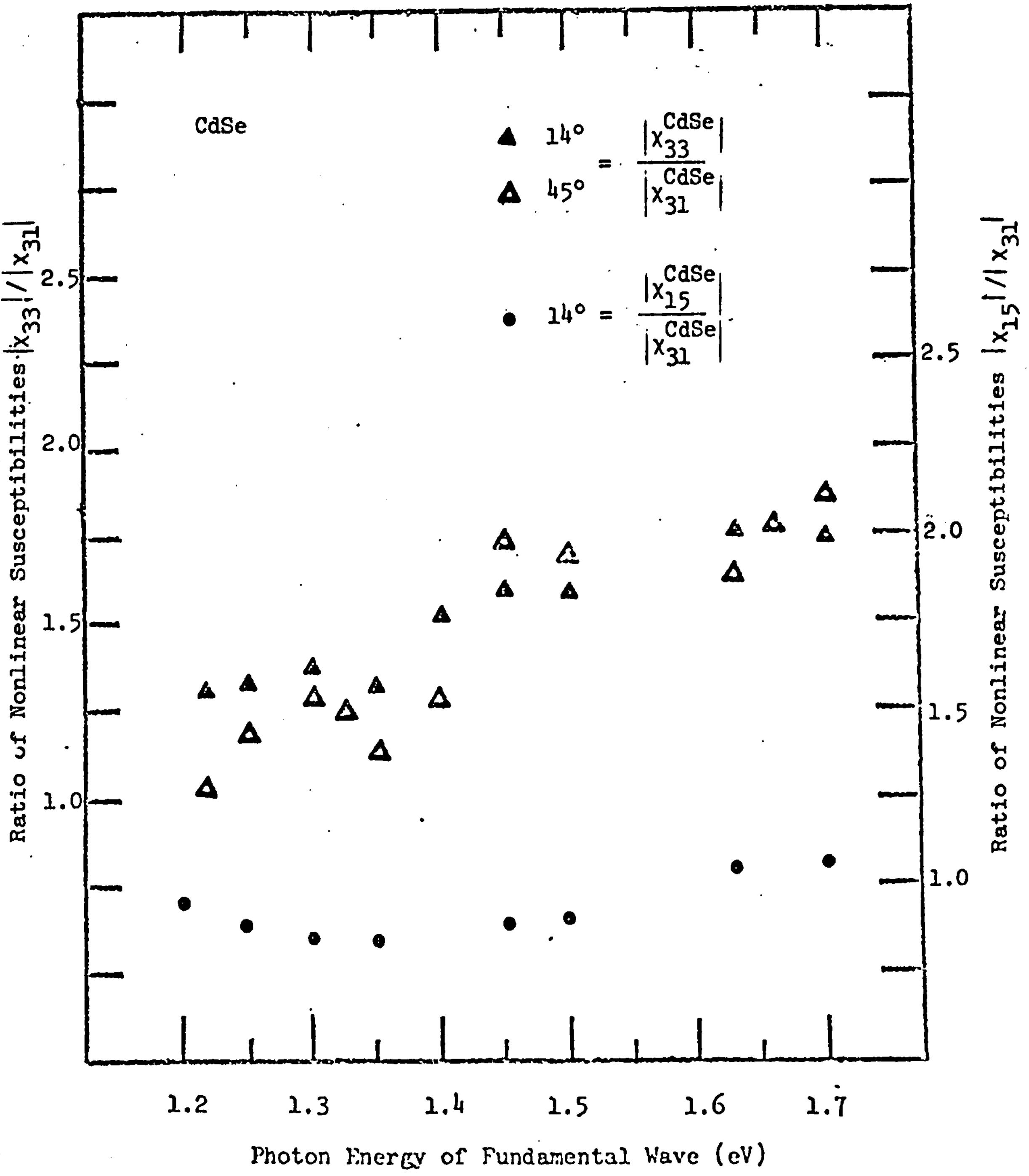

Figure 4.16

Ratio of the Moduli of the Nonlinear Susceptibilities of CdSe as a Function of the Photon Energy of the Fundamental Wave

Chapter 5

Measurement of the Relative Sign of the Wurtzite Nonlinear Coefficients for CdS and CdSe.

5.1 Introduction

In Chapter 4 the dispersion of χ_{33}, χ_{31}, and χ_{15} were measured for CdS and CdSe. Nothing was said about the relative phase angle ϕ of the coefficients, $\chi = |\chi| e^{i\phi}$.

The nonlinear susceptibility is in general complex when the material absorbs at the fundamental and/or second harmonic. The imaginary part of the nonlinear susceptibility is not related to the absorption in the material, as the imaginary part of the linear susceptibility is. Instead it introduces a phase shift between the fundamental frequency electric field and the second harmonic.

Recently the problem of the sign has become an interesting topic since several authors (Robinson 1968, Levine 1969,70, and Phillips and Van Vechten, 1970) have predicted the signs of the nonlinear coefficients for all zinc-blende and wurtzite materials. Robinson (Robinson, 1968) predicted, as was discussed in Chapter 4 $\frac{\chi_{33}}{\chi_{31}} = -2$ and $\frac{\chi_{15}}{\chi_{31}} = 1$ from purely geometric arguments. Only ZnO had an absolute sign opposite to that given by theory. In fact, this recent observation led to a better understanding of the contributions to the nonlinear susceptibility in semiconductors (Levine, 1970). It was from this perspective that a quest for the relative signs of the nonlinear coefficients χ_{15}, χ_{31} , and χ_{33} was undertaken for the materials CdS and CdSe.

Two authors (Miller and Nordland, 1970) have recently measured the absolute phase angle for two of the three nonlinear susceptibilities in CdS and CdSe. These measurements were done at 1.06μ. CdS is transparent at $\hbar\omega$ and $2\hbar\omega$. The results for CdSe were "difficult to analyze" due to absorption at $2\hbar\omega$. Their technique was basically an interference technique identical to the procedure first used by Chang et. al. (Chang, Ducuing and Bloembergen, 1965a).It involved using two crystals one whose sign is to be determined and another whose sign is known. The second harmonic generated from the unknown was passed through the "known" crystal along with the original fundamental beam. The harmonic generated from the "known" crystal then interfered with the harmonic from the "unknown". The relative phase between the two waves could be altered by changing the effective optical path length between the two nonlinear crystals. Variable optical path was achieved by placing both crystals in an evacuated chamber and filling with a gas. The optical path was altered by changing the pressure of the gas. Clearly this was quite a project since the temperature and pressure must be monitored while the maxima and minima in the total in the total harmonic signal are measured.

However, to measure the <u>relative</u> phase angle among the nonlinear coefficients, the author has devised a <u>new</u> technique. This technique is particularly useful when the crystal absorbs $2\hbar\omega$ or both $\hbar\omega$ and $2\hbar\omega$. It is much simpler than the previously described technique. The new technique does not require a second nonlinear crystal or a means of changing the effective optical path length. Its disadvantage is that it measures only the relative phase of the coefficients. For testing Robinson's relationships $\frac{\chi_{33}}{\chi_{31}} = -2$ and $\frac{\chi_{15}}{\chi_{31}} = +1$ this is all that is necessary.

The experiment will now be described.

5.2 The Experimental Technique.

The new technique makes use of the interference among the P^{NLS} produced by each of the nonlinear coefficients within the crystal itself. This was done by rotating the crystal about its face normal ("a" axis). A qualitative idea as to how the sign measurement was made can best be described by referring to Figure 5.1.

Figure 5.1 shows the three possible effective polarizations (P^{NLS}_{eff}) that would result by various combinations of relative signs for the three independent $\chi^{\mu L}$. The effective nonlinear polarization is produced by the vector sum of the three contributions χ_{15} , χ_{31} , and χ_{33} to the nonlinear polarization. If an analyzer were placed perpendicular to the plane of reflection as is shown in Figure 5.1c, no second harmonic would be observed (for the θ shown in the diagram). This would not be true of the situations shown in Figures 5.1a and 5.1b. It is this kind of cancellation among the nonlinear susceptibility components that is the essance of the technique.

If the crystal were rotated about its face normal, the angular dependence of the harmonic intensity polarized perpendicular and parallel to the reflection plane will imply the relative signs of the nonlinear coefficients. Figures 5.2 and 5.3 show the harmonic intensity versus angle of rotation for the three distinct possibilities of the relative signs among the nonlinear susceptibilities. These curves are not corrected for variations in the linear susceptibility as a function of angle of rotation. This correction would be necessary in the final analysis.

The measured intensity distributions are analyzed in terms of the nonlinear reflection laws outlined in Chapter 4. The angular dependence for the nonlinear source polarization, $P^{NLS}(2\omega, \theta)$, was given in equation 4.2. The electric field at the second harmonic was then proportional to:

eq. 5.1 $$E_R(2\omega,\theta) = \frac{V_2\,(n_r \times u_1) - v_1\,(n_r \times u_2)}{n_r \cdot (u_1 \times u_2)}$$

where the quantities were described by equations 4.7, 4.9, 4.10 and F.4 (from Appendix F). These relationships take into account the dependence of the linear dielectric constants on angle, as one should for uniaxial crystals.

The angular dependence of the second harmonic intensity from CdS and CdSe was studied. The linear dielectric constant data used was obtained from Cardona and Harbeke as in Chapter 4. The angular dependence for CdS was studied at two photon energies 1.7 and 1.25 eV (fundamental). The 1.25 eV energy was chosen since 2 is resonant to the exciton energy. Using the appropriate ratios $\frac{|\chi_{15}|}{|\chi_{31}|}$ and $\frac{|\chi_{33}|}{|\chi_{31}|}$ obtained in Chapter 4, the theoretical were fitted to the measured intensity distributions. The same done for CdSe at 1.7 eV.

5.3 The Discussion of Experimental Results

Figure 5.4 shows, at $\hbar\omega = 1.7$ eV, the angular dependence of the second harmonic intensity for CdS polarized horizontally in the reflection plane. Figure 5.5 shows the case for vertically polarized harmonic radiation. The fundamental light impinged at 45° angle of incidence. The data was fitted assuming the relative phase shifts between χ_{31} and χ_{15} was 0°, and between χ_{31} and χ_{33} was 180°. This assumption is in accord with Robinson's theory. The magnitudes of their ratios $\frac{|\chi_{15}|}{|\chi_{31}|}$ and $\frac{|\chi_{33}|}{|\chi_{31}|}$ were taken to be 1.07 and 1.5, respectively (see Chapter 4). The good fit between theory and experiment implies that the relative phase shift assumptions are justified.

The angular dependence of harmonic intensity at 1.25 eV (fundamental) for CdS is shown in Figure 5.6 for parallel polarization and in Figure 5.7 for perpendicular polarization. The data was fitted by assuming the relative phase shift between χ_{31} and χ_{15} was 0° and between χ_{31} and χ_{33} was 180°. The magnitudes of their ratios $\frac{|\chi_{15}|}{|\chi_{31}|}$ and $\frac{|\chi_{33}|}{|\chi_{31}|}$ were taken to be .95 and 2.25 respectively (see Chapter 4). Discrepancy exists between the theory and experiment. This is due to incorrect assumptions on the relative phase shifts, which must have changed in going from 1.7 to 1.25 eV.

The angular dependence of the harmonic intensity at 1.7 eV (fundamental) for CdSe is shown in Figure 5.8 for parallel polarization and in Figure 5.9 for perpendicular polarization. Again the data was fit assuming the relative phase shifts between χ_{31} and χ_{15} was 0° and between χ_{31} and χ_{33} was 180°. The magnitudes of their ratios $\left|\frac{\chi_{15}}{\chi_{31}}\right|$ and $\left|\frac{\chi_{33}}{\chi_{31}}\right|$ were taken to be 1.09 and 1.78, respectively (see

Chapter 4). Again we observe good fit between the theory and experiment. This justifies our assumptions on the relative phase shifts.

These results are the first measurements of the relative phase shifts between χ_{15} and χ_{31} in CdS and CdSe. For CdS and CdSe at 1.7 eV the phase difference between χ_{15} and χ_{31} was found to be zero. This verifies Robinson's relationship $\chi_{15} = \chi_{31}$.

In addition, the results of Miller and Nordland (1970) have been verified. The relative phase shift between χ_{33} and χ_{31} was found to be 180° for CdS and CdSe at 1.7 eV. Robinson's other relationship $-2 \cdot \chi_{31} = \chi_{33}$ has also been verified further.

In CdS at 1.25 eV it has been shown that the phase relationships that held at 1.7 eV are no longer true. At this photon energy there is large absorption due to the exciton lines.

Summarizing further, a new and simple technique has been demonstrated for measuring the relative phase shifts of the χ^{NL} for wurtzite materials.

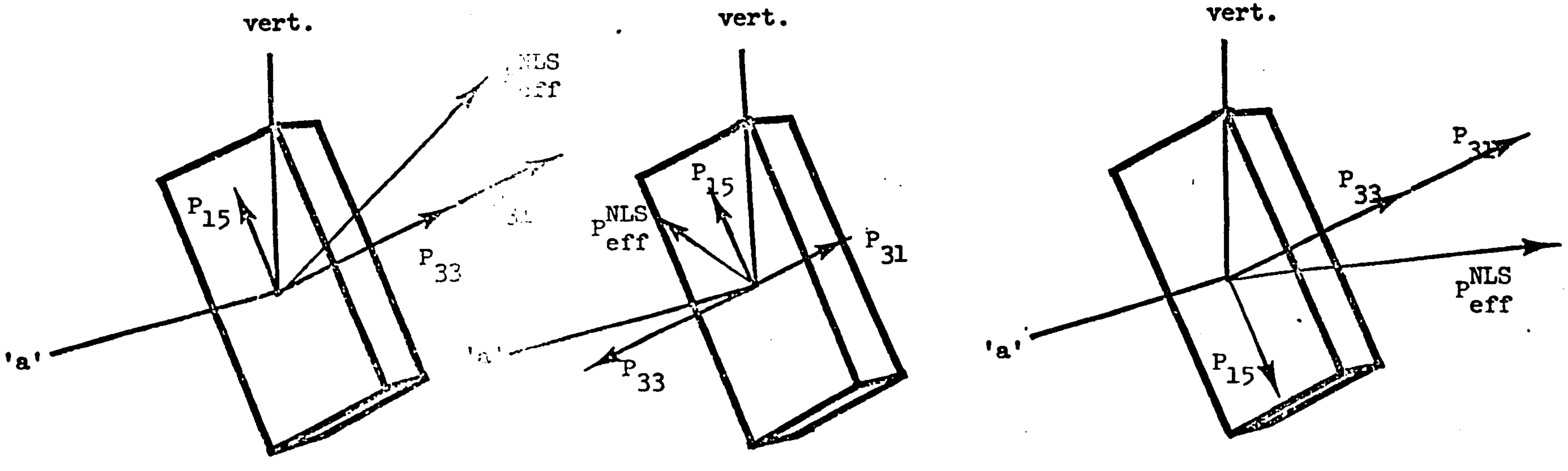

(a) (b) (c)

P_{33} is the nonlinear polarization arising from χ_{33}, P_{31} from χ_{31} etc.

Figure 5.1

The Vector Addition of the Three Seperate Nonlinear Source Polarizations assuming:

a) The Three Nonlinear Coefficients have the same sign.

b) χ_{33} and χ_{31} have Opposite Signs but χ_{15} and χ_{31} do not.

c) χ_{33} and χ_{31} have the Same Sign but χ_{15} and χ_{31} do not.

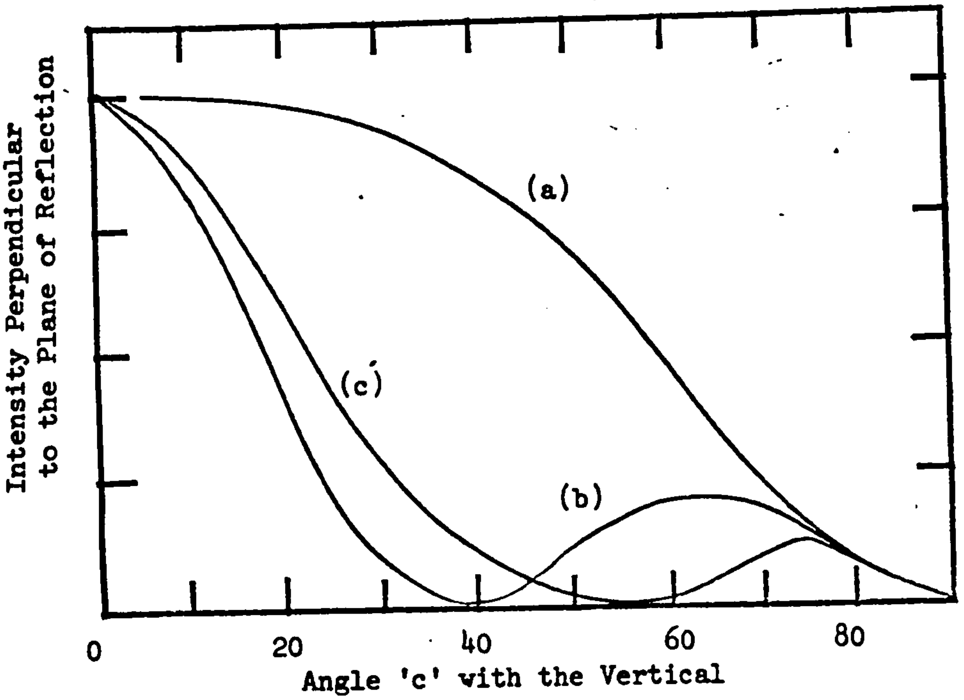

Figure 5.2

Relative Intensity as a Function of Angle for the 3 Cases Mentioned in Figure 5.1

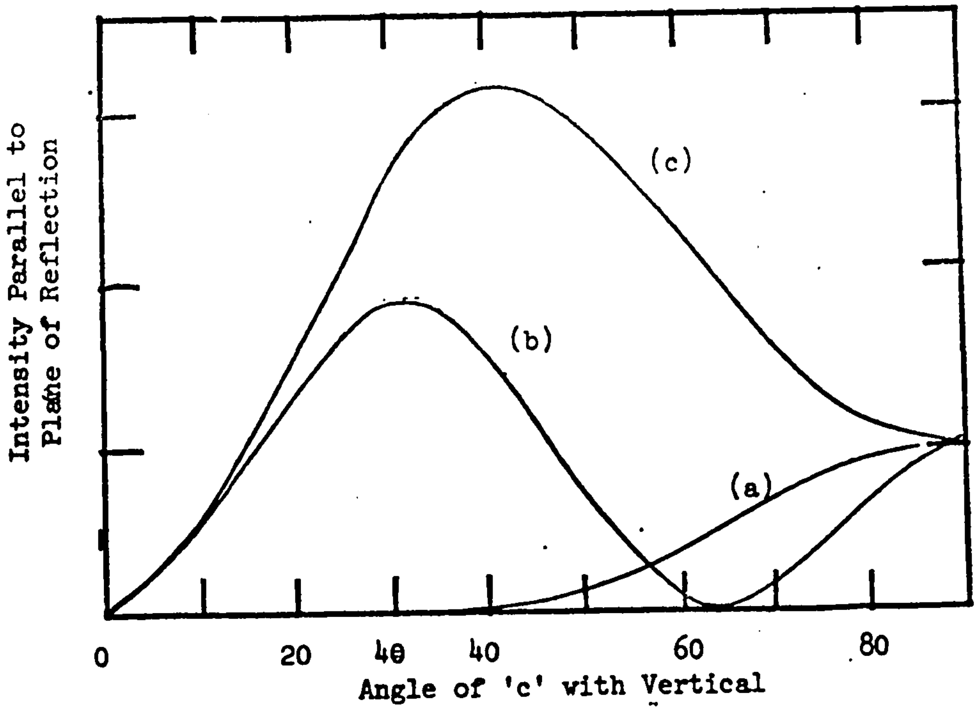

Figure 5.3

Relative Intensity as a Function of Angle for the 3 Cases Mentioned in Figure 5.1

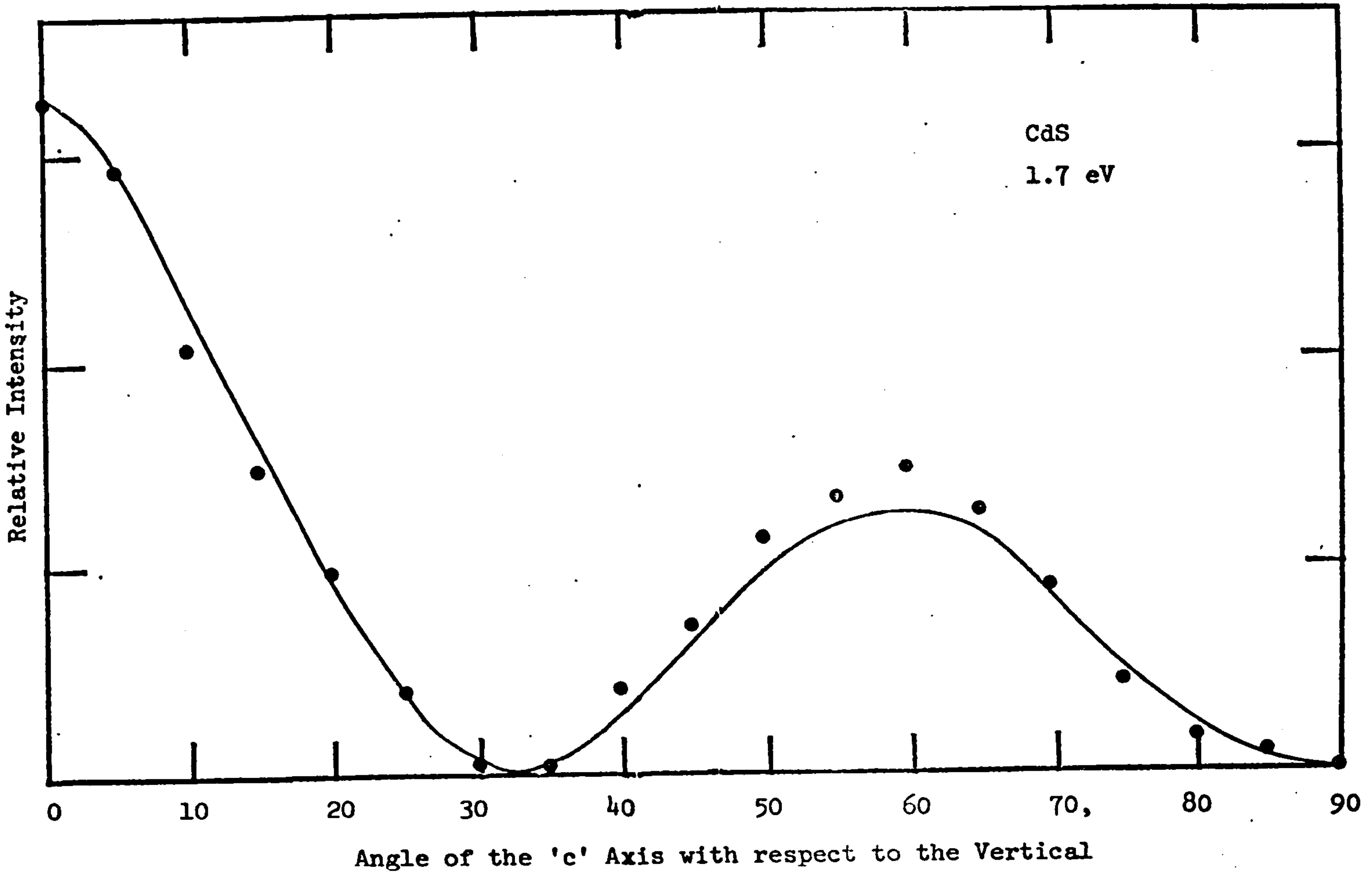

Figure 5.4

The Relative Intensity of the Second Harmonic Perpendicular to the Plane of Reflection for CdS as a Function of the Angle of the 'c' Axis with respect to the Vertical (1.7 eV)

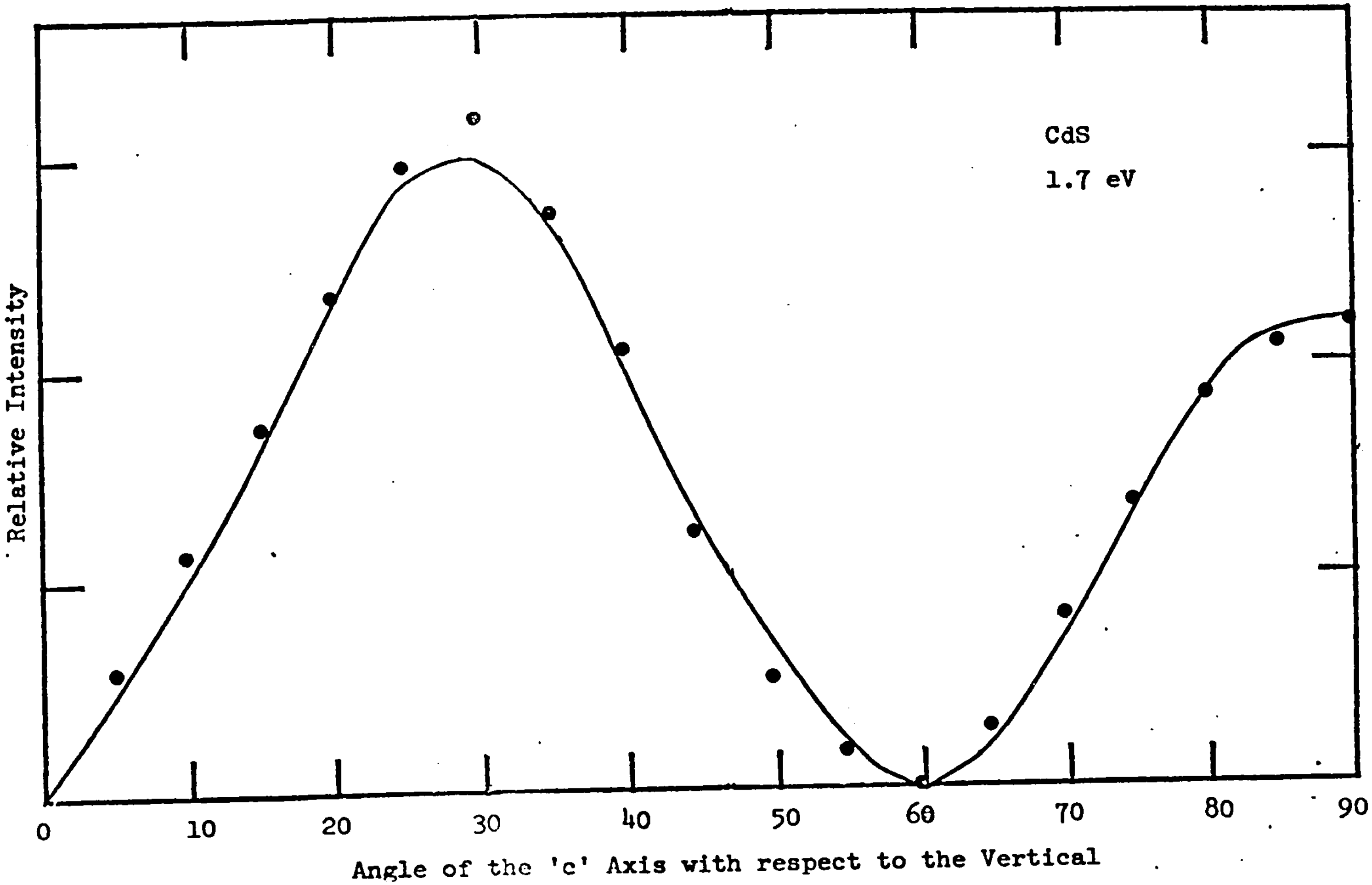

Figure 5.5

The Relative Intensity of the Second Harmonic in the Plane of Reflection for CdS as a Function of the Angle of the 'c' Axis with respect to the Vertical (1.7 eV)

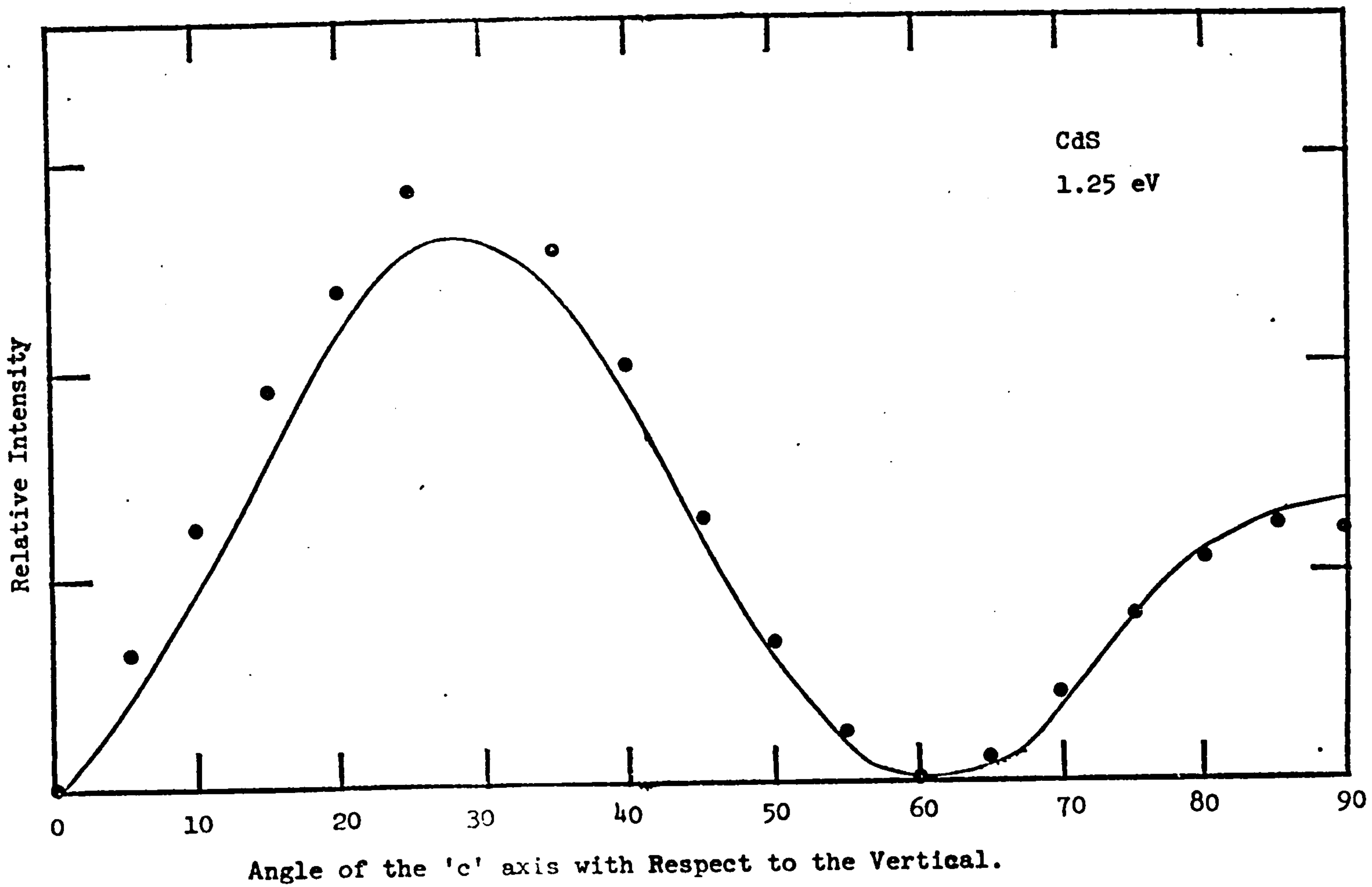

Figure 5.6

The Relative Intensity of the Second Harmonic in the Plane of Reflection for CdS as a Function of the Angle of the 'c' Axis with respect to the Vertical. (1.25 eV)

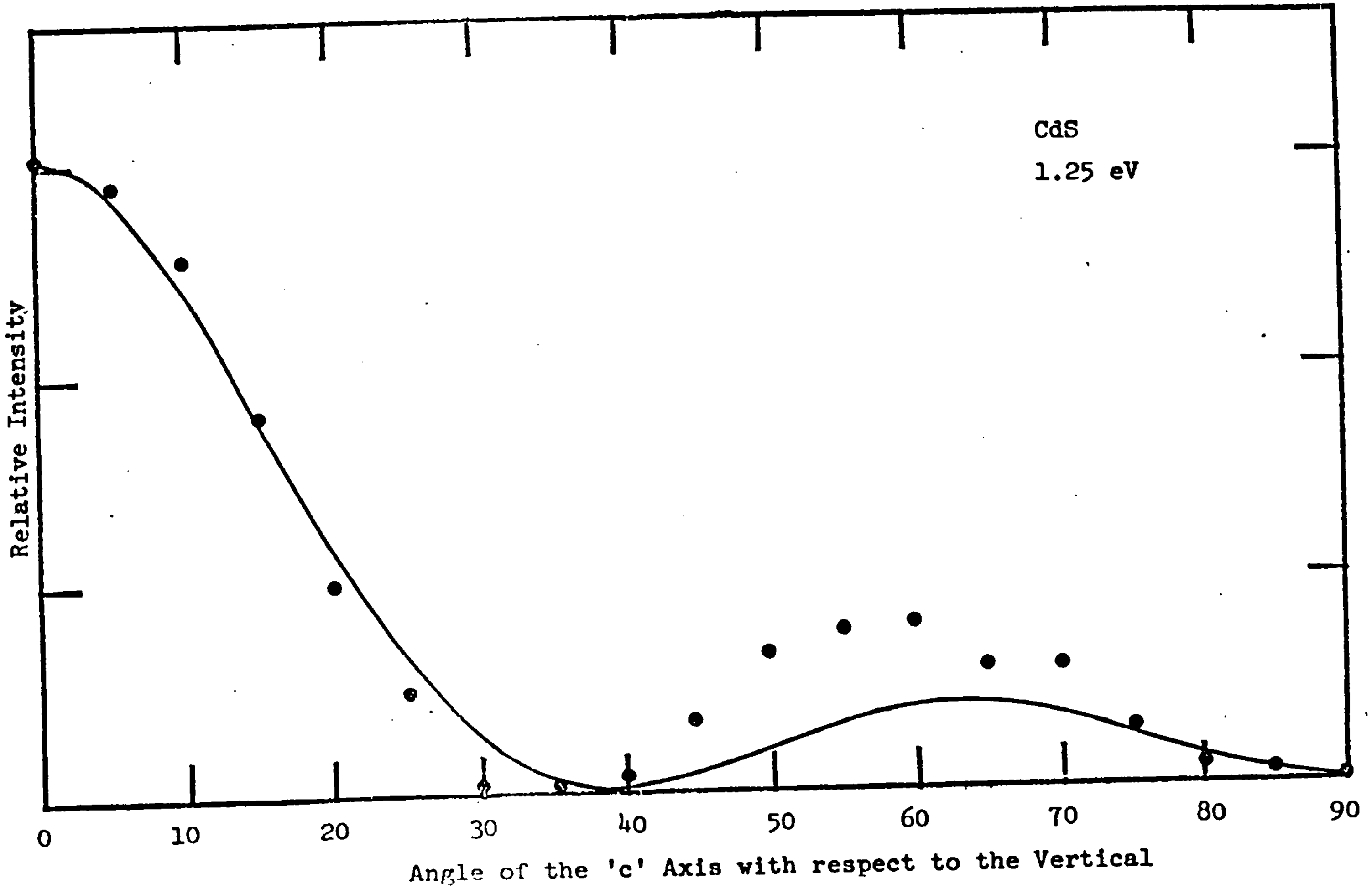

Figure 5.7

The Relative Intensity of the Second Harmonic Perpendicular to the Plane of Reflection for CdS as a Function of the Angle of the 'c' axis with respect to the Vertical (1.25 eV)

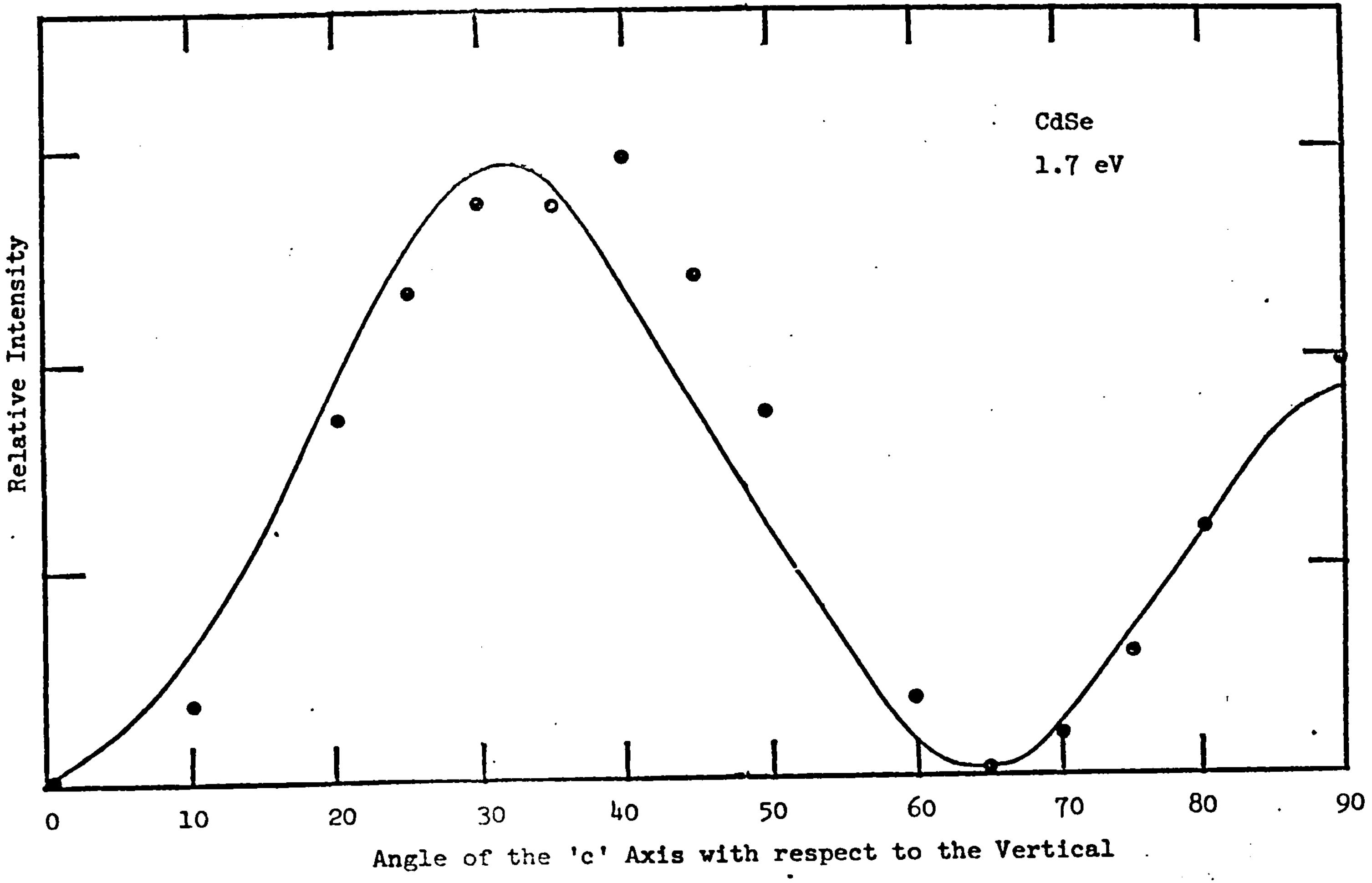

Figure 5.8

The Relative Intensity of the Second Harmonic in the Plane of Reflection for CdSe as a Function of the Angle of the 'c' Axis with respect to the Vertical (1.7 eV)

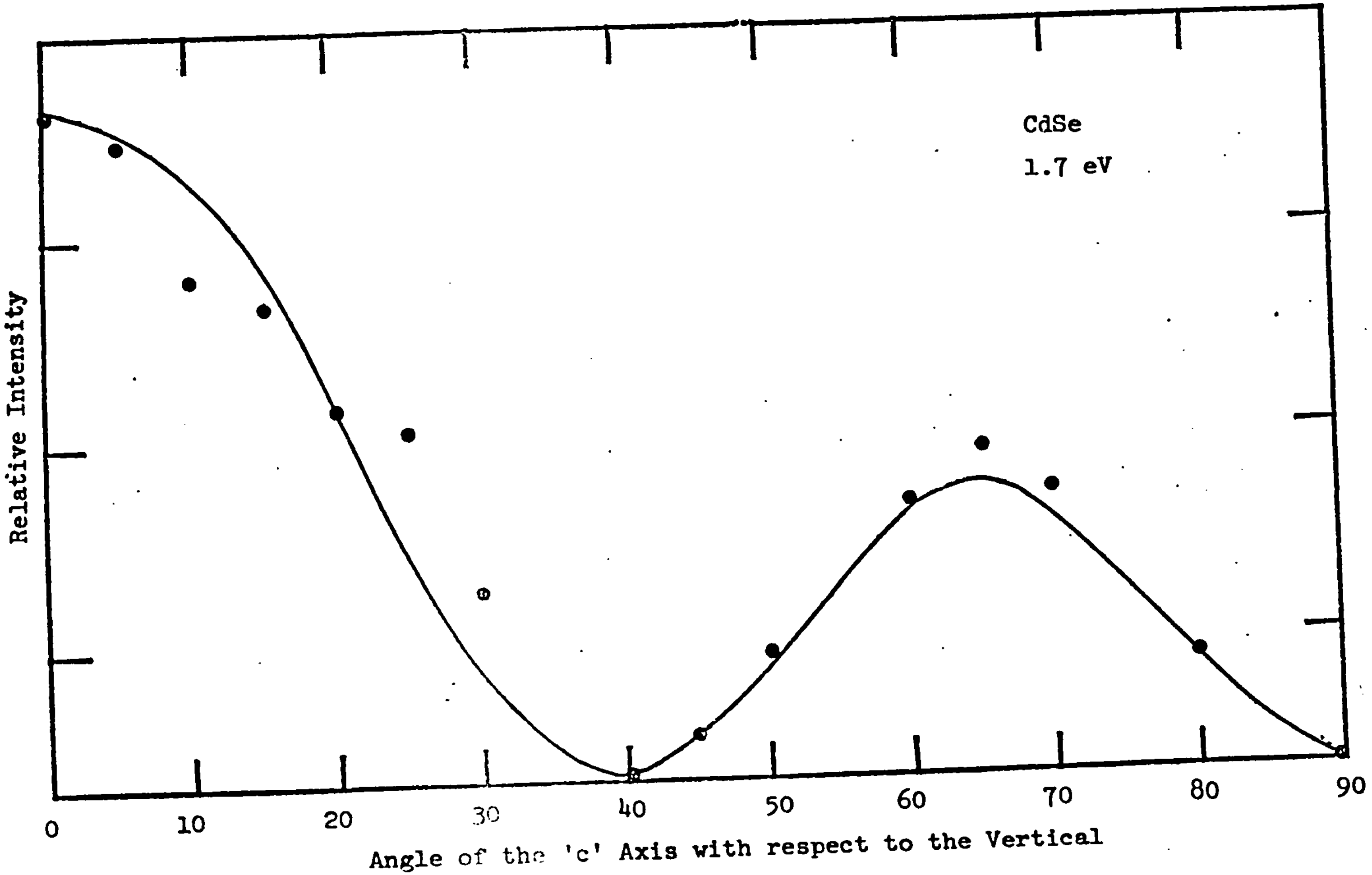

Figure 5.9

The Relative Intensity of the Second Harmonic Perpendicular to the Plane of Reflection for CdSe as a Function of the Angle of the 'c' Axis with respect to the Vertical (1.7 eV)

Chapter 6

Future Studies

Using a tunable high power laser many interesting nonlinear spectroscopic experiments can be performed.

One such experiment would be the measurement of the dispersion of the phase of the nonlinear susceptibility for zinc-blende and wurtzite materials.

Another experiment would be the measurement of the difference frequency, extending this work into the infared. The nonlinear susceptibility dispersion could be studied from 10μ to 1μ by optical difference mixing using a ruby and a dye laser and/or a frequency doubled Nd laser and a dye laser. The nonlinear susceptibility measurements performed on zinc blende and wurtzite materials could then be linked to their 10.6μ values as measured by other authors (Wynne and Bloembergen, 1969; McFee, Boyd and Schmidt, 1970).

The large peak in the nonlinear susceptibility of GaAs should be studied in more detail. The relation of doping and impurity effects to the nonlinear susceptibiility, as seen in the linear reflectivity data, should be studied.

Lowering the temperture of CdS would enhance the exciton structures. Studing the nonlinear susceptibility dispersion near the exciton structure would help in the overall understanding of the nonlinear properties.

With the help of a mode locked dye laser, measurements of the third order optical nonlinear susceptibility would be readily feasible. Such coefficients are of interest in materials where inversion symmetry does not allow second order effects. Recent theoretical work (Levine, 1969) has predicted the values of these coefficients, again in the crystal transparency region. Frequency dispersion measurements might give aid to the theoretical understanding of the nonlinear properties of these materials.

The dispersion of the nonlinear susceptibility is now being studied further into the visible region of the spectrum. A frequency doubled ruby laser is used to pump the dyes. Tunable emission in the .4 to .7μ region has been achieved. It will be interesting to study the nonlinear susceptibility behavior for wurtzite materials such as CdS deeper into the absorption region. The dispersion of χ_{33} χ_{31} and χ_{15} further into the absorbing region might tell more about the bond polarizablilty contributions to the nonlinear susceptibility.

Appendix A

Notes on the Dye Laser

In the range of 1.7 to 1.2 eV six polymethine dyes have been used.

It has been reported (Sorokin, Lankard, Hammond, and Moruzzi, 1967) that the efficiencies of these dyes as lasers is highest when then are dissolved in dimethyl sulfoxide (DMSO). This is the only solvent used in this work. Care should be exercised when working with this solvent. The solvent is rapidly absorbed by the skin, taking with it all materials dissolved in it (such as polymethine dyes). Since the toxic properties of these dyes have not been throughly investigated, one should wear disposable rubber gloves when handling DMSO as a solvent.

The polymethine dyes were all contained in standard absorption cells. The cell path was chosen to be 5 cm in most of the dyes. Two dyes lased better in 1 cm cells. This can be explained by looking at the absorption spectra of the "host" DMSO itself. It contains several absorption peaks. One is at .9 μ , another at 1.0 μ . Both are about .06 μ broad. Using a short absorption cell lessens the absorption near these wavelengths and improves the dye laser efficiency. It was noticed that when dyes 10 and 11 (see Table A.1) were pumped in 5 cm cells the schlieren effects were so bad as to cause lasing to cease after one or two laser shots. A 1 cm cell helped minimize this, although flowing the liquid dye would do the same.

Focusing the ruby laser beam was also necessary for dyes 10 and 11 since the thresholds for these dyes, when in 1 cm cells, (irregardless of the concentration) were observed to be higher than the other dyes in 5 cm cells.

The dyes were obtained from Koch Light Ltd., Colnbrook, Bucks, England; Gallard-Schlesinger Chem. Co., New York; and Nippon Kankoh-shikiso Kenkyusho, Okayama, Japan.

The author would like to report a deficiency in the quality of the dyes obtained from Koch-Light. Dye 10 was reported to lase from 890 to 970 nm. The Koch Light version of this dye would not lase at all up to pumping powers of greater than 50 MW/cm^2. This was a direct contradiction to the Miyazoe and Maeda papers (Miyazoe and Maeda, 1968; Miyazoe and Maeda, 1970). The author also obtained a sample of dye 10 from Dr. Sorokin who had purchased his from Koch Light. This dye would not lase. Dr. Sorokin was not able to lase this dye either. Finally a sample of dye 10 was obtained from Nippon Kankoh-Shikiso Kenkyusho. This dye was strikingly different in color (green not gray-brown) and lased well from

890 to 970 nm. Since this called into question the purity of dye 10 from the other sources, absorption spectra were taken. It was observed that the absorption cross section for dye 10 obtained from Koch - Light was smaller than that of the sample from Nippon Kankoh-Shikiso Kenkyusho. It was also noted that the absorption tail of the Koch-Light dye was much longer. A complete analysis of the dye would have to be done with chromatography but it is likely that an impurity exists in the Koch-Light dye.

Koch-Light dye 11 lased, but not strongly, in the region 970 to 1020 nm. Efficiencies were a factor of 10 lower than those reported by Miyazoe and Maeda in 1968. This dye was a brownish-green in solution with DMSO. A sample of this dye was obtained from Nippon Kankoh-Shkish Kenkyusho. Its color was a brilliant green in DMSO. Absorption spectra comparing the Japanese dye to the Koch-Light dye showed features similar to those mentioned for dye 10. The Nippon Kankoh-Shikiso Kenkyusho sample lased efficiently in DMSO over a wavelength range 990 to 1020 nm. It is suggested that the dyes used for experiments in the future be obtained from the Japanese corporation.

Table A.1

DYE #*	CHEMICAL NAME	WAVELENGTH	PHOTON ENERGY	SUPPLIER	FOCUSING?	CELL PATH
1	3,3'-diethyl-2,2'-thiadicarbocyanine iodide	730-765	1.7-1.62	Koch-Light	No	5 cm.
2	3,3'-diethyl-2,2'-thiatricarbocyanine iodide	810-840	1.53-1.48	Koch-Light	No	5 cm.
4	3,3'-diethyl-2,2'-(4,5,4',5') dibenzo thiatricarbocyanine iodide	844-918	1.45-1.35	Koch-Light	No	5 cm.
10	1,1'-diethyl-2,2'-tricarbocyanine iodide	no lase	----	Koch-Light P.P. Sorokin	Yes,No	1-5 cm.
10	as above	885-970	1.4-1.28	Nippon K-S K.	Yes	1 cm.
11	1,1'-diethyl-4,4'-tricarbocyanine iodide	weak lase 970-1020	1.28-1.21	Koch-Light	Yes	1 cm.
11	as above	990-1020	1.25-1.21	Nippon K-S K.	Yes	1 cm.
17	1,3,3,1',3',3'-Hexamethyl-2,2'-indotricarbocyanine iodide	780-840	1.59-1.48	Gallard-Sch.	No	5 cm.

* as numbered by Miyazoe and Maeda, 1968

All wavelengths in nm. All Photon Energies in eV.

Appendix B

The Optical Filters

Traditionally a saturated acqueous solution of copper sulfate was used to seperate the second harmonic from its fundamental at .694 μ . A 65 mm path length of this solution offered the advantage of high attenuation of the fundamental ($T = 10^{-37}$ at .69μ) without large loss of the second harmonic ($T = 10^{-2}$ at .347μ). The absorption characteristics of a saturated copper sulfate solution (65 mm path) made this filter suitable for work from .7 to 1.1μ ($T = 10^{-37}$). Transmission at the second harmonic was quite high ($t = 10^{-2}$ to .7).

For other wavelength regions (from .41 to .69μ , fundamental) one would use other filters designated in Table B.1. The table shows the filters and their respective transmissions at the fundamental and second harmonic.

When studing second harmonics, one must be sure that the only light impinging on the sample is the desired frequency with no second harmonics present in the beam. To accomplish this a Corning CS-2-64 filter was used from .72 to 1.02 μ . For other wavelength regions, .35 to .69 μ filters listed in Table B.2 perform the task.

TABLE B.I

Filters to Attenuate the Fundamental

FILTER MATERIAL	TRANSMISSION (Fundamental)	TRANSMISSION (Second Harmonic)
$CuSO_4$ saturated (65 mm path)	$< 10^{-37}$ from .72 to 1.02	$> .15$ from .36 to .51
$CoCl_2$ saturated (65 mm path)	$< 6X10^{-33}$ from .68 to .56	$> .1$ from .28 to .34
UG-5* Glass (7 mm path)	$< 10^{-20}$ from .50 to .63	$> .1$ from .25 to .315
UV-R-220* (Interference filter)	$< 10^{-20}$ from .41 to .49	$> .1$ from .205 to .245

Table B.2

Filters to Attenuate the Second Harmonic

FILTER MATERIAL	TRANSMISSION (Fundamental)	TRANSMISSION (Second Harmonic)
Corning CS-2-64 (4 mm)	$> .8$ from .68 to 1.02	$< 10^{-5}$ from .34 to .51
GG-14* glass (4 mm)	$> .9$ from .53 to .69	$< 10^{-4}$ from .265 to .345
BG-38* glass (4 mm)	$> .9$ from .35 to .55	$< 10^{-5}$ from .175 to .275

* Manufactured by the Schott Glass Co.

Appendix C

The Pulse Amplitude Encoder

The pulse amplitude encoder is a charge integrating analog-to-digital converter. This unit replaced photographing the oscilloscope traces of the second harmonic signals and then manually measuring the pulse height or area.

This unit performed two main tasks. First, it integrated the total current from the photomultipliers which detected the optical second harmonic intensities. Second,it converted the value of integrated current to digital form. Integration was accomplished by a capacitor connected to the output of the photomultiplier. Conversion of this capacitor voltage to digital form was accomplished by an analog-to-digital converter.

The unit can be described as having five main parts; i) charge integrating electronics; ii) sample-hold and analog-to-digital converter; iii) semiconductor memory; iv) digital nixie tube display; and v) hardwired logic to sequence the above mentioned parts.

C.1 Charge Integrating Electronics

The integration of the photomultiplier's photocurrent uses a small capacitor. The total charge on the capacitor is directly proportional to the number of photoelectrons emitted from the photocathode times the gain of the photomultiplier. The capacitor voltage is sampled by a high impedance amplifier. The measured voltage is proportional to the number of photoelectron events.

The capacitor can take on two values. One capacitor value was chosen so that a digital "4" represented one photoelectron event. The other capacitor value was chosen so that 10 photoelectrons read "4" on the nixie tube readout. The design information needed for these capacitor values was: 1) 1 volt across the capacitor read full scale on the analog-to-digital converter (digit "1000" on the nixie tubes); and 2) the overall gain of the EMI 9635 QD photomultiplier tubes at 900 V was about 3.6 X 10^6.

To minimize dark current noise from the photomultipliers two precautions were taken. First, the capacitor was turned on just before the laser pulse and turned off at the end of the laser pulse. Second, the phototube chosen had a low dark count (10 photoelectrons per second).

The capacitor switching was accomplished by inserting in parallel with the capacitor a high impedance field effect transistor (FET) which acted as a high speed shorting switch (see Figure C.1). The electronics used were not fast enough to open the

FET at the beginning of a Q-switch pulse (approximately 50 ns total duration). Instead a trigger pulse, initiated by the laser flashlamp, opened the FET before the arrival of the Q-switch pulse. The Q-switch laser pulse itself was used to close the FET again. The open state time of the FET was measured by an internal clock. An internal register temporarily stored this time interval.

Due to the nature of the FET, a small amount of charge was placed on the capacitor when the switching occured. Furthermore dark current pulses could have placed some charge on the capacitor, although with small probability, during the FET open state. In order to overcome these effects, a logic circuit was designed two subtract these two effects. During the time immediately after a Q-switch pulse, the FET was opened a second time precisely as long as the FET was first opened when the Q-switch pulse occured. The capacitor charge acquired during this second FET open time is subtracted from the charge acquired during the first FET open state. This canceled the FET switching effect and possible dark current pulses. Only the photoelectron charges resulting from the harmonic radiation remained on the capacitor.

C.2 The Sample-Hold and Analog-to-Digital Conversion

There were two sample-hold circuits in the encoder. Each sample-hold circuit performed the task of sampling the output from the two operational amplifiers connected to the two charging capacitors. One charging capacitor was associated with the "signal" photomultiplier and the other charging capacitor was associated with the "monitor" photomultiplier. The voltages of the operational amplifiers were sampled at the end of the Q-switch pulse, and then sequentially transferred by a FET to the analog-to-digital converter (Hybird Systems model 501 10 bit converter). The sample hold circuits were then set to zero and resampling of the operational amplifier voltages occured for the subtract cycle mentioned above.

C.3 The Semiconductor Registers

To store the two digital information results a small semiconductor memory (local memory) is included in the encoder. The contents of this memory can be either erased or transferred. If the decision is made to transfer, a "manual data transfer" switch is activated. Then the contents of the local memory are numerically added to the contents of another memory (primary memory). If the decision is made to erase the contents of the local memory an erase button is activated. A "primary memory erase" button erases the contents of the primary memory. A "logic control" switch is also included on the front panel to allow the unit to automatically transfer the contents of the local memory to the primary memory after every laser pulse.

C.4 The Digital Display

Nixie tubes were employed to display the two digital results of the local memory, one for the "signal" and one for the "monitor" photomultiplier outputs. The display consisted of six digits for each digital result.

The tubes displayed positive numbers only. If, by chance, the subtraction cycle produced a negative number in the local memory, a special display light would indicate that fact. Negative could not be added to the primary memory.

In pratice, the contents of the local memory were displayed after each laser pulse. The data was then transferred by activating the "manual data transfer" switch. After numerous laser firings the accumulated contents of the primary memory could then be displayed by pushing a "reset" button.

C.5 The Hardwired Logic Control

The control and sequencing of events performed by the encoder was accomplished by the hardwired logic. This logic consisted of a series of clocks and "one shot" pulse generators which gate on and off the main parts of the unit. This logic kepts track of whether a laser pulse occured during the FET open state and also the sequencing of the sample-hold, analog-to-digital conversion and add-subtract cycles.

The operation of the unit begins (see Figure C.2) when the flashlamp is triggered. Both FET are closed. A "one shot" pulse generator provides the time delay before the FET is opened. This delay time is variable from the front panel of the unit. The Q-switch pulse usually occured 500 ± 50 microseconds after the flashlamp was triggered. This interval depended upon the concentration of the Q-switch solution, the voltage of the pump lamp, and the Q of the optical cavity.

After 450 microseconds delay time the FET is opened making the capacitors susceptible to charge. At the same time a 500 KC clock is set into operation. When a Q-switch pulse occurs, a 100 KC clock, caller the sequencer, is then set into operation. The sequencer activates the sample-hold circuits and stops the 500 KC clock. The total number of pulses from the 500 KC clock is thus proportional to the time the FETs were in the open state. This resultant number is stored in a register (A), as it will be needed for the subtraction cycle.

The sequencer then triggers the analog-to-digital converter to start digitizing the sample-hold voltage from the "signal" channel. The sequencer waits until this has been acomplished. If the signal did not "over range" (overload the analog-to-digital converter) the sequencer loads the digital information into the signal register (SR). The sequencer then throws the FET (on the input to the analog-to digital converter) and reperforms the same analog-to-digital conversion for the "monitor" channel. The result is stored in the monitor register.(MR). The sequencer now opens the FETs for a time equal to that stored by register (A). In this the subtraction cycle, the 500 KC is used again until the total number of counts from it equals the contents of register (A). The sequencer is now reset and restarted. It reperforms the sample-hold and analog-to-digital conversion cycle. Now though, the digital results are subtracted from the contents of the SR and MR. Both the 100 and 500 KC clocks, their counters,and the register (A) are reset to their original state. The sequence of events is now finished. Another "signal" and "monitor" pulse can now be so processed.

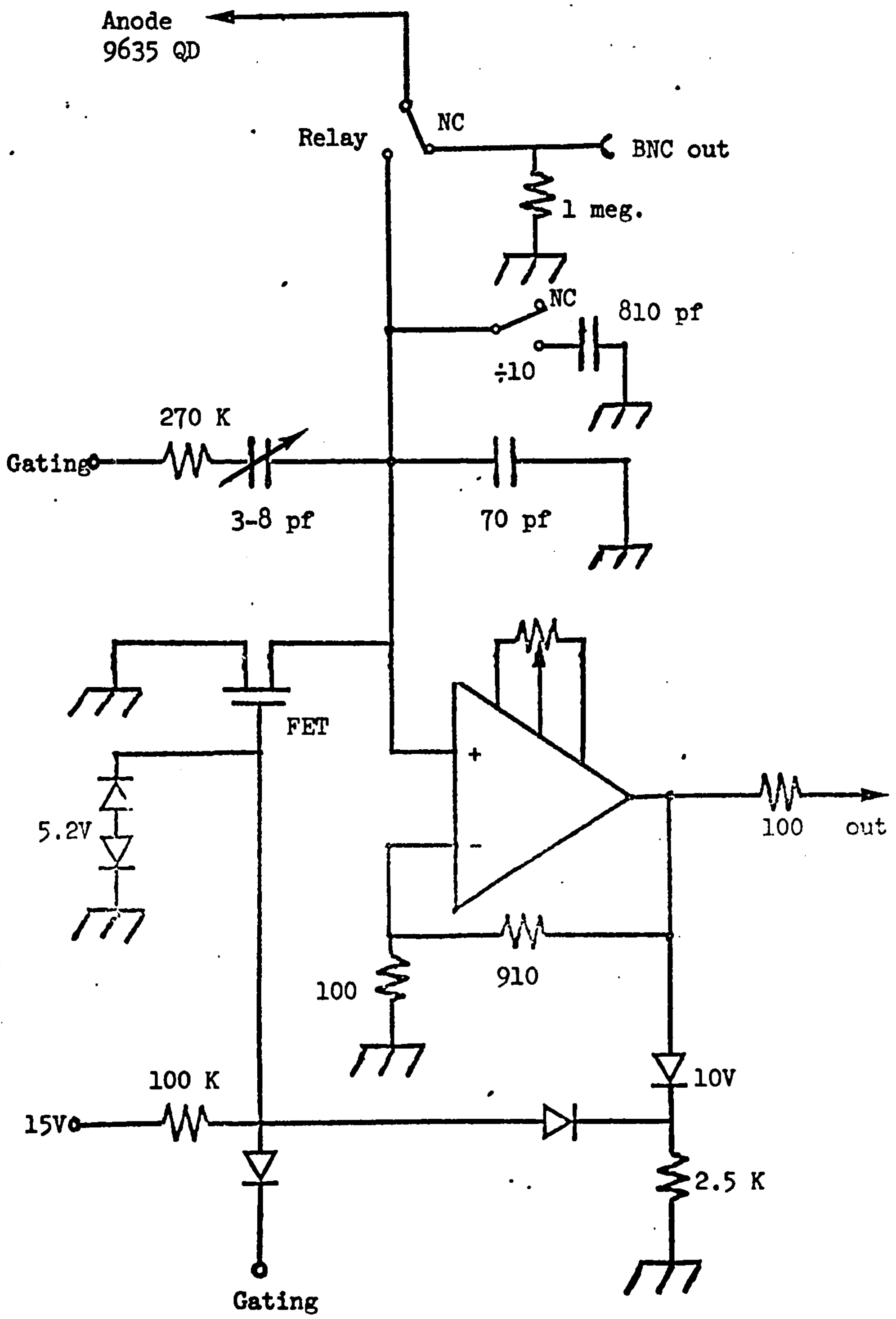

Figure C.1

Schmatic of Charge Integrate Electronics

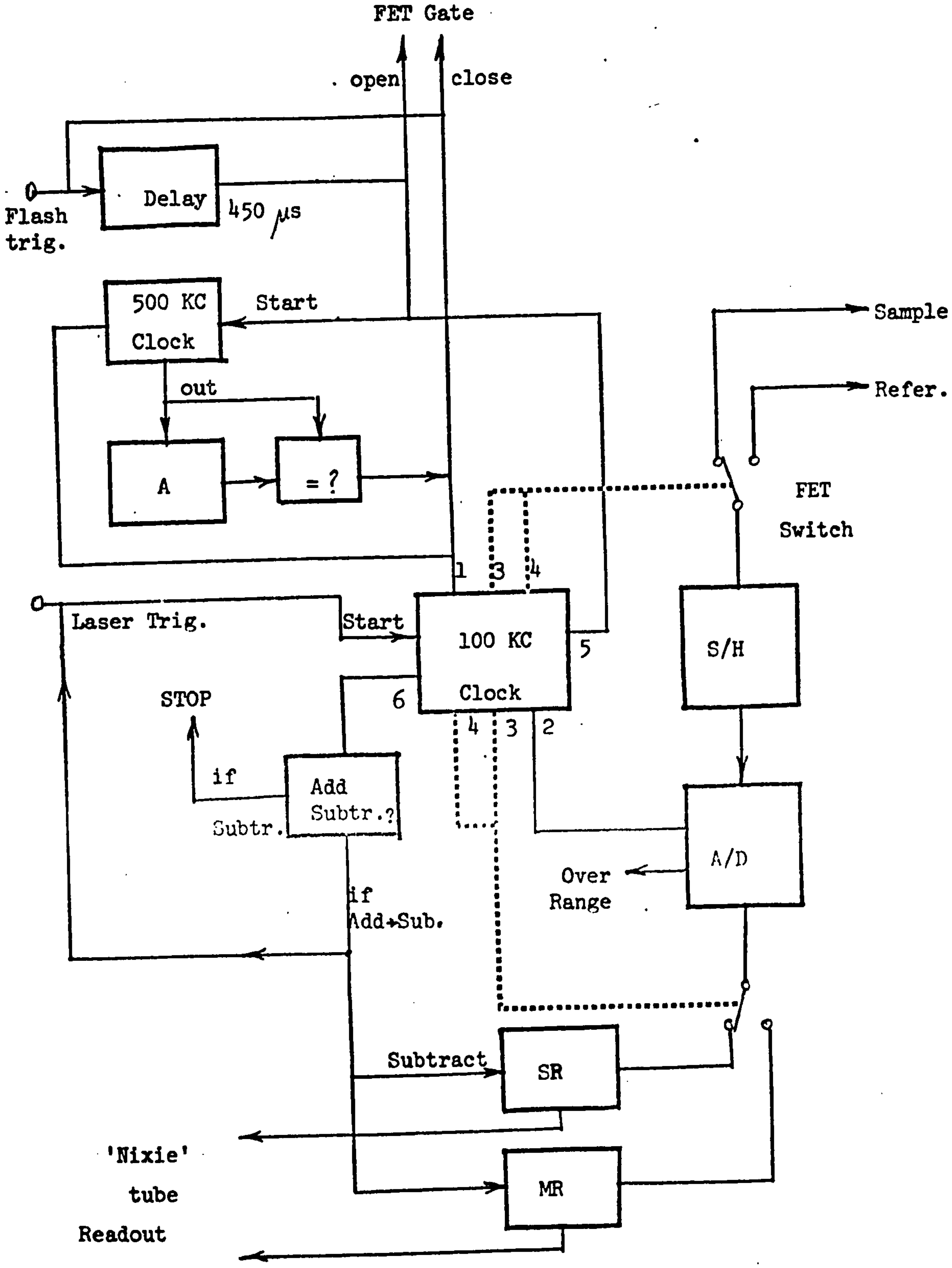

Figure C.2

Block Diagram of Sequencing

(see text)

Appendix D

Etching the Samples

To remove the damage layer from the surface of the semiconductors, all the samples used in this work were mildly etched.

The etching procedure first included the cleaning of the samples with an organic solvent such as acetone, followed by distilled water. The samples were rubbed gently with a Q-tip applicator. From then on the samples were handled only with teflon tweezers. The etchants were all held in nalgene beakers, due to the hydrofluoric acid in most of the etchants. Using the teflon tweezers the crystal was inserted into the etchant. The etching action was halted by diluting the etchant with water while the crystal was still in the beaker.

The etchants used and their etching times are found in Table D.1.

The zinc-blende semiconductors were all etched according to Gatos and Lavine (Gatos and Lavine, 1963). The etchant for InSb was the authors own mixture. The CdSe etchant was previously published (Cardona and Harbeke, 1965), while that for CdS was from Cardona (private communication).

TABLE D.1

CRYSTAL	ETCHANT	TIME
GaAs	1 HF 5 HNO_3 5 H_2O	5 seconds
InAs	15 HF 75 HNO_3 .06 Br_2	5 seconds
InSb	1 HF 1 HNO_3	1 second
InP	1 Br_2 10 CH_3COOH	10 seconds
ZnTe	3 HNO_3 4 HF	2 seconds, rinse in conc. HCl, then dist. H_2O
CdS	.5 M $K_2Cr_2O_7$ 16 N H_2SO_4	60° C. 1.5 hr.
CdSe	.5 M $K_2Cr_2O_7$ 16 N H_2SO_4	60° C. 20 minutes

Appendix E

The Computer Programming

E.1 Introduction

Two computer programs were used in this work. They were both processed on a time-shared PDP-10 computer. One program was used to calculate the Fresnel factors for the zinc-blende materials. The other was used for the wurtzite materials.

The two programs are quite different from each other. The emphasis of the zinc-blende program was on interpolating dielectric constant data at any wavelength from the optical constants at discrete wavelengths used as the input data. The emphasis of the wurtzite program was on performing all the necessary matrix and vector manipulations necessary for solving the Fresnel factor. No interpolation procedure was incorporated into this program. The optical constants at the particular wavelength of interest had to be fed into the machine. In practice, this was not found a handicap.

E.2 The Zinc-Blende Program

The zinc-blende program is reproduced on the following pages. Two files are called, "ADP" and "INP", a listing of dielectric constants of ADP and the particular zinc-blende material being studied.

The input data format in the file was:

photon energy (eV), Re $\epsilon(\hbar\omega)$, Im $\epsilon(\hbar\omega)$

for the zinc-blende material and:

wavelength (λ), ordinary index at λ , extra ord. at $\lambda/2$

for the ADP.

The order of the data in each file was arbitrary. New data, at any wavelength, could be added to the end of the file at any time.

Once the data was in the memory, the machine would request the wavelength range over which the Fresnel factor was to be computed and the spacing of the interpolation (ie. every 2 Å etc.).

The computer then computed $Y(\epsilon_1, \epsilon_2, n_e, n_o)$ as per the formula of equation 3.15. A listing was made of the photon energy of the fundamental wave verses $Y(\epsilon_1, \epsilon_2, n_e, n_o)$.

E.3 The Wurtzite Program

The wurtzite program is also reproduced in the following pages. The program solved for $E_R(2\omega)$ from equations 4.8 to 4.10. The input data was based on the format:

$$Pe(eV), e^r_{ao}(2\omega), e^i_{ao}(2\omega), e^r_o(2\omega), e^i_o(2\omega), e^r_{ao}(\omega), e^i_{ao}(\omega), e^r_o(\omega), e^i_o(\omega), n_e(\ ), n_o(\omega)$$

where: Pe(eV) was the photon energy of the fundamental wave.

$e^r_{ao}(2\omega), e^i_{ao}(2\omega)$ were the real and imaginary dielectric constants for the wurtzite at 2ω, respectively.

$e^r_o(2\omega), e^i_o(2\omega)$ were the real and imaginary dielectric constants for wurtzite at 2ω, respectively.

$n_e(2\omega), n_o(\omega)$ were the indices of refraction of ADP at the second harmonic and fundamental, respectively

For each photon energy, the computer printed out the vector equation:

$$\overline{E_R} = \bar{a}_1(\theta)\chi_{31} + \bar{a}_2(\theta)\chi_{33} + \bar{a}_3(\theta)\chi_{15}$$

as was mentioned in Chapter 4. A typical printout sheet is reproduced after the program.

```
C THIS IS THE FILE FRED ALSO KNOWN AS F
      DIMENSION WAVOUT(500,2),EXPTS(6),FEXPTS(6),PROD(6),RDINDX(500)
      DIMENSION EXINDX(500),E(2,100,5),WAVE(100,5),C(6),DIELEC(500,2)
      COMPLEX Y,DIE(500)
      CALL IFILE(1,'ADP ')
      GO TO 808
708   CALL IFILE(1,'INAS')
808   N=1
      TYPE 14
      TYPE 13
      PRINT 709
      PRINT 710
710   FORMAT(' WAVELENGTH OR P.E., EPS1,EPS2,NS,N',/)
709   FORMAT(' THE INPUT DATA',/)
      READ (1,1) NXTAL
      TYPE 1,NXTAL
4     READ (1,2) WAVE(N,NXTAL),E(1,N,NXTAL),E(2,N,NXTAL),NS
      PRINT 15,WAVE(N,NXTAL),E(1,N,NXTAL),E(2,N,NXTAL),NS,N
      IF (NS)3,3,717
3     N=N+1
      GO TO 4
717   IF(NXTAL-1)5,5,617
617   DO 718 I=1,N
718   WAVE(I,NXTAL)=1.24/WAVE(I,NXTAL)
5     CALL ARRANG(WAVE,E,NXTAL,N)
      IF(NXTAL-1)609,609,610
610   PRINT 12
      GO TO 611
609   PRINT 612
612   FORMAT(' WAVELENGTH,ORDINARY,EXTRAORD,CORRES,PE.,ARR',/)
611   DO 10 I=1,N
      SOWAT=1.24/WAVE(I,NXTAL)
10    PRINT 11, WAVE(I,NXTAL),E(1,I,NXTAL),E(2,I,NXTAL),SOWAT
12    FORMAT(' WAVELENGTH MICRONS    EPS 1    EPS 2 , CORRES PE, ARR',/)
1      FORMAT(I)
2      FORMAT(3F,I)
11     FORMAT(4F10.4)
14     FORMAT(' TYPE IN A XTAL #,THEN WAVELENGTH,EPS 1,2, AND 0 OR 1')
13     FORMAT(' IF IT IS THE LAST CARD TYPE A 1')
15     FORMAT(3F8.3,2I3)
       IF (NXTAL-1)616,619,619
618   TYPE 17
17    FORMAT(' SPECIFY WAVELENGTH DIVISIONS',/)
      ACCEPT 16,DIVINT
16    FORMAT(F)
      TYPE 21
21    FORMAT(' SPECIFY THE WAVELENGTH TO START AND STOP',/)
      ACCEPT 22,WASTR,WASTP
22    FORMAT (2F)
      IF(WASTR-WAVE(1,NXTAL))23,23,26
23    TYPE 24
24    FORMAT(' INCR THE LOWER WAVELENGTH',/)
      ACCEPT 25,WAST
      WASTR=WAST
26    IF(WASTP-WAVE(N,NXTAL))28,27,27
27    TYPE 29
29    FORMAT(' LOWER THE UPPER WAVELENGHT',/)
      ACCEPT 25,UPWAY
25    FORMAT (F)
      WASTP=UPWAY
28    SPRO= WASTP-WASTR
```

```
      NDIV=SPRD/DISINT
      TYPE 409,NDIV
409   FORMAT (I4,' THIS IS THE # OF DIVISIONS')
619   DO 34 NOT=1,2
      IBIG=1
      WAVOUT(IBIG,NOT)=WASTR
262   J=1
261   IF (WAVE(J,NXTAL)-WAVOUT(IBIG,NOT)) 251,30,30
251   J=J+1
      GO TO 261
30    JE=4
301   EXPTS(JE)=WAVE(J,NXTAL)
      IF (JE-6) 310,31,31
310   JE=JE+1
      J=J+1
      GO TO 301
31    JE=JE-3
      J=J-3
33    EXPTS(JE)=WAVE(J,NXTAL)
      IF (JE-1)32,32,321
321   JE=JE-1
      J=J-1
      GO TO 33
32    DO 331 JF=J,J+5
      FEXPTS(JE)=E(NOT,JF,NXTAL)
331   JE=JE+1
      CALL SAL(EXPTS,FEXPTS,WAVOUT,SUM,IBIG,NOT)
      DIELEC(IBIG,NOT)=SUM
      IBIG=IBIG+1
      WAVOUT(IBIG,NOT)=WAVOUT(IBIG-1,NOT)+DISINT
      IF (IBIG-2-NDIV) 262,262,101
101   IF(NXTAL-1) 613,613,701
613   PRINT 614,NOT
614   FORMAT ('INTER. WAVE,MICRONS,INDEX ',I3,' 1=ORF,2=EX-COR-PE')
      GO TO 615
701   PRINT 35,NOT
35    FORMAT(' INTERPOLATED WAVELENGTH MICRONS,ESPILION',I3,' P.E.')
615   DO 34 KBIG=1,NDIV+2
      FOX=1.24/WAVOUT(KBIG,NOT)
34    PRINT 36,WAVOUT(KBIG,NOT),DIELEC(KBIG,NOT),FOX
36    FORMAT (F10.4,'          ',F10.4,'          'F10.4)
      IF(NXTAL-1) 605,605,607
605   DO 606 KLAG=1,NDIV+2
      EXINDX(KLAG)=DIELEC(KLAG,2)
606   PDINDX(KLAG)=DIELEC(KLAG,1)
      GO TO 703
607   PRINT 603
603   FORMAT(' WAVE    Y REAL    YIMG    YABS    P.E.    CHANG')
      IWAYL=WAVOUT(NDIV+2,1)*10000.
      IWAYF=WAVOUT(1,1)*10000.
      IDELWA=IWAYL-IWAYF
      JINT=1+((IWAYF*(NDIV+1))/IDELWA
      TYPE 818,JINT
818   FORMAT(' THIS IS THE INITIAL INDEX    ',I3)
      DO 820 JBI=1,NDIV+2
820   DIE(JBI)=CMPLX(DIELEC(JBI,1),DIELEC(JBI,2))
      CALL OFILE(1,'PUT')
      WRITE (1,603)
      DO 601 JBIG=JINT,NDIV+2,2
      IPART=WAVOUT(JBIG,1)*10000.
      JDEL=((IWAYL-IPART/2)*(NDIV+1))/IDELWA
```

```
      J=NDIV+2-JDEL
      CALL YCHANG(WAVOUT,DIE,JBIG,EXINDX,RDINDX,Y,J)
      YREAL=REAL(Y)
      YIMG=AIMAG(Y)
      WATER=1.24/WAVOUT(JBIG,1)
      YABS=CABS(Y)
      WRITE(1,602) WAVOUT(JBIG,1),YREAL,YIMG,YABS,WATER,WAVOUT(J,1)
601   PRINT 602,WAVOUT(JBIG,1),YREAL,YIMG,YABS,WATER
      PRINT 904
      WRITE(1,904)
904   FORMAT(' WAVE    YREAL    YIMG     YABS    P.E.   FRED')
      DO 901 JBIG=JINT,NDIV+2,2
      IPART=WAVOUT(JBIG,1)*10000.
      JDEL=((IWAVL-IPART/2)*(NDIV+1))/IDELWA
      J=NDIV+2-JDEL
      CALL YFRED(WAVOUT,DIE,JBIG,EXINDX,RDINDX,Y,J)
      YREA=REAL(Y)
      YIM=AIMAG(Y)
      WATE=1.24/WAVOUT(JBIG,1)
      YAB=CABS(Y)
      WRITE(1,602) WAVOUT(JBIG,1),YREA,YIM,YAB,WATE,WAVOUT(J,1)
901   PRINT 602,WAVOUT(JBIG,1),YREA,YIM,YAB,WATE,WAVOUT(J,1)
602   FORMAT(F10.4,' ',E12.6,' ',E12.6,' ',E12.6,' ',F8.3,' ',F10.4)
      END
C   THIS IS THE FIRST LINE OF THE FILE YOU HAVE JUST MADE'AR'
      SUBROUTINE ARRANG(WAVE,E,NXTAL,N)
      DIMENSION WAVE(1005,5),E(2,1005)
      DO 9 I=1,N-1
      IF=I
8     IF(WAVE(IF,NXTAL)-WAVE(IF+1,NXTAL))6,6,7
7     S=WAVE(IF,NXTAL)
      FSO=E(1,IF,NXTAL)
      FST=E(2,IF,NXTAL)
      WAVE(IF,NXTAL)=WAVE(IF+1,NXTAL)
      E(1,IF,NXTAL)=E(1,IF+1,NXTAL)
      E(2,IF,NXTAL)=E(2,IF+1,NXTAL)
      WAVE(IF+1,NXTAL)=S
      E(1,IF+1,NXTAL)=FSO
      E(2,IF+1,NXTAL)=FST
      GO TO 8
6     IF=IF-1
      IF(IF) 9,9,8
9     CONTINUE
      RETURN
        END
C THIS IS THE FIRST LINE OF THE FILE   'SUMA'.
       SUBROUTINE SAL(EXPTS,FEXPTS,WAVOUT,SUM,IBIG,NOT)
       DIMENSION EXPTS(6),FEXPTS(6),WAVOUT(500,2),PROD(6)
       DO 18 K=1,6
       PROD(K)=1
       DO 18 I=1,6
       IF(I-K) 19,18,19
19    PROD(K)=(PROD(K)*(WAVOUT(IBIG,NOT)-EXPTS(I)))/(EXPTS(K)-EXPTS(I))
18    CONTINUE
      SUMA=0.
      DO 602 J=1,6
602   SUMA=SUMA+FEXPTS(J)*PROD(J)
      SUM=SUMA
      RETURN
      END
```

```
C THIS IS THE FIRST LINE OF THE FILE 'WHY'
      SUBROUTINE WHY(WAVOUT,DIE,JBIG,EXINDX,RDINDX,Y,J)
      COMPLEX Y,DIE(500)
      DIMENSION WAVOUT(500,2),EXINDX(500),RDINDX(500)
      IMX=J
      YINT=((3.**.5)*EXINDX(IMX))/(EXINDX(IMX)-RDINDX(JBIG))
      YINT=YINT/(EXINDX(IMX)+RDINDX(JBIG))
      YINT=YINT/(((EXINDX(IMX)+1.)**2.)*(RDINDX(JBIG)+1.))
      Y=((CSQRT(2.*DIE(JBIG)-1.)+1.)**2.)*(CSQRT(2.*DIE(IMX)-1.)+1.)
      Y=Y*(CSQRT(2.*DIE(JBIG)-1.))+(CSQRT(2.*DIE(IMX)-1.))
      Y=Y*YINT
      RETURN
      END
C THIS IS THE FIRST LINE OF THE FILE 'WHYFR'
      SUBROUTINE WHYFRE(WAVOUT,DIE,JBIG,EXINDX,RDINDX,Y,J)
      COMPLEX Y,DIE(500)
      DIMENSION WAVOUT(500,2),EXINDX(500),RDINDX(500)
      IMX=J
      YINT2=1./((EXINDX(IMX)-RDINDX(JBIG))*(EXINDX(IMX)+RDINDX(JBIG)))
      YINTR=YINTR/(RDINDX(JBIG)+1.)
      Y=(CSQRT(2.*DIE(JBIG)-1.)+CSQRT(2.*DIE(IMX)-1.))
      Y=Y*(CSQRT(2.*DIE(IMX)-1.)+1.)*(CSQRT(2.*DIE(IMX)-1.)+1.)
      Y=Y/(SQRT(2.)*(CSQRT(2.*DIE(IMX)-1.)))
      Y=Y*((CSQRT(2.*DIE(JBIG)-1.)+1.)**2.)
      Y=Y*YINT2/2.
      RETURN
      END
```

Reproduced with permission of the copyright owner. Further reproduction prohibited without permission.

```
C THIS IS THE FIRST LINE OF THE FILE MAIN
        COMPLEX  V1,UNIT(3,3).X(3),S2, BF(3),RN(3)
        COMPLEX   A(3),B(3),V2,S,D(3,3), ASSE(3,3),FE,C(3)
        COMPLEX  E(3,3),F(3,3),G(3,3),H(3.3),EO,EAO,BN(3)
        COMPLEX  AMIN1(3,3),AMIN2(3,3),AMIN3(3,3),TR,DFF
        COMPLEX U1(3),U2(3),ER(3),ER1(3),ER2(3),ER3(3),NAF(3)
        COMPLEX NR2W(3),NO2W(3),NAO2W(3),E2WO(3),E2WAO(3),NRR(3)
        COMPLEX P(3),DEX ,   AM(3,3),QAP(3)   ,NAP(3),NOW(3),NAOW(3)
        COMPLEX NAP1(3),NAP2(3),NAP3(3),QAP3(3),QAP2(3),QAP1(3)
        REAL NOZ,NEZ,FISSER
        DIMENSION E11(3),E22(3),E33(3)
        COMPLEX ATEN(3,3),AMI(3,3) ,ANSW(3,3),ET(3),T ,EWO,EWAO
        TYPE  29
29      FORMAT (' TYPE IN THE ANGLE OF THE C AXIS WITH RESP.TO VERT',/)
        ACCEPT 30,THETA
        TYPE 972
972     FORMAT(' TYPE IN THE ANGLE OF INCIDENCE.',/)
        ACCEPT 30,FISSER
30      FORMAT (F)
        CALL IFILE(1,'CDS')
C       ENTERS WAVELENGTH,EPSILON REAL,IMAG,PERP THEN PARA AT 2W THEN W.
        CALL OFILE(20,'TEN')
4       READ (1,1) WAVE,EPR,EPI,ESR,ESI,FPR,FPI,FSR,FSI,NEZ,NOZ
1       FORMAT(11F )
        TYPE 31,WAVE
31      FORMAT (' PHOTON ENERGY FOR XTAL ',F10.4)
C       DEFINE THE UNIT MATRIX.
2       DO 5 I=1,3
        DO 5 J=1,3
        IF(I-J)6,7,6
6       UNIT (I,J) = 0
        GO TO 5
7       UNIT (I,J) = 1.
5       CONTINUE
C       DEFINE THE COMPLEX DIELECTRIC CONSTANT AT 2W.
        EAO=CMPLX(EPR,EPI)
        EO =CMPLX(ESR,ESI)
C       DEFINE THE UNIT VECTOR
        X(1)=1.
        X(2)=0
        X(3)=0
C       COMPUTING THE ASSOCIATED TENSOR E(2W) BAR.
C       FIRST THE OPTIC AXIS IS 'C' A VECTOR GIVEN BY.
        C(1)=0.
        C(2)=COSD(THETA)
        C(3)=SIND(THETA)
C       NOW CALCULATE THE ASSOCIATED TENSOR CALLED ASSE.
        CALL ASS(C,EAO   ),UNIT,ASSE)
C       COMPUTING THE TRACE OF E(2W) CALLED TR.
        TR=2.*EO+EAO
C       COMPUTING E(2W) CALLED BY E(I,J)
        CALL SCAL(EO,UNIT.F)
        CALL DYAD(C,C,D)
        S2=EAO-EO
        CALL SCAL(S2,D,G)
        CALL SUM(G,F,E)
C       WRITE (20,50) THETA
        TYPE 34,TR
C          DO 98 I=1,3
C 98        WRITE(20,49) E(I,1),E(I,2),E(I,3)
50      FORMAT (' DIELECTRIC TENSOR,THETA=',F,'WAVE=',F)
```

```
 49      FORMAT(6E12.3)
 34      FORMAT (' E(I,J) HAS BEEN COMPUTED AND TR IS',2F)
 C       COMPUTE FOR ALFA 1,2,3 A1,A2,A3
         NALFA =1
         FE=CMPLX(FSR,FSI)
         NOW(3)=SIND(FISSER)
         NOW(2)=0.
         NOW(1)=CSQRT(FE-NOW(3)**2)
         CALL VEQUL(NRR,NOW)
 999     CALL AMTX(NRR,E,UNIT,ATEN)
 C       WRITE(20,24) NALFA
 24      FORMAT (' THE MATRIX A FOR ALFA =',I2)
 C       DO 199 I=1,3
 C199     WRITE(20,20) ATEN(I,1),ATEN(I,2),ATEN(I,3)
         CALL ABR(ATEN,UNIT,AMI)
 C       WRITE (20,44) NALFA,THETA
 C          DO 23 I=1,3
 C  23      WRITE(20,20) AMI(I,1),AMI(I,2),AMI(I,3)
 C       CHECK A TIMES INVERSE GIVES IDENTITY.
         CALL MAMUL(ATEN,AMI,ANSW)
 C       TYPE 447
 C        DO 444 I=1,3
 C444      TYPE 20 ,ANSW(I,1),ANSW(I,2),ANSW(I,3)
 447     FORMAT (' THE A TIMES ITS INVERSE')
         IF (NALFA-2) 14,15,16
 14      CALL MEQUL(AMIN1,AMI)
         FE = CMPLX(FPR,FPI)
         NAOW(2)=0
         NAOW(3)=SIND(FISSER)
         NAOW(1)=CSQRT(FE-NAOW(3)**2)
         CALL VEQUL(NRR,NAOW)
         NALFA =2
         GO TO 999
 44      FORMAT(' THE MAT A TO THE -1 TIMES 4 PI,ALFA=',I2,'  THETA=',F)
 15      CALL MEQUL(AMIN2,AMI)
         NRR(1)=NOW(1)/2.+NAOW(1)/2.
         NRR(2)=0.
         NRR(3)=NOW(3)/2.+NAOW(3)/2.
         NALFA=3
         GO TO 999
 20      FORMAT ( 6E12.3)
 16      CALL MEQUL(AMIN3,AMI)
 C       PN IS THE VECTOR NE(W), IE AN INCIDENT VECTOR.
         RN(2)=0.
         RN(3)=SIND(FISSER)
         RN(1)=COSD(FISSER)
 C       CALCULATE THE REFRACTION AND POLARISATION VECTORS
         CALL CROSS(RN,X,BE)
         CALL CROSS(X,BE,BN)
         CALL NR(BN,X,NR2W)
 C       TYPE 599 ,NR2W(1),NR2W(2),NR2W(3)
         CALL NAO(BN,X,EO,EAO,E,NAO2W)
         CALL NO(BN,X,EO,NO2W)
         WRITE(20,159)
 159     FORMAT(' NO2W IS:  AND NAO2W IS:',/)
         WRITE(20,599) NO2W(1),NO2W(2),NO2W(3)
         WRITE(20,599) NAO2W(1),NAO2W(2),NAO2W(3)
         TYPE 599,C(1),C(2),C(3)
 599     FORMAT (6E12.3)
         CALL POVEC(EO,NAO2W,NO2W,UNIT,C,E2WO,E2WAO)
 C       DEFINE P VECTOR FOR ALFA=1.
```

```
      WRITE(20,343)
343   FORMAT (' THE POLARISATION VECTORS E2W0 AND E2WAO')
      WRITE(20,499) E2WO(1),E2WO(2),E2WO(3)
      WRITE(20,499) E2WAO(1),E2WAO(2),E2WAO(3)
499   FORMAT(6E12.3)
C     TYPE 391
C     ACCEPT 392,GOOK
      P(1)=0.
      P(2)=((SIND(THETA))**2)*COSD(THETA)
      P(3)=(SIND(THETA))**3
C     THE COMPLEX DIELECTRIC CONSTANT AT W IS DEX.
      DEX=CMPLX(FSR,FSI)
      DEF=CSQRT(DEX)
      CALL VEQUL(NAF,NOW)
      NBETA=1
C     EQUATE ALFA 1 MATRIX A WITH AM.
      CALL MEQUL(AM,AMIN1)
102   CALL QAPE(X,AM,P,QAP)
      CALL NAPE(NAF ,AM,P,NAP)
C     TYPE 569,NBETA
C     TYPE 589,NAP(1),NAP(2),NAP(3)
C     TYPE 589,QAP(1),QAP(2),QAP(3)
      WRITE (20,606) NBETA
606   FORMAT (' THE POLARISATION VECTORS FOR ALFA=',I2)
      WRITE(20,579) P(1),P(2),P(3)
391   FORMAT(' PUSH RET TO CONTINUE')
C     TYPE 391
C     ACCEPT 392,GOOK
392   FORMAT(F)
579   FORMAT(6E12.3)
569   FORMAT(' ALFA=',I,'     NAP QAP AND P ARE AS FOLLOWS:')
589   FORMAT(6E12.3)
      IF (NBETA-2)103,104,105
103   NBETA=2
      CALL MEQUL(AM,AMIN2)
      CALL VEQUL(NAP1,NAP)
      CALL VEQUL(QAP1,QAP)
      P(2)=(COSD(THETA))**3
      P(3)=((COSD(THETA))**2)*SIND(THETA)
      CALL VEQUL(NAF,NAOW)
      DEX=CMPLX(FPR,FPI)
      DEF=CSQRT(DEX)
      GO TO 102
104   NBETA=3
      CALL VEQUL(NAP2, NAP)
      CALL MEQUL(AM,AMIN3)
      CALL VEQUL(QAP2,QAP)
      P(3)= -2.*((COSD(THETA))**2)*SIND(THETA)
      P(2)=2.*((SIND(THETA))**2)*COSD(THETA)
       NAF(1)=NOW(1)/2.+NAOW(1)/2.
      NAF(2)=NOW(2)/2.+NAOW(2)/2.
      NAF(3)=NOW(3)/2.+NAOW(3)/2.
      GO TO 102
105   CALL VEQUL(NAP3,NAP)
      CALL VEQUL(QAP3,QAP)
C     COMPUTATION OF TH VECTORS U1 AND U2.
      CALL YOU1(E2WO,F2WAO,NO2W,NAO2W,X,NR2W,U1)
      CALL YOU2(      E2WAO,NO2W,NAO2W,X,NR2W,U2,E2WO)
C     WRITE(20,607)
C     DO 77 I=1,3
607   FORMAT(' THE U VECTORS',/,'      U-1 REAL      IMAG      U-2')
```

```
C77      WRITE(20,99) U1(I),U2(I)
99      FORMAT (4E12.3)
C       CAL OF THE LINEAR TRANS FACTOR SQUARED: T
        EWO=CMPLX(FSR,FSI)
        EWAO=CMPLX(FPR,FPI)
        CALL TRANS(EWO,EWAO,THETA,T,FISSER)
        TYPE 834,T
834     FORMAT (' THE SQUARE OF THE LINEAR FRESNEL FACTOR',2E12.3)
C       CAL OF THE SCALS V1 AND V2.
        JGAM=1
        CALL VEQUL(NAP,NAP1)
        CALL VEQUL(QAP,QAP1)
109     CALL VE1(E2WO,E2WAO,QAP,NAP,X,NO2W,NAO2W,V1)
        CALL VE2(E2WO,E2WAO,QAP,NAP,X,NO2W,NAO2W,V2)
C       WRITE(20,699) V1,V2,JGAM
699     FORMAT(4E12.3,' V1   V2,ALFA=',I2)
C       CALCULATE ER(2W) FOR ALFA =1,2,3 AND STORE.
        CALL EAR(NR2W,U1,U2,V1,V2,ET)
        CALL SVEC(T,ET,ER)
        TYPE 431,JGAM
431     FORMAT ( ' THE E REFLECTED VECTOR CONTRIBUTION ALFA=', I2 )
        TYPE 69,ER(1),ER(2),ER(3)
        TYPE   391
C       ACCEPT 392,GOOK
69      FORMAT(6E12.3)
        IF(JGAM-2)106,107,108
106     JGAM=2
        CALL VEQUL(QAP,QAP2)
        CALL VEQUL(NAP,NAP2)
        CALL VEQUL(ER1,ER)
        GO TO 109
107     JGAM=3
        CALL VEQUL(QAP,QAP3)
        CALL VEQUL(NAP,NAP3)
        CALL VEQUL(ER2,ER)
        GO TO 109
108     CALL VEQUL(ER3,ER)
        WRITE(20,110) THETA
        WRITE (20,113) WAVE
113     FORMAT(' THE PHOTON ENERGY IS',E12.3,'  ELECTRON VOLTS',/)
        Y=8.*3.14159/((NOZ+1.)*(NEZ**2-NOZ**2))
        WRITE (20,118)Y
        WRITE (20,165),NEZ,NOZ
165     FORMAT(' THE EXTRA ORDINARY INDEX OF ADP AT 2W',E12.4,/ ,' THE
     3  ORDINARY INDEX OF ADP AT W          ',E12.4,/)
118     FORMAT(' LITTLE Y',E12.4,/ )
        WRITE(20,146)
        WRITE(20,148)EAD,EO
        WRITE(20,158)FPR,FPI,FSR,FSI
146     FORMAT(' THE DIELECTRIC CONSTANTS ENTERED FOR THIS P. E.',/)
158     FORMAT(' EXTRA E(W)',2E12.3,/,' ORDIN. E(W)',2E12.3,/)
148     FORMAT(' EXTRA E(2W)',2E12.3,/,' ORDIN. E(2W)',2E12.3,/)
        DO 119 I=1,3
        WRITE(20,112) I
        WRITE(20,111) ER1(I),ER2(I),ER3(I)
111     FORMAT(' D32',2E12.3,/,' D33',2E12.3,/,' D15',2E12.3,/ )
110     FORMAT(' THE ANGLE OF THE C AXIS WITH RESP TO VERT.=',F,/)
112     FORMAT('          REAL PART   IMAGINARY',/,'ER(',I1,')',/)
119     TYPE 111,ER1(I),ER2(I),ER3(I)
        WRITE (20,138)
        DO 133 I=1,3
```

```
      E11(I)=CABS(ER1(I))
      E22(I)=CABS(ER2(I))
      E33(I)=CABS(ER3(I))
      WRITE(20,139)I
139   FORMAT(' ER(',I1,')',/)
133   WRITE(20,132)E11(I),E22(I),E33(I)
132   FORMAT('D32',E12.3,/,' D33',E12.3,/,' D15',E12.3,//)
138   FORMAT(' THE ABSOLUTE VALUE OF THE COFF. OF D(IJ)',/)
      GO TO 4
117   CONTINUE
      END

C     THIS IS THE FIRST LINE OF THE FILE 'FIN'

C     THIS FILE CALCULATES U1 PARSONS

      SUBROUTINE YOU1(E2WO,E2WAO,NO2W,NAO2W,X,NR2W,U1)
      COMPLEX EX(3),E2WAO(3),NO2W(3),NAO2W(3),EN(3),ER(3)
      COMPLEX DYA(3,3),X(3),U1(3),E2WO(3),PT(3),NR2W(3),FISH
      CALL CROSS(E2WAO,X,EX)
      CALL CROSS(E2WAO,E2WO,EN)
      CALL DYAD(EN,EX,DYA)
      CALL VMAT(NO2W,DYA,EX)
      CALL CROSS(E2WAO,NR2W,EN)
      CALL CROSS(E2WAO,E2WO,ER)
      CALL DYAD(ER,EN,DYA)
      CALL VMAT(X,DYA,ER)
      FISH=-1.
      CALL SVEC(FISH ,ER,PT)
      CALL VSUM(EX,PT,U1)
      RETURN
      END

C     HERE IS THE CALCULATION OF THE VECTOR U2.PARSONS

      SUBROUTINE YOU2(      E2WAO,NO2W,NAO2W,X,NR2W,U2,E2WO)
      COMPLEX EX(3),E2WAO(3),E2WO(3),NO2W(3),NAO2W(3),EN(3),ER(3)
      COMPLEX DYA(3,3),X(3),U2(3),PR(3) ,NR2W(3),FISH
      CALL CROSS(E2WO,X,EX)
      CALL CROSS(E2WAO,E2WO,ER)
      CALL DYAD(ER,EX,DYA)
      CALL VMAT(NAO2W,DYA,EN)
      CALL CROSS(E2WO,NR2W,ER)
      CALL CROSS(E2WAO,E2WO,EX)
      CALL DYAD(EX,ER,DYA)
      CALL VMAT(X,DYA,EX)
      FISH=-1.
      CALL SVEC(FISH ,EX,PR)
      CALL VSUM(PR,EN,U2)
      RETURN
      END

C     CALCULATION OF ER(2W) FOR EACH ALFA.

      SUBROUTINE EAR(NR2W,U1,U2,V1,V2,ER)
      COMPLEX H(3),A(3),B(3),C(3),HSUM(3),UCROS(3),Z
      COMPLEX SALOR,ER(3),V1,V2,U1(3),U2(3),NR2W(3)
      CALL CROSS(NR2W,U1,A)
      CALL CROSS(NR2W,U2,B)
      Z=-V1
      CALL SVEC(V2,A,C)
      CALL SVEC( Z ,B,H)
      CALL VSUM(C,H,HSUM)
      CALL CROSS(U1,U2,UCROS)
      CALL DOT(NR2W,UCROS,SALOR)
      SALOR=1./SALOR
      CALL SVEC(SALOR,HSUM,ER)
      RETURN
      END
```

```
C     CALCULATION OF V2 BY PARSONS FORMULA
      SUBROUTINE VE2(E2WO,E2WAO,QAP,NAP,X,NO2W,NAO2W,V2)
      COMPLEX E2WAO(3),E2WO(3),QAP(3),NAP(3),X(3),NO2W(3),NAO2W(3)
      COMPLEX V2,A(3),S,B(3),U,DIA(3,3),EOT(3,3),EOU(3,3),DIB(3,3)
      COMPLEX T,TP,SE,SP
      CALL CROSS(E2WAO,E2WO,A)
      CALL DOT(X,A,T)
      CALL DOT(E2WO,NAP,TP)
      S=T*TP


      CALL DOT(E2WO,QAP, SE)
      CALL DOT(NAO2W,A, SP)
      U= SE*SP
      TYPE 1
1     FORMAT (' THE U AND S SCALORS FOR V2 ARE')
      TYPE 2,U,S
2     FORMAT (4E12.3)
      V2=S-U
      RETURN
      END

C     CALCULATION OF V1 BY A SECOND METHOD.(PARSONS)
C
      SUBROUTINE VE1(E2WO,E2WAO,QAP,NAP,X,NO2W,NAO2W,V1)
      COMPLEX E2WO(3),E2WAO(3),DIA(3,3),EOT(3,3),S,B(3),U,X(3),T,TP
      COMPLEX V1,DIB(3,3),EOU(3,3),NAP(3),QAP(3),A(3),NO2W(3),NAO2W(3)
      COMPLEX SE,SP
      CALL CROSS(E2WAO,E2WO,A)
      CALL DOT(X,A,T)
      CALL DOT (NAP,E2WAO,TP)
      S= TP*T
      CALL DOT(NO2W,A,SE)
      CALL DOT(E2WAO,QAP,SP)
      U=SE*SP
      TYPE 1
1     FORMAT (' THE U AND S FOR V1:')
      TYPE 2,U,S
2     FORMAT(4E12.3)
      V1=S-U
      RETURN
      END

C     THE CALCULATION OF THE SQ OF LINEAR FRESNEL TRANS.
      SUBROUTINE TRANS(EWO,EWAO,THETA,T,FISSER)
      COMPLEX EWO,EWAO,T,SL,SA,EFF,ROOT,TEF
      REAL FISSER
      SL=((SIND(THETA))**2)/EWO
      SA=((COSD(THETA))**2)/EWAO
      EFF=1./(SA+SL)
      ROOT=SIND(FISSER)*CSQRT(EFF-(SIND(FISSER))**2)
      TEE=2./(ROOT+(SIND(FISSER))*(COSD(FISSER)))
      TEF=TEE*COSD(FISSER)*SIND(FISSER)
      T=TEE**2
      RETURN
      END
```

```
C     THIS IS THE FIRST LINE OF THE FILE SUB
C     SOME MATRIX AND VECTOR ROUTINES.
      SUBROUTINE DOT(A,B,S)
      COMPLEX   A(3),B(3),S
      S=0
      DO 5 I=1,3
5     S=S+A(I)*B(I)
      RETURN
      END
      SUBROUTINE CROSS(A,B,C)
      COMPLEX   A(3),B(3),C(3)
      C(1)=A(2)*B(3)-B(2)*A(3)
      C(2)=A(3)*B(1)-B(3)*A(1)
      C(3)=A(1)*B(2)-B(1)*A(2)
      RETURN
      END
      SUBROUTINE DYAD(A,B,D)
      COMPLEX   A(3),B(3),D(3,3)
      DO 6 I=1,3
      DO 6 J=1,3
6     D(I,J)=A(I)*B(J)
      RETURN
      END
C     MATRIX TIMES A VECTOR.
      SUBROUTINE MAVEC(D,B,C)
      COMPLEX   D(3,3),B(3),C(3)
      DO 1 I=1,3

1     C(I)=0
      DO 2 I=1,3
      DO 2 J=1,3
2     C(I)=D(I,J)*B(J)+C(I)
      RETURN
      END
C     THE SCALOR MATRIX PRODUCT.
      SUBROUTINE SMAMA(D,E,S)
      COMPLEX   D(3,3),E(3,3),S
      S=CMPLX(0.,0.)
      DO 2 I=1,3
      DO 2 J=1,3
2     S=S+D(J,I)*E(I,J)
      RETURN
      END
C     SCALOR TIMES A MATRIX.
      SUBROUTINE SCAL(S,D,E)
      COMPLEX S,D(3,3),E(3,3)
      DO 10 I=1,3
      DO 10 J=1,3
10    E(I,J)=D(I,J)*S
      RETURN
      END
```

```
C     THE SUBTRACTION OF TWO MATRICIES.

      SUBROUTINE SUTRA(E,F,D)
      COMPLEX  E(3,3),F(3,3),D(3,3)
      DO 11 I=1,3
      DO 11 J =1,3
11    D(I,J)=E(I,J)-F(I,J)
      RETURN
      END

C     SUM OF TWO MATRICIES.

      SUBROUTINE SUM(E,F,G)
      COMPLEX E(3,3),F(3,3),G(3,3)
      DO 20 I=1,3
      DO 20 J=1,3
20    G(I,J)=E(I,J)+F(I,J)
      RETURN
      END

C     MULTIPLICATION OF MATRICIES.

      SUBROUTINE MAMUL(D,F,G)
      COMPLEX D(3,3),E(3,3),G(3,3)
      DO 21 I=1,3
      DO 21 J=1,3
21    G(I,J)=0.
      DO 23 K=1,3
      DO 23 I=1,3
      DO 23 J=1,3
23    G(I,K)=D(I,J)*E(J,K)+G(I,K)
      RETURN
      END


C     REFRACTION VECTOR SUBROUTINES.

C     CALCULATION OF THE REFLECTED INDEX VECTOR.

      SUBROUTINE NR(BN,X,NR2W)
      COMPLEX BN(3),S,NR2W(3),ETA,NQ(3),X(3)
      CALL DOT(BN,BN,S)
      ETA=-CSQRT(1.-S)
      CALL SVEC(ETA,X,NQ)
      CALL VSUM(NQ,BN,NR2W)
      RETURN
      END

C     CALCULATION OF THE ORDINARY RAY REFRACTION VECTOR

      SUBROUTINE NO(BN,Y,EO,NO2W)
      COMPLEX   X(3)
      COMPLEX BN(3),EO,NO2W(3),NQ(3),S,ETA
      CALL DOT(BN,BN,S)
      ETA=CSQRT(EO-S)
      CALL SVEC(ETA,X,NQ)
      CALL VSUM(NQ,BN,NO2W)
      RETURN
      END

C     CALCULATION OF THE EXTRAORDINARY RAY REF. VECTOR.

      SUBROUTINE NAO(BN,X,EO,EAO,E,NAO2W)
      COMPLEX E(3,3),X(3),S,D(3,3),V,BN(3),EB(3,3),EOB
      COMPLEX   DYA(3,3),EO,EAO,NAO2W(3),ETA,NQ(3)
      CALL DYAD(X,X,DYA)
```

```
      CALL SMAMA(E,DYA,S)
      CALL DYAD(X,BN,D)
      CALL SMAMA(E,D,V)
      CALL DYAD(BN,BN,PB)
      CALL SMAMA(E,PB,EDB)
      EDB=S*(EDB-EO*FAO)
      EDB=CSQRT(V**2-EDB)
      ETA=(-V+EDB)/S
      CALL SVEC(ETA,X,NO)
      CALL VSUM(NO,BN,NAO2W)
      RETURN
      END
C     CALCULATION OF THE POLARISATION VECTORS.
      SUBROUTINE POVEC(EO,NAO2W,NO2W,UNIT,C,E2WO,E2WAO)
      COMPLEX NAO2W(3),NO2W(3),E2WO(3),F2WAO(3),DYA(3,3),DYAP(3,3)
      COMPLEX   UNIT(3,3),C(3),EO,DYAR(3,3)
      CALL CROSS(NO2W,C,F2WO)
      CALL DYAD(NAO2W,NAO2W,DYA)
      CALL SCAL(EO,UNIT,DYAP)
      CALL SUTRA(DYAP,DYA,DYAR)
      CALL MAVEC(DYAR,C,F2WAO)
      RETURN
      END
C     SUM OF TWO VECTORS ROUTINE.
      SUBROUTINE VSUM(A,B,C)
      COMPLEX A(3),B(3),C(3)
      DO 1 I=1,3
 1    C(I)=A(I)+B(I)
      RETURN
      END
C     VECTOR TIMES A SCALOR ROUTINE.
      SUBROUTINE SVEC(S,A,B)
      COMPLEX S, A(3), B(3)
      DO 1 I=1,3
 1    B(I)=A(I)*S
      RETURN
      END
C     VECTOR TIMES A MATRIX.
      SUBROUTINE VMAT(A,D,F)
      COMPLEX A(3),D(3,3),F(3)
      DO 1 I=1,3
 1    F(I)=0.
      DO 2 J=1,3
      DO 2 I=1,3
 2    F(J)=A(I)*D(I,J) +F(J)
      RETURN
      END
C     THIS CALCULATES NSUB ALFA CROSS A TO -1 TIMES P
      SUBROUTINE  NAPE(INDEX,AMIN,P,NAP)
      COMPLEX PEE(3),INDEX(3),AMIN(3,3),NAP(3),P(3)
```

```
      CALL MAVEC(AMIN,P.PEF)
      CALL CROSS(INDEX,PEF,NAP)
      RETURN
      END
C     CALCULATION OF Q X A -1   TIMES P.
      SUBROUTINE QAPE(X.AMIN,P,QAP)
      COMPLEX X(3),AMIN(3,3),P(3),QAP(3),QEE(3)
      CALL MAVEC(AMIN,P,QEE)
      CALL CROSS(X,QEE,QAP)
      TYPE 2
2     FORMAT(' THE VALUE OF AMIN      PUSH RET TO CONT.')
      DO 3 I=1,3
3     TYPE 1,AMIN(I,1),AMIN(I,2),AMIN(I,3)
      TYPE 5
5     FORMAT('THESE ARE THE P')
      TYPE 6,P(1),P(2),P(3)
6     FORMAT(6E12.3)
      TYPE 7
      TYPE 1,QEE(1),QEE(2),QEE(3)
C     ACCEPT 4,GOOK
7     FORMAT(' THE QEE')
4     FORMAT(F)
1     FORMAT (6E12.3)
      RETURN
      END
C     EQUATE TWO VECTORS.
      SUBROUTINE VEQUL(A,B)
      COMPLEX A(3),B(3)
      DO 1 I=1,3
1     A(I)=B(I)
      RETURN
      END
C     EQUATE 2 MATRICIES
      SUBROUTINE MEQUL(D,F)
      COMPLEX D(3,3),F(3,3)
      DO 1  I=1,3
      DO 1  J=1,3
1     D(I,J)=F(I,J)
      RETURN
      END
C     THE SUBROUTINE FOR THE ASSOCIATED TENSOR ASSE.
C
      SUBROUTINE ASS(C,EAO,EO,UNIT,ASSE)
      COMPLEX C(3),EAO,EO,UNIT(3,3),ASSE(3,3),D(3,3)
      COMPLEX S,F(3,3),G(3,3),H(3,3)
      CALL DYAD(C,C,D)
      S=EAO-EO
      CALL SCAL(EAO,UNIT,F)
      CALL SCAL(S,D,C)
      CALL SUTRA(F,G,H)
      CALL SCAL(EO,H,ASSE)
      RETURN
      END
```

```
C     THE SUBROUTINE THAT CALCULATES THE MATRIX A.
      SUBROUTINE AMTX(NRR,E,UNIT,A)
      COMPLEX NRR(3),E(3,3),UNIT(3,3),A(3,3),B(3,3)
      COMPLEX CE(3,3),SCALE,BE(3,3)
      CALL DYAD(NRR,NRR,B)
      CALL SUM(B,E,CE)
      CALL DOT(NRR,NRR,SCALE)
      CALL SCAL(SCALE,UNIT,BE)
      CALL SUTRA(CE,BE,A)
      RETURN
      END
C     CALCULATION OF A TO THE MINUS 1 TIMES 4 PI.
      SUBROUTINE ABR(ATEN,UNIT,AMI)
      COMPLEX ATEN(3,3),A1.A2,A3,A2I(3,3),PART1(3,3)
      COMPLEX PART2(3,3),AMITX(3,3),ACURE(3,3),ASQURE(3,3)
      COMPLEX TRCE1,TRCE2,TRCE3,FISH,AMI(3,3),UNIT(3,3)
      CALL TRACE(ATEN,TRCE1)
      CALL MAMUL(ATEN,ATEN,ASQURE)
      CALL TRACE(ASQURE,TRCE2)
      CALL MAMUL(ASQURE,ATEN,ACUBE)
      CALL TRACE(ACUBE,TRCE3)
      A1=-TRCE1
      A2=-(A1*TRCE1+TRCE2)/2.
      A3=-(A2*TRCE1+A1*TRCE2+TRCE3)/3.
      CALL SCAL(A2,UNIT,A2I)
      CALL SUM(A2I,ASQURE,PART1)
      CALL SCAL(A1,ATEN,PART2)
      CALL SUM(PART1,PART2,AMITX)
      FISH=-4.*3.14159/A3
      CALL SCAL(FISH,AMITX,AMI)
      RETURN
      END
C     SUBROUTINE CALCULATES THE TRACE
      SUBROUTINE TRACE(D,S)
      COMPLEX D(3,3),S
      S=0.
      DO 1 I=1,3
 1    S=S+D(I,I)
      RETURN
      END
```

```
NO2W  IS:  AND NAO2W  IS:

   0.202E+01   0.821E+00   0.000E+00   0.000E+00   0.707E+00   0.000E+00
   0.222E+01   0.798E+00   0.000E+00   0.000E+00   0.707E+00   0.000E+00
THE POLARISATION VECTORS E2WO AND E2WAO
   0.000E+00   0.000E+00  -0.202E+01  -0.821E+00   0.000E+00   0.000E+00
  -0.157E+01  -0.564E+00   0.000E+00   0.000E+00   0.339E+01   0.331E+01
THE POLARISATION VECTORS FOR ALFA= 1
   0.000E+00   0.000E+00   0.000E+00   0.000E+00   0.100E+01   0.000E+00
THE POLARISATION VECTORS FOR ALFA= 2
   0.000E+00   0.000E+00   0.000E+00   0.000E+00   0.000E+00   0.000E+00
THE POLARISATION VECTORS FOR ALFA= 3
   0.000E+00   0.000E+00   0.000E+00   0.000E+00   0.000E+00   0.000E+00
THE ANGLE OF THE C AXIS WITH RESP TO VERT.=       89.9999999

THE PHOTON ENERGY IS   0.170E+01  ELECTRON VOLTS

LITTLE Y  0.1612E+03

THE EXTRA ORDINARY INDEX OF ADP AT 2W   0.1518E+01
THE  ORDINARY INDEX OF ADP AT W         0.1497E+01

THE DIELECTRIC CONSTANTS ENTERED FOR THIS P. E.

EXTRA E(2W)    0.487E+01   0.349E+01
ORDIN. E(2W)     0.389E+01    0.331E+01

EXTRA E(W)    0.644E+01    0.206E+01
ORDIN. E(W)    0.589E+01    0.300E+01

          REAL PART     IMAGINARY
ER (1)

D32    -0.847E-01     0.101E+00
D33     0.000E+00     0.000E+00
D15     0.000E+00     0.000E+00

          REAL PART     IMAGINARY
ER (2)

D32     0.000E+00     0.000E+00
D33     0.000E+00     0.000E+00
D15     0.000E+00     0.000E+00

          REAL PART     IMAGINARY
ER (3)

D32    -0.847E-01     0.101E+00
D33     0.000E+00     0.000E+00
D15     0.000E+00     0.000E+00

THE ABSOLUTE VALUE OF THE COEFF. OF D(IJ)

ER(1 )

D32     0.132E+00
 D33     0.000E+00
 D15     0.000E+00


 ER(2 )

D32     0.000E+00
 D33     0.000E+00
 D15     0.000E+00


 ER(3 )

D32     0.132E+00
 D33     0.000E+00
 D15     0.000E+00
```

Appendix F

The Reflected Second Harmonic Electric Field Strength from the Boundary of a Nonmagnetic Uniaxial Piezo-Electric Material

The details of the calculation used to arrive at equations 4.8 through 4.10 are dealt with in this appendix.

In Chapter 4 it was noted that the solution to the wave equation 4.6:

eq. F.1 $$\nabla \times (\nabla \times \overrightarrow{E}(r,t)) + \frac{1}{c^2}\frac{\partial}{\partial t^2}\epsilon(2\omega)\cdot\overrightarrow{E}(r,t) = -\frac{4\pi}{c}\frac{\partial^2}{\partial t^2}P^{NLS}(r,t)$$

consisted of bound waves (inhomogeneous solution) and free waves (homogeneous solution) whose general forms were given (Fischer, 1967) as:

eq. F.2 $$\overrightarrow{E}_{hcm}(r,t) = \left(\bar{e}_o E_o(2\omega)\, e^{i\frac{2\omega}{c}(\bar{n}_o(2\omega)\cdot\bar{r})} + \overrightarrow{e}_{ao} E_{ao}(2\omega)\, e^{i\frac{2\omega}{c}(\bar{n}_{ao}(2\omega)\cdot\bar{r})}\right) e^{i2\omega t}$$

where $\bar{e}_o$ and $\bar{e}_{ao}$ were the polarization vectors of the ordinary and extraordinary waves, respectively.

and:

eq. F.3 $$\overrightarrow{E}_{inh}(r,t) = \sum_{\alpha=1,2,3}(-1)\,\overrightarrow{p}_\alpha(2\omega)\, e^{2\frac{\omega}{c}i(\bar{n}_\alpha(2\omega)\cdot\bar{r} - ct)}$$

where $$\bar{p}_\alpha = 4\pi A^{-1}\bar{P}^{NLS}(2\omega)$$

and $$A = \bar{n}_x\bar{n}_x + \epsilon(2\omega) - \bar{n}_\alpha^2\cdot I$$

Recall that the electric fields used to describe the nonlinear source polarization are for inside the medium. These are related to their values outside the medium by a linear Fresnel factor given by:

eq. F.3 $$E_{inside} = E_0(\omega)\left[\frac{2\sin\alpha\cos\alpha}{\sin\alpha\sqrt{\epsilon_f - \sin^2\alpha} + \sin\alpha\cos\alpha}\right] \; ; \; \epsilon_f = \frac{1}{\frac{\sin^2\theta}{\epsilon_o(\omega)} + \frac{\cos^2\theta}{\epsilon_{ao}(\omega)}}$$

where $E_o(\omega)$ is the electric field outside the material, θ is the angle of the "c" axis with respect to the electric field vector $E_o(\omega)$ and α is the angle of incidence of the incident wave.

The wave equation solutions must be matched at the boundary. The tangential components of both E and H must be continous across the boundary for all time.

We postulate that the solution of the wave equation for the second harmonic wave reflected from the boundary:

eq. F.4 $$\bar{E}_R(r,t) = \bar{E}_R(2\omega)\, e^{2i\frac{\omega}{c}(\bar{n}_r \cdot \bar{r} - ct)}$$

consists of two orthoginal vectors that form a plane normal to the direction of propagation of the wave:

eq. F.5 $$\bar{E}_R(2\omega) = v_2\bar{V}_1(2\omega) - v_1\bar{V}_2(2\omega)$$

where $\bar{E}_R(2\omega)$ is the reflected electric field vector and $\bar{V}_1$ and $\bar{V}_2$ are the above mentioned vectors.

We know that $\bar{n}_r \cdot \bar{E}_R(2\omega) = 0$ (transverse waves), where $\bar{n}_r$ is the propagation vector of $\bar{E}_R(2\omega)$. Thus $\bar{E}_R(2\omega)$ can be represented as:

eq. F.6 $$\bar{E}_R(2\omega) = v_2(\bar{n}_r \times \bar{u}_1) - v_1(\bar{n}_r \times \bar{u}_2)$$

and therefore:

eq. F.7 $$v_2 = \frac{-\bar{u}_1 \cdot \bar{E}_R}{\bar{n}_r \cdot (\bar{u}_1 \times \bar{u}_2)} \qquad v_1 = \frac{-\bar{u}_2 \cdot \bar{E}_R}{\bar{n}_r \cdot (\bar{u}_1 \times \bar{u}_2)}$$

and $$\bar{E}_R(2\omega) = \frac{1}{\bar{n}_r \cdot (\bar{u}_1 \times \bar{u}_2)} \left[(u_2 \cdot E_R)(n_r \times u_1) + u_1 \cdot E_R (n_r \times u_2) \right]$$

eq. F.8

The boundary conditions give us:

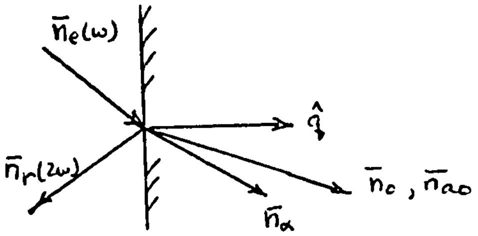

eq. F.9 $$\hat{q} \times \bar{E}_R = \hat{q} \times \bar{E}_{inh} + (\hat{q} \times \bar{e}_{ao}) E_{ao} + (\hat{q} \times \bar{e}_o) E_o$$

eq. F.10 $$\bar{n}_r \times \bar{E}_R = \bar{n}_\alpha \times \bar{E}_{inh} + (\bar{n}_{ao} \times \bar{e}_{ao}) E_{ao} + (\bar{n}_o \times \bar{e}_o) E_o$$

Rearranging the equation F.9, scalor multiplying it by $\bar{e}_o$ and $\bar{e}_{ao}$ then inserting it into F.10 yields:

eq F.11 $$(\hat{q} \cdot [\bar{e}_{ao} \times \bar{e}_o])(\bar{n}_r \times \bar{E}_R) - (\bar{n}_{ao} \times \bar{e}_{ao}) \bar{e}_o \cdot (\hat{q} \times \bar{E}_R) + \bar{e}_{ao} \cdot (\hat{q} \times \bar{E}_R)(\bar{n}_o \times \bar{e}_o) = \bar{A}$$

where

eq. F.12 $$\bar{A} = -\bar{e}_o \cdot (\hat{q} \times \bar{E}_{inh})(\bar{n}_{ao} \times \bar{e}_{ao}) + \bar{e}_{ao} \cdot (\hat{q} \times \bar{E}_{inh})(\bar{n}_o \times \bar{e}_o) + \hat{q} \cdot (\bar{e}_{ao} \times \bar{e}_o)(\bar{n}_\alpha \times \bar{E}_{inh})$$

Scalor multiplying this result by $\bar{e}_{ao}$ reduces F.11 to:

eq. F.13 $$\bar{E}_R \cdot \left[\bar{n}_o \cdot (\bar{e}_{ao} \times \bar{e}_o)(\bar{e}_{ao} \times \hat{q}) - \hat{q} \cdot (\bar{e}_{ao} \times \bar{e}_o)(\bar{e}_{ao} \times \bar{n}_r) \right] = \bar{e}_{ao} \cdot A$$

and we define:

eq. F.14 $$\bar{E}_R \cdot \bar{u}_1 = \bar{e}_{ao} \cdot \bar{A}$$

if, instead, equation F.11 were multiplied by $\bar{e}_o$, it would become:

eq. F.15 $$\bar{E}_R \cdot \left[\bar{n}_{ao} \cdot (\bar{e}_{ao} \times \bar{e}_o)(\bar{e}_o \times \hat{q}) - \hat{q} \cdot (\bar{e}_{ao} \times \bar{e}_o)(\bar{e}_o \times \bar{n}_r) \right] = \bar{e}_o \cdot \bar{A}$$

and we define:

eq. F.16 $$-\bar{E}_R \cdot \bar{u}_2 = \bar{e}_o \cdot \bar{A}$$

Recalling the definition of $\bar{A}$ (equation F.12) and using equation F.6 yields v_1 and v_2.

eq. F.17
$$v_1 = [\bar{e}_{ao} \cdot (\bar{n}_\alpha \times \bar{E}_{inh})][\hat{q} \cdot (\bar{e}_{ao} \times \bar{e}_o)] + [\bar{e}_{ao} \cdot (\bar{n}_o \times \bar{e}_o)][\bar{e}_{ao} (\hat{q} \times \bar{E}_{inh})]$$
$$v_2 = [\bar{n}_{ao} \cdot (\bar{e}_{ao} \times \bar{e}_o)][\bar{e}_o \cdot (\hat{q} \times \bar{E}_{inh})] - [\bar{e}_o \cdot (\bar{n}_\alpha \times \bar{E}_{inh})][\hat{q} \cdot (\bar{e}_{ao} \times \bar{e}_o)]$$

and the correct result as was described in Chapter 4 equations 4.8 to 4.10.

Caution must be used in deriving this result when eliminating terms from equation F.11. Fischer's result (Fischer, 1967) can be reproduced by multiplying equation F.11 by $\bar{n}_o$ and $\bar{n}_{ao}$ instead of $\bar{e}_o$ and $\bar{e}_{ao}$. $\bar{n}_o$ and $\bar{n}_{ao}$ are a poor choice of vectors. The space spanned by these vectors does not describe all possible $E_R(2\omega)$. $\bar{n}_o$ and $\bar{n}_{ao}$ are both in the plane of $\bar{n}_r$. Therefore in taking the dot product information is lost. Fischer's results, while possibly correct for some special cases, are not general.

BIBLIOGRAPHY

Armstrong, J.A., Bloembergen, N., Ducuing, J., and Perchan, P.S., "Interactions between Light Waves in a Nonlinear Dielectric," Phys. Rev. 127, 1918 (1962).

Armstrong, J.A., and Ducuing, J., "Experimental Observations of Random Fluctuations in Optical Harmonic Generation," Bull. Am. Phys. Soc. 8, 233 (1963).

Bell, Michael I., "Frequency Dependence of Miller's Rule for Nonlinear Susceptibilities," (to be published).

Bell, Michael I., "Nonlinear Optical Susceptibility of Semiconductors with Zinc-Blende Structure," Proc. 3rd Materials Res. Symp., Electron Density of States, Gaithersburg, MD. 1969 (in Press).

Bloembergen, N., "Optical Nonlinear Susceptibilities," Comments Solid State Phys. 11, 161 (1970).

Bloembergen, N., Chang, R.K., and Ducuing, J., "Dispersion of the Optical Nonlinearity in Semiconductors," Physics of Quantum Electronics, P.L. Kelly, B. Lax, and P.E. Tannenwald, editors (McGraw-Hill Book Co., New York, 1966), p. 67.

Bloembergen, N., Chang, R.K., Ducuing, J., and Lallemand, P., "Non-Linearieites Optiques de Quelques Composes III - V," Proc. of the 7th International Conf. on Semiconductors, (Dunod, Paris, 1964).

Bloembergen, N. and Ducuing, J., "Experimental Verification of the Optical Laws of Non-linear Reflection," Phys. Lett. 6, 5 (1963).

Bloembergen, N., and Pershan, P.S., "Light Waves at Boundary of Nonlinear Media," Phys. Rev. 128, 606 (1962).

Boyd, G.D., Buehler, E., and Storz, F.G., "Linear and Nonlinear Optical Properties of $ZnGeP_2$ and CdSe," Appl. Phys. Lett. 18, 301 (1971).

Bradley, D.J., Gale, G.M., Moore, M., and Smith, P.D., "Longitudinally Pumped Narrow Band Continuously Tunable Dye Laser," Phys. Lett. 26A, 378 (1968).

Brust, D., "Electronic Spectra of Crystaline Ge and Si," Phys. Rev. 134, A1337 (1964).

Butcher, P. and McClean, T., "Nonlinear Constitutive Relations in Solids at Optical Frequencies," Proc. Phys. Soc. 81, 219 (1963).

Cardona, M., "Infared Dielectric Constants and UV Optical Properties of Solids with the Diamond, ZB, Wurtzite, and Rocksalt Structures," J. Appl. Phys. 36, 2181 (1965).

Cardona, M., and Harbeke, G., "Optical Properties and Band Structure of Wurtzite-type Crystals and Rulite," Phys. Rev. 137, A1467 (1965).

Cardona, M., Shaklee, K.L., and Pollak, F.H., "Electroreflectance at a Semiconductor Electrolyte Interface," Phys. Rev. 154, 696 (1967).

Chang, R.K., and Bloembergen, N., "Experimental Verification of the Laws of the Reflected Intensity of Second-Harmonic Light," Phys. Rev. 144, 775 (1966).

Chang, R.K., Ducuing, J., and Bloembergen, N., "Relative Phase Measurement between Fundamental and Second Harmonic Light," Phys. Rev. Lett. 15, 6 (1965a).

Chang, R.K., Ducuing, J., and Bloembergen, N., "Dispersion of Optical Nonlinear Semiconductors," Phys. Rev. Lett. 15, 415 (1965).

Degiorgio, V., and Potentza, G., "Energy Losses in a Passive Q-Switched Ruby Laser," IEEE J. Quantum Electron. QE-3, 59 (1967).

Ducuing, J., and Bloembergen, N., "Observation of Reflected Light Harmonics at the Boundary of Piezoelectric Crystals," Phys. Rev. Lett. 10, 474 (1963).

Ducuing, J., and Bloembergen, N., "Statistical Fluctuations in Nonlinear Optical Processes,"Phys. Rev. 133, A1493 (1964).

Fischer, R., "Zur Theorie der Erzeugung der Zweiten Harmonischen an der Oberfläche eines Unmagnetischen Quadratischen, Optisch Einachsign Kristalls," Phys. Stat. Sol. 19, 757 (1967).

Francois, G.E., "CW Measurement of the Optical Nonlinearity of Ammonium Dyhydrogen Phosphate," Phys. Rev. 143, 2 (1966).

Franken, P.A., and Ward, J.F., "Optical Harmonics and Nonlinear Phenomena," Rev. Modern Phys. 36, 23 (1963).

Gatos, H.C., and Lavine, M.C., "Chemical Behavior of Semiconductors: Etching Characteristics," Lincoln Lab., Tech. Report 293 (1963).

Hercher, M., Chu, W., and Stockman, D., "An Experimental Study of Saturable Absorbers for Ruby Lasers," IEEE J. Quantum Electron. QE-6, 954 (1968).

Jerphagnon, J., and Kurtz, S.K., "Maker Fringes," App. Phys. 41, 1667 (1970).

Kelly, P.L., "Nonlinear Effects in Solids," J. Phys. Chem. 24, 607 (1963a).

Kelly, P.L., "Second Harmonic Generation in Solids," J. Phys. Chem. 24, 1113 (1963b).

Kleinman, D.A., "Theory of S.H.G. of Light," Phys. Rev. 128, 1761 (1962).

Knight, W., Kohanzadeh, G., and Lengyel, G., "Evaluation of Magnetic Defocussing for a Photomultiplier Tube with Large Area Semitransparent Photocathode," Appl. Optics 7, 1115 (1968).

Levine, B.F., "Electrodynamical Bond-Charge Calculation of Nonlinear Optical Susceptibilities," Phys. Rev. Lett. 22, 787 (1969).

Levine, B.F., "A New Contribution to the Nonlinear Optical Susceptibility Arising from Unequal Atomic Radii," Phys. Rev. Lett. 25, 440 (1970).

Loudon, R., "Theory of Nonlinear Optical Processes in Semiconductors and Insulators," Proc. Phys. Soc. 80, 952 (1962).

McFee, J.H., Boyd, G.D., and Schmidt, P.T., "Redetermination of the Nonlinear Optical Coefficients of Te and GaAs by Comparison with Ag_3SbS_3," Appl. Phys. Lett. 17, 57 (1970).

Miller, R.C., "Optical Second Harmonic Generation in Piézoelectric Crystals," Appl. Phys. Lett. 5, 17 (1964).

Miller, R.C., and Nordland, W.A., "Absolute Signs of Second Harmonic Generation Coefficients of Piezoelectric Crystals," Phys. Rev. 12, 4896 (1970).

Miller, R.C., and Savage, S., "Harmonic Generation and Mixing of $CaWo_4$: Nd^{3+} and Ruby Pulsed Laser Beams in Piezoelectric Crystals," Phys. Rev. 128, 2175 (1962).

Miyazoe, Y., and Maeda, M., "Stimulated Emission form 19 Polymethine Dyes - Laser Action over the Continuous Range from 710-1060 m , Appl. Phys. Lett. 12, 206 (1968).

Miyazoe, Y., and Maeda, M., "Polymethine Dye Lasers," Opto. Electron 2, 227 (1970).

Nye, J.F., Physical Properties of Crystals, Oxford, 1957.

Parsons, F.G., and Chang, R.K., "Measurement of the Nonlinear Susceptibility Dispersion by Dye Lasers," Opt. Comm. 3, 173 (1971).

Patel, C.K.N., "Optical Harmonic Generation in the Infrared Using a CO_2 Laser," Phys. Rev. Lett. 16, 613 (1966).

Phillips, J.C., "Covalent Bond in Crystals I: Elements of a Structural Theory." Phys. Rev. 166, 832 (1968a).

Phillips, J.C., "Covalent Bond in Crystals II: Partially Ionic Binding," Phys. Rev. 168, 905 (1968b).

Phillips, J.C., and Van Vechten, J.A., "Nonlinear Optical Susceptibilities of Covalent Crystals," Phys. Rev. 183, 709 (1969).

Robinson, F.N.H., "Relations Between the Components of the Nonlinear Polarizability Tensor in Cubic and Hexagonal II-VI Compounds," Phys. Lett. 26A, 435 (1968).

Seraphin, B.O., and Bennett, H.E., "Optical Constants," Semiconductors and Semimetals, Vol. 3, R.K. Willardson and A.C. Beer, editors (Academic Press, 1967), p. 499.

Soffer, B. and McFarland, B.B., "Continuously Tunable Narrow Band Organic Dye Lasers," Appl. Phys. Lett. 10, 266 (1967).

Soref, R.A. and Moos, H.W., "Optical Second Harmonic Generators in ZnS-CdS and CdS-CdSe Alloys," J. Appl. Phys. 35, 2152 (1964).

Sorokin, P.P., " End Pumped Stimulated Emission from a Thiacarboncyanine Dye," IBM Journ. (Sept. 1966).

Sorokin, P.P. and Lankard, J.R., "Stimulated Emission Observed from an Organic Dye Chloro Aluminum Phthalocyanine," IBM J. Res. & Dev. 10, 162 (1966).

Sorokin, P.P., Lankard, J.R., Hammond, E.C., and Moruzzi, V.L., "Emission from Organic Dyes, Experimental Studies and Analytical Comparisons, Flashlamp Excitation of Organic Dye Lasers, IBM J. Res. & Dev. 11, 130 (1967).

Sorokin, P.P., Lankard, J.R., Moruzzi, V.L., and Hammond, E.C., "Flash-Lamp Pumped Organic Dye Lasers," IBM Research Report RC 1950 (1967).

Sorokin, P.P., Luzzi, J.J., Lankard, J.R., and Pettit, G.D., "Ruby Laser Q-Switching Elements Using Phthalocyanine Molecules in Solution," IBM J. RES. & Dev. 8, 182 (1964).

Wynne, J.J., and Bloembergen, N., "Measurement of the Lowest-order Non-linear Susceptibility in III-IV Semiconductors by Second-Harmonic Generation with a CO_2 Laser," Phys. Rev. 188, 1211 (1969).

Yariv, A., Quantum Electronics, (John Wiley & Sons, Inc., New York, 1967) Chapters 18 and 21.

Zernike, F., "Refractive Indices of Ammonium Dihydrogen Phosphate and Potassium Dihydrogen Phosphate between 2000A-1.5μ," J. Opt. Soc. Am. 10, 1215 (1964).